Remodeling of airway epithelium and lung extracellular matrix in COPD and IPF

Hedström, Ulf

2018

Document Version:
Publisher's PDF, also known as Version of record

Remodeling of airway epithelium and lung extracellular matrix in COPD and IPF

ULF HEDSTRÖM | FACULTY OF MEDICINE | LUND UNIVERSITY

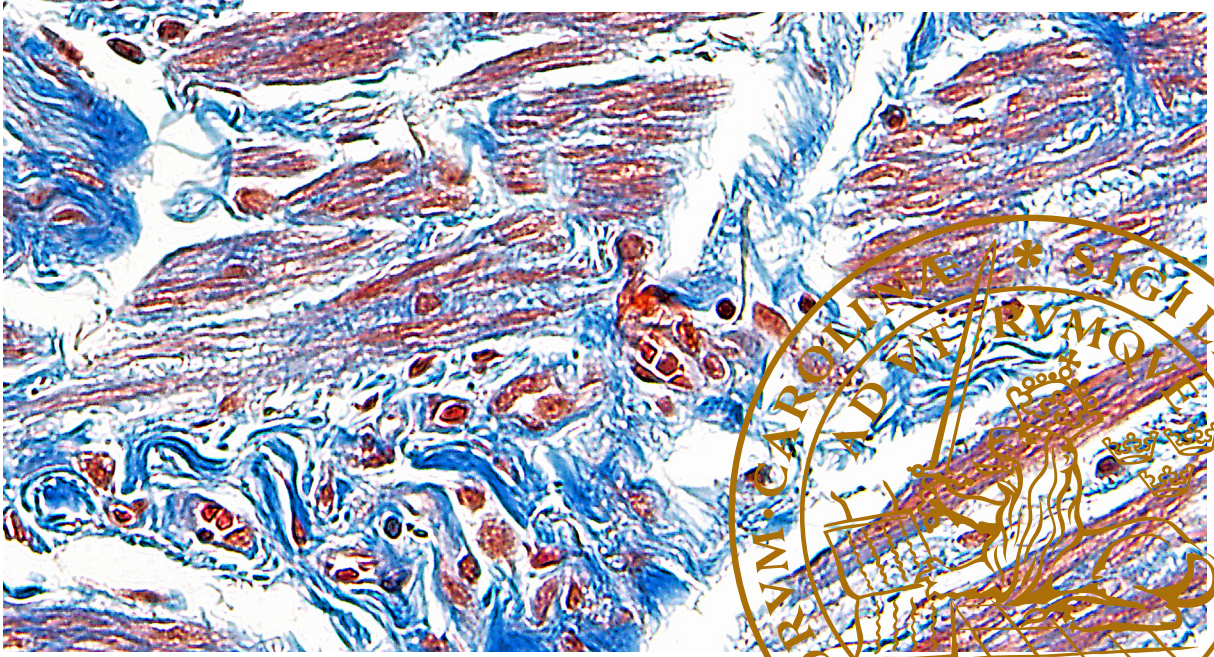

Remodeling of airway epithelium and lung extracellular matrix in COPD and IPF

Remodeling of airway epithelium and lung extracellular matrix in COPD and IPF

Doctoral thesis
by
Ulf Hedström

LUND
UNIVERSITY

DOCTORAL DISSERTATION

by due permission of the Faculty of Medicine, Lund University, Sweden.
To be defended at Belfragesalen D15, BMC, Lund on 6 December 2018 at 13:00.

Faculty opponent

PD Dr. Claudia Staab-Weijnitz

Helmholtz Zentrum München

Organization	Document name
LUND UNIVERSITY	Doctoral dissertation
Department of Experimental Medical Science	Date of issue 2018-12-06
Author: Ulf Hedström	Sponsoring organization

Title: Remodeling of airway epithelium and lung extracellular matrix in COPD and IPF

Abstract

In chronic obstructive pulmonary disease (COPD) and idiopathic pulmonary fibrosis (IPF), the lungs are subjected to remodeling, which affects cellular architecture and function as well as extracellular matrix (ECM) composition. COPD lungs show localized, peribronchiolar fibrosis, but is generally characterized by chronic airway inflammation and degradation of the alveolar parenchyma, which lead to irreversible airflow limitation. In addition, airway epithelial remodeling contributes to the pathology of the disease and increases the risk of respiratory infections. In IPF, exaggerated deposition of ECM proteins in the lung interstitium causes lung scarring, reduced compliance and impaired gas exchange.

Much is yet to be learned about the nature of pulmonary ECM alterations in COPD and IPF and how they modulate cell function in the diseased lung. The aim of this thesis work was to study in detail how the pulmonary ECM is remodeled in COPD and IPF, with a particular focus on how pathological alterations in the bronchial ECM modulate epithelial cell phenotype in COPD airways. An ex vivo model was developed in which diseased and normal primary human bronchial epithelial cells (HBEC) repopulate decellularized bronchial scaffolds derived from COPD patients and healthy individuals. Global gene expression analysis was performed on the repopulated cells. Furthermore, proteomics and immunohistochemistry were used to examine the ECM composition of COPD and IPF lungs.

Bronchial scaffolds from COPD patients induced altered gene expression in repopulated HBEC. Ciliated cell differentiation was induced by the scaffolds regardless of scaffold origin, but COPD HBEC had an impaired ability to initiate the differentiation. Moreover, COPD HBEC showed increased cell cycle progression when cultured on bronchial scaffolds from COPD patients. Glycosaminoglycan content was increased in IPF lungs along with an altered structure of heparan sulfate. IPF lungs showed increased deposition of asporin and altered expression of ECM proteins that regulate cell adhesion. Lungs from COPD patients showed altered expression of ECM proteins that regulate proteolytic activity and elastic fiber homeostasis. In summary, this thesis provides novel insight into phenotypic modulation of epithelial cells in COPD airways and remodeling of the pulmonary ECM in COPD and IPF. Hopefully, these findings will eventually help to facilitate development of more efficient therapies to improve the clinical outcome of patients suffering from COPD or IPF.

Keywords: chronic obstructive pulmonary disease, idiopathic pulmonary fibrosis, extracellular matrix, epithelial cells, remodeling.

Classification system and/or index terms

Supplementary bibliographical information	Language English
ISSN and key title 1652-8220 Lund University, Faculty of Medicine Doctoral Dissertation Series 2018:153	ISBN 978-91-7619-722-6

Recipient's notes	Number of pages 204	Price
	Security classification	

Remodeling of airway epithelium and lung extracellular matrix in COPD and IPF

Doctoral thesis
by
Ulf Hedström

LUND
UNIVERSITY

DOCTORAL DISSERTATION

by due permission of the Faculty of Medicine, Lund University, Sweden.
To be defended at Belfragesalen D15, BMC, Lund on 6 December 2018 at 13:00.

Faculty opponent

PD Dr. Claudia Staab-Weijnitz

Helmholtz Zentrum München

Cover photo by: Ulf Hedström

Faculty of Medicine

Department of Experimental Medical Science

ISBN 978-91-7619-722-6

ISSN 1652-8220

Lund University, Faculty of Medicine Doctoral Dissertation Series 2018:153

Printed in Sweden by Media-Tryck, Lund University

Lund 2018

MADE IN SWEDEN

Contents

List of papers

This thesis is based on the following papers, which will be referred to in the text by their Roman numerals.

I. Ulf Hedström, Oskar Hallgren, Lisa Öberg, Amy DeMicco, Outi Vaarala, Gunilla Westergren-Thorsson*, Xiaohong Zhou*. **Bronchial extracellular matrix from COPD patients induces altered gene expression in repopulated primary human bronchial epithelial cells**. *Scientific Reports* 8:3502 (2018).

II. Ulf Hedström, Lisa Öberg, Outi Vaarala, Göran Dellgren, Martin Silverborn, Gunilla Westergren-Thorsson*, Oskar Hallgren*, Xiaohong Zhou*. **Bronchial epithelial cells from COPD patients show impaired ciliary development and altered cell cycle progression after repopulation on bronchial scaffolds**. *Manuscript in preparation for submission*.

III. Gunilla Westergren-Thorsson, Ulf Hedström, Annika Nybom, Emil Tykesson, Emma Åhrman, Marie Hornfelt, Marco Maccarana, Toin H. van Kuppevelt, Göran Dellgren, Marie Wildt, Xiao-Hong Zhou, Leif Eriksson, Leif Bjermer, Oskar Hallgren. **Increased deposition of glycosaminoglycans and altered structure of heparan sulfate in idiopathic pulmonary fibrosis**. *The International Journal of Biochemistry and Cell Biology* 83, 27-38 (2017).

IV. Emma Åhrman, Oskar Hallgren, Lars Malmström, Ulf Hedström, Anders Malmström, Leif Bjermer, Xiao-Hong Zhou, Gunilla Westergren-Thorsson, Johan Malmström. **Quantitative proteomic characterization of the lung extracellular matrix in chronic obstructive pulmonary disease and idiopathic pulmonary fibrosis**. *Journal of Proteomics* 189, 23-33 (2018).

* These authors share senior authorship

Selected abbreviations

ALI	Air-liquid interface
CS	Chondroitin sulfate
COPD	Chronic obstructive pulmonary disease
DS	Dermatan sulfate
ECM	Extracellular matrix
FN	Fibronectin
GAG	Glycosaminoglycan
HS	Heparan sulfate
HBEC	Human bronchial epithelial cells
HSPG	Heparan sulfate proteoglycan
HA	Hyaluronic acid
IHC	Immunohistochemistry
IPF	Idiopathic pulmonary fibrosis
KS	Keratan sulfate
SLRP	Small leucine-rich proteoglycan

Preface

Chronic obstructive pulmonary disease (COPD) is a considerable global health problem that affects hundreds of millions of people worldwide[1]. It is a progressive disease that leads to a largely irreversible airflow limitation and ultimately a severely decreased lung function caused by airflow obstruction and destruction of peripheral lung tissue. In addition, remodeling of the airway epithelium contributes to the disease pathology and increases the risk of respiratory infections[2]. Idiopathic pulmonary fibrosis (IPF) is characterized by progressive lung scarring due to exaggerated extracellular matrix (ECM) deposition, which leads to reduced lung compliance[3]. COPD and IPF have similar risk factors but are different with respect to the tissue remodeling that takes place during disease progression.

The ECM is a complex macromolecular network that impart tensile strength and elasticity to tissues and organs, but it can also influence cell function by harboring mediators such as growth factors or by participating in activation of cell surface receptors[4]. The ECM is subjected to remodeling in COPD and IPF lungs, but much is yet to be learned about these ECM alterations and especially how they affect cell function in the diseased lung.

The aim of this thesis work was to study in detail how the pulmonary ECM is remodeled in COPD and IPF, with a particular focus on how pathological alterations in the bronchial ECM modulate epithelial cell phenotype in COPD airways. To this end, we developed an ex vivo model in which primary human bronchial epithelial cells (HBEC), isolated from COPD or normal lungs, repopulate and differentiate on decellularized bronchial scaffolds derived from COPD patients or healthy individuals. Immunohistochemistry and RNA sequencing were used to investigate the phenotype of the repopulated cells. Furthermore, the pulmonary ECM in patients with COPD and IPF was examined by mass spectrometry, high-performance liquid chromatography and immunohistochemistry.

Introduction

Chronic obstructive pulmonary disease

COPD is characterized by chronic airway inflammation, loss of small airways and destruction of the lung parenchyma. It is a progressive disease that leads to a largely irreversible airflow limitation and common symptoms are dyspnea, cough, wheezing and recurrent respiratory infections. Prolonged inhalation of tobacco smoke is the primary cause of COPD, but other risk factors include exposure to biomass fuels and air pollution, frequent respiratory infections during childhood and genetic factors. Exacerbations are common in COPD patients and lead to increased morbidity and mortality. Although inflammation and remodeling of lung tissue architecture are both crucial aspects of COPD pathology, the main focus of this thesis is on the remodeling.[5-7]

Pathophysiology

Narrowing and destruction of the small conducting airways known as bronchioles is one of the earliest events in COPD pathogenesis and has been shown to precede emphysematous destruction[8]. Bronchioles offer little resistance in the normal lung, but in COPD lungs they constitute the major site of airway obstruction[9]. In COPD lungs, hypersecretion of mucus[10], ciliary dysfunction[11,12] and dysregulated tissue repair lead to increased susceptibility to respiratory infections, mucus plugs and airway wall thickening[13]. Many of these changes are related to airway epithelial remodeling, which can include goblet cell hyperplasia[10], squamous cell metaplasia[14] and decreased epithelial integrity[15]. Degradation of elastic fibers[16] and alveolar septa lead to loss of elastic recoil, airway collapse and emphysema. However, the extent of parenchymal destruction varies a lot between patients with COPD, which is a very heterogeneous disease in general. In COPD, lung tissue destruction is intimately connected to increased proteolytic activity resulting from a dysregulated tissue repair response[17]. Tissue damage caused by chronic exposure to inhaled noxious agents leads to persistent infiltration of inflammatory cells, which secrete proteolytic enzymes like matrix metalloproteinase 8 (MMP8), MMP9, MMP12 and neutrophil elastase. This causes enzymatic degradation of the ECM and generation of short peptide fragments derived from ECM proteins like collagen and elastin. These ECM fragments have chemotactic

properties and therefore promote continued infiltration of neutrophils and monocytes, which leads to perpetuated tissue damage. The progressive degradation of alveolar septa eventually leads to decreased oxygenation of the blood[18] as well as increased resistance in pulmonary arteries, which augments the risk of developing comorbidities like pulmonary arterial hypertension and right heart failure[19]. COPD patients also have an increased risk of developing lung cancer[20].

Diagnosis and treatment

Spirometry is a pulmonary function test and the principal diagnostic tool for COPD. An essential readout from this test is the forced expiratory volume in 1 second (FEV_1), which is the volume of air exhaled by the patient during the first second of a forced expiration after administration of bronchodilators. The total volume of air expelled from the lungs during the expiration is referred to as the forced vital capacity (FVC) and an $FEV_1/FVC<0.70$ indicates airway obstruction. FEV_1 is then calculated as the percentage of a predicted value, which is based on spirometry data from individuals of the same gender, age, race and height. The Global Initiative for Chronic Obstructive Lung Disease (GOLD) has defined four clinical stages of COPD (table 1) based on the percentage of the predicted FEV_1 value (FEV_1% predicted) in patients with $FEV_1/FVC<0.70$.[7]

Table 1. GOLD stage classification in patients with $FEV_1/FVC<0.70$.

GOLD stage	Disease severity	FEV_1% predicted
GOLD 1	Mild	$FEV_1 \geq 80\%$ predicted
GOLD 2	Moderate	$50\% \leq FEV_1 < 80\%$ predicted
GOLD 3	Severe	$30\% \leq FEV_1 < 50\%$ predicted
GOLD 4	Very severe	$FEV_1 < 30\%$ predicted

The standard of care for COPD typically includes the use of bronchodilators and corticosteroids. Bronchodilators increase airflow by inducing smooth muscle relaxation in the airway wall and include two main classes of drugs: beta 2 adrenergic receptor agonists and muscarinic acetylcholine receptor antagonists. Corticosteroids act by suppressing the inflammatory response. Bronchodilators and corticosteroids can be administered orally or via the inhaled route and are often combined to increase therapeutic efficacy. Other treatment options include methylxanthines and phosphodiesterase 4 inhibitors.[7,21-23]

Idiopathic pulmonary fibrosis

IPF is a chronic interstitial lung disease of unknown cause that leads to progressive scarring of the lung interstitium[24]. It presents with dyspnea, cough and eventually a severely decreased quality of life. Risk factors include prolonged inhalation of tobacco smoke or other noxious particles and gases, chronic pulmonary viral infections and genetic factors, which have been estimated to constitute up to one third of the risk of developing IPF[25].

Pathophysiology

Pathological hallmarks of IPF are progressive lung scarring because of exaggerated extracellular matrix (ECM) deposition, and the presence of a radiological and/or histopathological pattern called usual interstitial pneumonia (UIP). The main characteristic of this pattern is honeycombing, which refers to subpleural, cystic airspaces with well-defined walls that are usually lined with bronchiolar epithelium. Traction bronchiectasis is also frequently associated with the UIP pattern. Histologically, IPF lung tissue shows a patchy fibrotic structure, with areas of dense fibrosis alternating with areas where a more normal alveolar structure can still be discerned, but with thickened alveolar septa. Another important characteristic of IPF histopathology is the presence of fibroblastic foci, which are areas of actively proliferating fibroblasts and myofibroblasts in a myxoid-like matrix. Fibroblastic foci have been suggested to represent sites of active fibrogenesis.[24,26,27]

Many of the pathological changes in IPF lungs are consistent with accelerated aging and aberrant activation of epithelial cells and fibroblasts[28]. Inflammation used to be viewed as a main driver of the disease, but this paradigm has been challenged by more recent data that support the idea of IPF as a disease driven by abnormally activated epithelial cells with an increased production of pro-fibrotic mediators, which stimulate hyperproliferation of fibroblasts, myofibroblast differentiation and exaggerated ECM deposition[24,29]. Epithelial cells in IPF lungs show signs of increased senescence[30] and telomere attrition[31] and gene variants associated with increased IPF risk are often found in genes involved in maintenance of telomere integrity[25]. The dysregulated epithelial function in IPF also appears to be connected to reactivation of signaling pathways related to development, such as Wnt and sonic hedgehog, and their crosstalk with transforming growth factor beta (TGF-β) signaling has been suggested to create a pro-fibrotic feedback loop[32].

Diagnosis and treatment

An IPF diagnosis is based on the absence of a known etiology and the presence of a pulmonary UIP pattern, identified by high-resolution computed tomography and sometimes additional histological evaluation[26]. Currently there are two main pharmacological treatment options for IPF patients. Pirfenidone is an anti-fibrotic agent with unknown mechanism of action that has been shown to improve survival and slow down physiological deterioration[33,34]. Nintedanib is an inhibitor of multiple tyrosine kinases, including platelet-derived growth factor, vascular endothelial growth factor and fibroblast growth factor (FGF) receptors, and has been demonstrated to slow down lung function decline in IPF patients[35]. Given that IPF is a restrictive lung disease, FVC is the most relevant spirometry readout for monitoring disease progression and response to treatment[36].

Airway epithelial cells

The airway epithelium in the central airways is made up of four principal cell types: ciliated cells, goblet cells, intermediate cells and basal cells[2]. Basal cells are cuboidal progenitor cells that are found near the basement membrane and can replenish an injured epithelium by differentiating into ciliated cells or goblet cells. Intermediate cells are undifferentiated cells that are believed to be in a transition state between basal cells and the terminally differentiated cell types. Interestingly, a novel airway epithelial cell type called the pulmonary ionocyte was also recently described and potentially plays an important role in the pathology of cystic fibrosis[37]. The epithelium has a pseudostratified morphology in the proximal segments of the tracheobronchial tree, but assumes a more cuboidal shape as the segments become more distal[38]. Mucus is produced by goblet cells together with submucosal glands and the mucus layer lining the airway surface is continuously transported towards the pharynx by ciliated cells due to coordinated ciliary beating. This machinery is sometimes referred to as the mucociliary escalator and constitutes a critical host defense mechanism responsible for clearing the lungs of pathogens. In addition, the lungs are protected from inhaled pathogens and other noxious particles by the airway barrier function, which exists thanks to tight junctions and adherens junctions that form connections between neighboring cells in the airway epithelium[39]. The airway epithelium also plays a crucial role in the innate host defense response by producing antimicrobial peptides[40] and cytokines for attracting leukocytes[41]. Differentiation towards the ciliated cell lineage in airway epithelium is controlled by the transcription factor forkhead box J1 (FOXJ1)[42], which is also a useful ciliated cell marker.

The transcriptional program governing goblet cell differentiation is regulated by FOXA3 and SAM-pointed domain-containing ETS transcription factor[43,44], but mucin 5AC (MUC5AC) is commonly used as a goblet cell marker, whereas basal cells are identified by their expression of keratin 5 or p63[2].

Remodeling of airway epithelium in COPD

Remodeling of the airway epithelium in COPD patients includes pathological changes such as goblet cell hyperplasia[10,45], basal cell hyperplasia[2], squamous cell metaplasia[14] and impaired epithelial integrity[15]. These alterations lead to exaggerated mucus production, defective mucociliary clearance and increased susceptibility to respiratory infections, which augments the risk of exacerbations[46].

Ciliary defects

Shortening of cilia and decreased ciliary beating have been observed in COPD airways[11,12] and multiple studies have shown that cigarette smoke has a detrimental effect on cilia in airway epithelium[47-49]. Cigarette smoke extract (CSE) has been shown to impair ciliated cell differentiation in vitro in a post-transcriptional manner[50], with a concomitant increase in the number of goblet cells and club cells[50]. Furthermore, it has been reported that the inhibitory effect of CSE on cilia growth in bronchial epithelial cells can be mitigated by overexpression of FOXJ1[51]. The same study also showed that exposure to CSE led to a broad suppression of genes linked to ciliary development, while expression of other types of genes was largely unaffected.

Impaired epithelial barrier function

The airway epithelial barrier function is dysfunctional in COPD lungs. Transcriptome analysis of airway epithelial cells has shown that the overall expression of adherens junctional complex genes is downregulated in healthy smokers compared to non-smokers and even further decreased in COPD smokers[15]. This is consistent with observations of downregulated tight junction proteins in COPD airway epithelium[52]. Moreover, CSE has been shown to reduce epithelial integrity of bronchial epithelial cells in vitro[53], and this effect was dependent on activation of the epidermal growth factor receptor (EGFR), which is in agreement with observations of increased EGFR expression in COPD airway epithelium[54].

Goblet cell hyperplasia

Mucus hypersecretion in COPD is mainly caused by goblet cell hyperplasia, hypertrophy of submucosal glands and insufficient mucociliary clearance[55]. Goblet cell hyperplasia is common in COPD[10,45], and especially in patients who are current smokers or have a chronic bronchitis phenotype[56]. The increased presence of

intraluminal mucus and the inability to clear it from the airways can lead to cough, mucus plugs and an elevated risk of respiratory infections. MUC5AC is one of the principal components of mucus in the central airways and mechanistic studies have shown that cigarette smoke-induced MUC5AC production is controlled by EGFR activation[57]. Moreover, the cystic fibrosis transmembrane conductance regulator (CFTR) ion channel is also dysfunctional in COPD airways[58], and both EGFR and CFTR have therefore been proposed to contribute to COPD pathogenesis.

Epithelial-mesenchymal transition

Epithelial-mesenchymal transition (EMT) is a process where epithelial cells transdifferentiate into mesenchymal cells. Epithelial markers like E-cadherin and cytokeratin are downregulated and the cells lose their polarity, become motile, degrade the basement membrane and migrate into the interstitium[59]. The transitioning cells start to express mesenchymal cell markers such as α-smooth muscle actin, vimentin, fibronectin and collagen I[60]. Studies have demonstrated increased EMT in the airway epithelium of COPD patients[61,62] and EMT has been proposed as a potentially important mechanism behind development of peribronchiolar fibrosis during small airway remodeling in COPD lungs.

Squamous metaplasia

In the lungs, squamous metaplasia occurs when normal airway epithelial cells are gradually replaced by squamous epithelium, often as a result of exposure to harmful agents such as tobacco smoke[14]. Squamous metaplastic lesions have been found in COPD airways and the extent of squamous metaplasia correlates with disease severity[14,63]. Although they are benign, squamous metaplastic lesions are considered pre-neoplastic and might eventually develop into bronchial carcinoma. It has been reported that squamous metaplasia triggers airway fibrosis in COPD by paracrine stimulation of airway fibroblasts with interleukin 1 beta[63]. The authors showed that enhanced production of interleukin 1 beta from squamous metaplastic cells induces fibroblast-mediated activation of latent TGF-β1 by an integrin-dependent mechanism, leading to subsequent pro-fibrotic changes in the airway fibroblasts.

Extracellular matrix

The ECM is a complex and dynamic macromolecular network of proteins and carbohydrates that provides all organs with both rigidity and flexibility. Its composition is highly tissue specific and reflects the different functional requirements of each tissue. Fibrous proteins with low solubility, especially collagens, are abundant in the ECM. However, it also includes more soluble proteins, such as mucins, growth factors and

enzymes that control assembly and degradation of components in the ECM and thereby contribute to its dynamic nature. Many ECM proteins have a modular structure and contain multiple domains that make them able to interact simultaneously with many other types of ECM molecules as well as cell surface receptors. This leads to intricate crosslinking within the ECM network and creates an organized tissue structure. Besides providing structural support, the ECM is also bioactive and can influence adhesion, migration, proliferation and differentiation of cells by harboring mediators that affect cell function or by interacting directly with cell surface receptors.[4,64]

The matrisome

Naba et al. have proposed a definition of what constitutes the ECM using an in silico approach[65]. A bioinformatic pipeline was established and candidate ECM proteins were extracted from bioinformatic databases based on the presence of signature protein domains that are commonly found in core ECM proteins or proteins known to regulate or be associated with the ECM. In parallel, exclusion domains were also defined and some of the extracted candidate ECM proteins were then removed if they contained such domains. Finally, the protein sequences for all remaining candidate ECM proteins were screened for predicted transmembrane domains and signal peptides to further refine the list. In the end, this approach identified 1062 proteins that were collectively referred to as the matrisome. This provided a broader definition of the ECM by including proteins that were previously not considered ECM components. The matrisome was subdivided into core matrisome proteins and matrisome-associated proteins (fig. 1). The core matrisome consists of the main structural proteins of the ECM and includes collagens, proteoglycans and ECM glycoproteins. Matrisome-associated proteins were divided into ECM regulators, ECM-affiliated proteins and secreted factors.

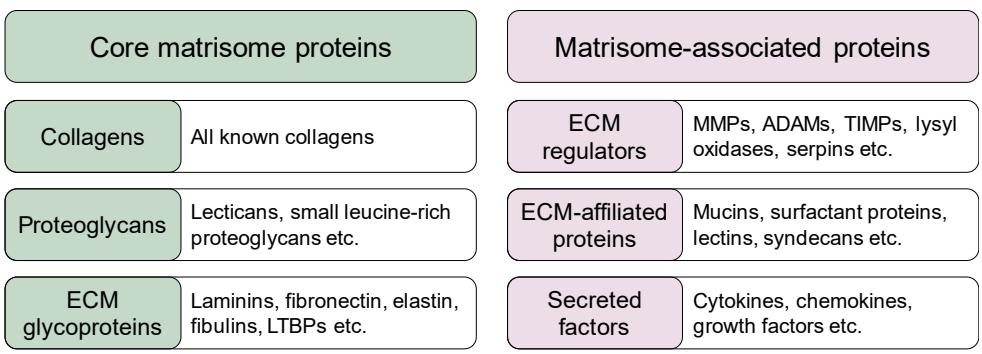

Figure 1. Matrisome protein categories with examples of proteins included in each category. LTBP=latent TGF-β-binding protein, MMP=matrix metalloproteinase, ADAM=disintegrin and metalloproteinase domain-containing protein, TIMP=tissue inhibitor of metalloproteinases.

Proteoglycans

Proteoglycans are complexes of linear proteins that are linked to polysaccharides known as glycosaminoglycans (GAGs). They are classified based on the type of GAGs the core protein is connected to. Most proteoglycans are found in the ECM, but they can also be membrane-bound or intracellular[66]. Proteoglycans are important for biomechanical properties of the ECM, but they are also involved in regulating biological processes that affect cellular functions. The heparan sulfate proteoglycan syndecan-4[67] is essential for FGF signaling[68], versican has been shown to have a negative impact on elastogenesis[69], and decorin regulates collagen fibrillogenesis[70] and TGF-β1 retention in the ECM[71,72].

Glycosaminoglycans

GAGs are long, unbranched polysaccharides composed of disaccharide repeats. They are grouped into five classes depending on their disaccharide composition: heparan sulfate (HS), chondroitin sulfate (CS), dermatan sulfate (DS), keratan sulfate (KS) and hyaluronic acid (HA) (also known as hyaluronan). Heparin is also a GAG and has the same disaccharide composition as HS but is mostly produced my mast cells and is more highly sulfated. All GAGs except HA are connected to a core peptide to form proteoglycans. The disaccharide repeats for all GAGs except KS are made up of one uronic acid (galactose for KS) and one amino sugar. The uronic acid is either D-glucuronic acid or L-iduronic acid and the amino sugar is N-acetyl-glucosamine (HS, KS, HA) or N-acetyl-galactosamine (CD, DS). Both the uronic acid and the amino sugar can also be sulfated at different positions, making GAGs a highly diversified group of molecules, based on varying disaccharide composition, chain length and sulfation patterns.[73,74]

Sulfation makes GAGs negatively charged at neutral pH, which increases their capacity to bind secreted mediators like cytokines and growth factors. GAGs are therefore important contributors to the ability of the ECM to act like a reservoir for such mediators. However, GAGs can also directly affect cell function by mediating binding between growth factors and their receptors[75,76]. One of the most well-known examples of a GAG influencing a biological function is the ability of heparin to act as an anticoagulant by potentiating the activity of antithrombin[77]. GAGs are also known to bind chemokines and may affect extravasation and migration of leukocytes by giving rise to chemokine gradients[73].

Lecticans

Lecticans are a family of large, extracellular CS/DS proteoglycans that all form aggregates with HA and include versican, aggrecan, neurocan and brevican. Neurocan and brevican are predominantly expressed in the central nervous system[78,79]. Aggrecan has a high GAG density and is a principal component of cartilage. Because of its high negative charge density, aggrecan has osmotic properties that make it able to easily bind

water. Its capacity to maintain a swelling potential in the cartilage ECM is essential for the ability of cartilage to resist compression.[80]

Versican is a multifaceted proteoglycan involved in numerous physiological and pathological processes. It regulates cell proliferation, differentiation, migration and adhesion, and has an influence on inflammation, tissue stability and remodeling. Fibroblasts are important producers of versican and its expression is regulated by TGF-β1. Versican has been implicated in chronic lung disease pathology and might contribute to remodeling during impaired tissue repair in the diseased lung.[81]

Small leucine-rich proteoglycans

The extracellular small leucine-rich proteoglycans (SLRPs) comprise the largest proteoglycan family. They are subdivided into five classes (table 2) based on structural homology and functional similarities. SLRPs can exist in soluble form in the ECM or be sequestered by other ECM components, which have implications for their biological activity. SLRPs that are not sequestered can modulate intracellular signal transduction by interacting with growth factor receptors, toll-like receptors or integrins. However, when bound to the ECM, SLRPs tend to be involved in regulating assembly of other ECM proteins. Most notably, several SLRPs regulate collagen fibrillogenesis. The most extensively studied SLRPs are decorin and biglycan. Decorin has been demonstrated to mitigate bleomycin-induced pulmonary fibrosis in vivo[82] and block TGF-β activity in cultured lung fibroblasts[83]. The antifibrotic properties of decorin have been attributed to its ability to sequester TGF-β. Indeed, several SLRPs, including biglycan, decorin and fibromodulin, can bind TGF-β[71] and thereby indirectly affect its activity. Asporin is another SLRP that is structurally similar to decorin and biglycan and has mainly been implicated in chondrogenesis, biomineralization and osteoarthritis. Several members of the SLRP family, including asporin, don't have any known GAG chains (table 2), but are still grouped with the GAG-bearing SLRPs because of a large degree of homology and functional similarity.[66,84]

Table 2. The five classes of small leucine-rich proteoglycans (SLRPs) and the type of glycosaminoglycan (GAG) chain each SLRP is attached to shown in parentheses. Asporin, ECM2, ECMX, opticin, chondroadherin, nyctalopin, tsukushi, podocan and podocan-like 1 don't have any known GAG chains. PRELP=proline/arginine-rich end leucine-rich repeat protein, CS=chondroitin sulfate, DS=dermatan sulfate, KS=keratan sulfate. Adapted from Nastase et al. (2014)[84].

SLRP class	SLRP (GAG)
I	Asporin (-), Biglycan (CS/DS), Decorin (CS/DS), ECM2 (-), ECMX (-)
II	Fibromodulin (KS), Keratocan (KS), Lumican (KS), Osteoadherin (KS), PRELP/prolargin (KS)
III	Epiphycan (CS/DS), Opticin (-), Osteoglycin (KS)
IV	Chondroadherin (-), Nyctalopin (-), Tsukushi (-)
V	Podocan (-), Podocan-like 1 (-)

Heparan sulfate proteoglycans

Heparan sulfate proteoglycans (HSPGs) are mainly present on cell surfaces and in basement membranes. They bind growth factors, cytokines and chemokines and regulate multiple biological functions[85]. Syndecans are transmembrane HSPGs that participate in various processes, such as endocytosis, exosome uptake and generation of morphogen gradients[66]. Syndecan-4 facilitate the interaction between FGFs and FGF receptors by acting as a coreceptor[67]. Also, syndecans cooperate with integrins during cell adhesion to ECM glycoproteins, such as fibronectin (FN), vitronectin and laminins[86]. It has also been shown that the ability of fibroblasts to form focal adhesions when grown on FN is dependent on both integrins and syndecan-4[87]. Glypicans are HSPGs that are attached to the plasma membrane via glycosylphosphatidylinositol anchors. They modulate the activity of Wnt and Hedgehog signaling and have been implicated in angiogenesis and tumor growth control[66]. The HSPGs perlecan, agrin and collagen XVIII are important constituents of basement membranes. Perlecan is widely expressed in all basement membranes and interacts with laminins and nidogens. It sequesters growth factors and its negative charge is important for the molecular sieving properties of basement membranes[64]. Agrin is mostly found in the nervous system and is responsible for postsynaptic acetylcholine receptor aggregation at the neuromuscular junction[88]. Collagen XVIII is highly expressed in basement membranes and is known to regulate angiogenesis[66].

Fibrous proteins

Collagens

Collagens are the most abundant group of proteins in the ECM. They have an unusual amino acid composition characterized by the presence of glycine-X-Y triple repeats, where X and Y represents any amino acid. Collagens are synthesized as α chains that combine to form a triple helix in the endoplasmic reticulum (ER). There are 28 known types of collagen, denoted by Roman numerals, and many of them include several different α chain isoforms. Over 40 distinct collagen α chains have been identified in humans and each triple helix can consist of three identical α chains or combinations of different α chains of the same collagen type. The glycine-X-Y triple repeat structure is essential for formation of the triple helix. Another distinguishing feature of collagens is the presence of hydroxyproline and hydrolysine. Prolines and lysines in the α chains are subjected to post-translational hydroxylation in the ER. This modification is crucial for formation of a stable tripe helix structure and for the lysyl oxidase-dependent crosslinking between mature triple helices that eventually takes place in the extracellular space during collagen fibrillogenesis. Following triple helix formation in the ER, additional post-translational modifications are made in the Golgi apparatus before secretion. Although all collagens contain at least one domain with glycine-X-Y triple

repeats (also known as a collagenous domain), not all collagens form fibrils. The fibril-forming collagens include collagen I, II, III, V, XI, XXIV and XXVII, but many collagens form other types of structures. Collagen IV is a network-forming collagen and one of the main components of basement membranes[89]. Fibril-associated collagens with interrupted triple helices (FACITs) associate with fibril-forming collagens without forming fibrils themselves, and include collagen IX, XII, XIV, XVI, XIX, XX, XXI and XXII. Collagen VI form beaded microfibrils that link connective tissue cells to the ECM[90]. In summary, collagens show considerable structural diversity due to a large variety of different collagen types and α chain isoforms, different post-translational modifications and alternative splicing. Consequently, collagens can form a multitude of suprastructures tailored to the specific needs of different tissues.[4,64]

Elastin

Elastic fibers impart elasticity to organs and tissues that require a lot of flexibility and are subjected to stretch, such as lungs, arteries and skin. Elastin is the main component of mature elastic fibers, but fibrillin-containing microfibrils are also present in the periphery of the fibers in association with other glycoproteins. Elastin is encoded by a single gene and secreted from the cells as tropoelastin monomers, which are then assembled into elastic fibers by extensive crosslinking catalyzed by lysyl oxidases. Modified lysine residues in lysine-rich regions of the protein form covalent desmosine and isodesmosine crosslinks, which are unique for elastic fibers. Alternating with the lysine-rich regions are stretches of hydrophobic amino acids that are essential for the elastic recoil properties of elastin. Elastic fibers are mainly produced during the embryological and neonatal periods, with minimal synthesis during adulthood, and the turnover of elastin is extremely low in the adult individual. Low solubility and high resistance to proteolytic degradation make elastic fibers resilient, but once they are degraded, for example by elastolytic proteases, they are unlikely to be properly replaced by new elastic fibers.[91,92]

Fibronectin

FN is a ubiquitously expressed ECM glycoprotein that is important for regulation of cell adhesion and migration, development and tissue repair. It is encoded by a single gene, but there are 20 isoforms of the protein because of alternative splicing and various post-translational modifications. FN has binding sites for a wide range of ECM proteins, many of which depend on FN for their own assembly, including collagens, fibrillin, fibulin and latent TGF-β-binding protein. Assembly of FN fibrils in the ECM requires direct interaction between soluble FN and integrin receptors. Several integrins can trigger formation of FN fibrils, but integrin $\alpha_5\beta_1$ is of particular importance. Binding of integrin $\alpha_5\beta_1$ to soluble FN activates intracellular signaling cascades in the integrin-expressing cell, which leads to reorganization of its actin cytoskeleton and increased cell contractility. This generates traction forces that will extend the integrin-

bound FN and expose cryptic sites that need to be exposed to allow additional FN molecules to bind. This process continues and leads to successive incorporation of soluble FN into growing, insoluble FN fibrils.[93,94]

Basement membranes

All epithelial and endothelial cells grow on thin sheets of specialized ECM known as basement membranes, which also surrounds muscle cells, adipocytes and peripheral nerves[95]. Basement membranes maintain the integrity of epithelial and endothelial linings by keeping them separated from the underlying connective tissue. They store growth factors and regulate transport of molecules and migration of cells. In the lungs, basement membranes are an integral part of the blood-air barrier by providing an interface between alveolar epithelial cells and capillary endothelial cells. Laminins, collagen IV, HSPGs (perlecan, collagen XVIII and/or agrin) and nidogens are core components of all basement membranes (fig. 2). Two separate polymer networks are formed by laminins and collagen IV, respectively, and these are interconnected by nidogens[96,97]. Apart from the core components, additional ECM proteins are also found in basement membranes, such as fibulins, SLRPs, vitronectin and growth factors[98]. The tissue-specific nature of basement membranes partially stems from the varying presence of such additional ECM proteins, but the tissue specificity is also highly dictated by expression of different laminin isoforms[95].

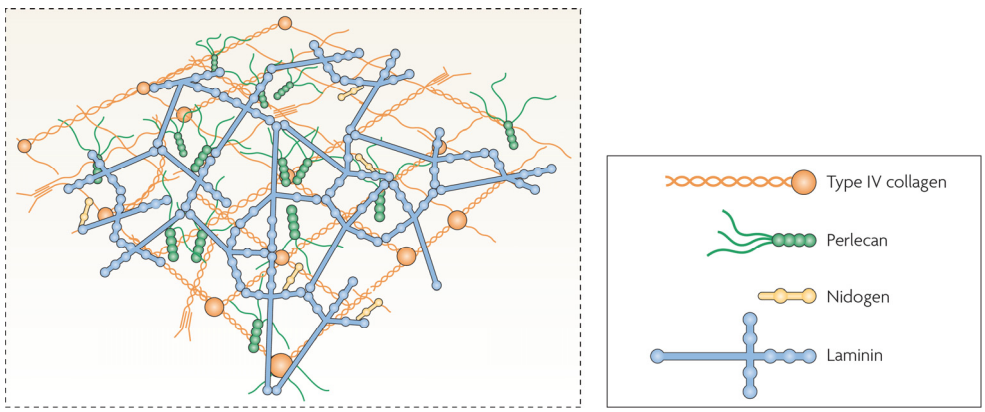

Figure 2. The basic structure of basement membranes. Adapted by permission from Springer Nature Customer Service Centre GmbH: Sorokin, L, The impact of the extracellular matrix on inflammation, Nature Reviews Immunology, volume 10, pages 712–723 (2010); DOI: 10.1038/nri2852.

Laminins

Laminins are large, heterotrimeric glycoproteins that are predominantly expressed in basement membranes, and they are crucial for anchoring of cells to the ECM. Each

heterotrimer consists of one α, one β and one γ chain. In mammals, five α chains, four β chains and three γ chains have been identified[96] and 18 laminin heterotrimers have so far been described[99]. Laminin nomenclature identifies each heterotrimer based on the names of its constituent chains, e.g. the laminin α5, β2 and γ1 chains form laminin-521[100]. The three chains are joined together via their C-terminal regions in a triple helical coiled-coil domain, creating a long, rod-shaped C-terminal arm. However, the N-terminal regions of the three chains are not bound to each other, which creates a cross-shaped structure with three short arms that are represented by the N-terminal regions of each chain. The complete structure of a laminin heterotrimer therefore includes four separate arms arranged in a cruciform shape (fig. 2), which makes laminins well adapted for interacting simultaneously with cell surface receptors, adjacent laminins and other ECM molecules. Laminins are assembled by a polymerization process where the heterotrimers bind to each other via their N-terminal domains[99]. The assembly is dependent on interaction with cell surface receptors, primarily integrins and dystroglycan, which bind to globular domains in the C-terminal end of the α chains[96]. The tissue dependent expression of laminins is mostly defined by varying expression of different α chain isoforms. Laminin γ1 has a broad expression pattern, whereas expression of the γ2 and γ3 chains is restricted to certain tissues. Examples of laminin subtypes that are expressed in lungs include laminin-521, laminin-511 and laminin-332[95,99].

Collagen IV

Collagen IV is a principal constituent of all basement membranes. There are six distinct collagen IV α chains that form three heterotrimers: α1α1α2, α3α4α5 and α5α5α6. Each collagen IV α chain is made up of a long collagenous domain, but also contains a cysteine/lysine-rich N-terminal domain (7S) and a non-collagenous C-terminal domain (NC1). The α chains can bind to each other via both the 7S and NC1 domains and then assemble to form the type of suprastructure that is characteristic of collagen IV, i.e. sheet-like, polygonal networks that associate with other molecules in the basement membrane (fig. 2). The α1α1α2 heterotrimer is expressed in all tissues, while α3α4α5 and α5α5α6 have a more restricted expression pattern. Mice that lack the α1 and α2 chains of collagen IV show normal basement membrane formation during early embryonic development, but die around embryonic day 11 due to structural deficiencies in their basement membranes.[89,101]

Perlecan

Perlecan is a large HSPG with a broad functional spectrum. It is abundantly expressed in basement membranes where it modulates cell adhesion, epithelial cell polarization and growth factor retention. The third domain of perlecan shows homology to laminin α chains and is likely involved in cell adhesion, and perlecan binds to both integrin β1[102] and the dystroglycan receptor[103]. In addition, its ability to interact with both

laminins and collagen IV[104] likely contributes to increased basement membrane stability. Perlecan regulates vascular function and promotes angiogenesis via its N-terminal HS chains, which can bind and present vascular endothelial growth factor A and FGFs to their cognate receptors. In contrast, its C-terminal domain, which can be proteolytically cleaved, has anti-angiogenic properties and inhibits endothelial cell motility by acting as an antagonist against both vascular endothelial growth factor receptor 2 and integrin $\alpha_2\beta_1$. Perlecan is also an important component of cartilage and has been implicated in lipid metabolism and autophagy.[105]

Nidogens

Nidogens are a family of sulfated glycoproteins that are highly expressed in basement membranes and include two members, nidogen-1 and nidogen-2. Nidogens stabilize basement membranes by interacting with laminins, collagen IV and perlecan. Knockout studies in mice have shown that loss of either nidogen gene has no pronounced effect on basement membrane formation or organ development, suggesting complementary functions of the two isoforms. However, mice that lack both nidogen isoforms die perinatally and show abnormal basement membrane formation, but only in certain organs, indicating that nidogens are not essential for assembly of all basement membranes. Loss of both nidogens had severe effects on late stage lung development, which was attributed to structural basement membrane deficiencies.[97]

Interactions between cells and extracellular matrix

The ECM can exert its influence on cell function by modulating the activity of cell surface receptors. Epithelial cell-ECM interactions are particularly important during wound healing when ECM proteins such as laminins and FN stimulate epithelial cell migration and spreading onto the provisional ECM[106]. In addition, polarization of epithelial cells depends on interaction with basement membranes, which leads to activation of signal transduction pathways and cytoskeletal rearrangement. Finally, cells also modify their extracellular environment by deposition of new ECM molecules[107], and this interplay between cells and ECM is important for tissue homeostasis.

Integrins

Integrins are heterodimeric transmembrane receptors that include one α and one β chain. Currently, 18 α chains and 8 β chains are known, and 24 heterodimers have been identified. Each chain contains a large, extracellular N-terminal domain, a single transmembrane domain and an intracellular C-terminal tail that is generally short. Integrins regulate cytoskeletal assembly and modulate signal transduction pathways that influence migration, survival, adhesion and proliferation of cells. Their main binding partners in the ECM are laminins, collagens and FN, but integrins also form

connections with adjacent cells by binding to cell surface receptors such as vascular cell adhesion molecule 1 and members of the intercellular adhesion molecule family.[108]

Activation of integrins by extracellular ligands requires integrin clustering, which is facilitated by their interactions with ECM proteins such as laminins. Binding of ligands to the extracellular domains of integrins leads to separation of the cytoplasmic tails of the α and β chains, which will allow the β chain to bind the cytoplasmic protein talin. Talin is a key protein since it provides a bridge between the cytoplasmic tail of β integrins and the actin cytoskeleton. A multitude of kinases, signaling proteins and adaptor proteins are then recruited to form a focal adhesion complex. The focal adhesion complex has two main functions. Firstly, it establishes a mechanical connection between the ECM and the actin cytoskeleton of the cell. Secondly, it induces activation of signal transduction pathways. Formation and activation of the focal adhesion complex lead to extensive cytoskeletal rearrangement. In addition, there will be significant crosstalk between the integrin-activated signal transduction cascade and growth factor signaling pathways, for example the Ras–MEK–MAP kinase and PI3 kinase/Akt kinase pathways. This kind of crosstalk is essential for anchorage-dependent growth of adherent cells, which depend on signals mediated by both integrins and growth factors for their survival.[108,109]

A characteristic feature of integrins is their ability to mediate bidirectional signaling. The integrin signaling mechanism described above is called outside-in signaling. However, in some cell types integrin signaling can also be triggered intracellularly. When this happens, talin is first released from an autoinhibitory conformation, which makes it available to bind the cytoplasmic integrin β tails. This interaction leads to separation of the α and β tails of the integrin heterodimer, which makes the extracellular domains switch from an inactive, low-affinity state into an active, high-affinity state. This type of integrin signaling is referred to as inside-out signaling and is primarily seen in non-adherent cells such as leukocytes and thrombocytes, which need to be able to quickly adhere during extravasation and coagulation, respectively.[108,109]

Non-integrin ECM receptors

Although integrins play a major role in cell-ECM interactions, several other ECM receptors also exist. Dystroglycan is a glycosylated laminin receptor that consists of a transmembrane β subunit bound to an extracellular α subunit. It is expressed in human airway epithelial cells, has been shown to regulate wound repair and can interact with perlecan, agrin and laminins via its carbohydrate chains[110,111]. Basal cell adhesion molecule/Lutheran blood group glycoprotein is a laminin receptor that belongs to the immunoglobulin superfamily and binds exclusively to laminin α5[112]. The 67 kDa laminin receptor promotes cell adhesion to basement membranes and has been implicated in metastatic cancer[113]. Sulfatides are sulfated glycolipids that also bind laminins, and they are particularly abundant in the brain[114]. CD44 is the main receptor

for HA, but also binds other ligands such as collagens, MMPs and the ECM protein osteopontin[115]. The CD44-HA interaction is known to promote signaling related to tumor progression[116]. Finally, discoidin domain receptor 1 (DDR1) and 2 (DDR2) are receptor tyrosine kinases that are activated by collagen and regulates ECM remodeling by upregulation of MMPs[117]. Also, DDR1 regulates collagen IV production[118], modulates E-cadherin-mediated cell aggregation[119] and promotes epithelial repair and MMP7 production in bronchial epithelial cells[120].

Extracellular matrix remodeling in COPD lungs

Remodeling of the pulmonary ECM in COPD (fig. 3) involves both large and small airways as well as the lung parenchyma. Several studies have presented quantitative differences in collagen deposition between patients and controls. Annoni et al. showed that collagen I is decreased in the airways of COPD patients compared to non-smokers[121], whereas results presented by Kranenburg et al. demonstrate increased abundance of collagen I and III in COPD airways[122]. Hogg et al. investigated collagen content in bronchioles in COPD lungs at different GOLD stages and found that the total amount of collagen increased between GOLD stage I and II, followed by a sharp decline at GOLD stage IV[123]. Meanwhile, the relative amount of collagen I and III in GOLD stage IV lungs was higher than in lungs from control subjects, indicating that the collagen composition is altered in lungs from patients with severe COPD.

Moreover, increased expression of FN, tenascin[121] and HA[16] has been reported in COPD airways, and reduced peribronchiolar expression of decorin and biglycan has

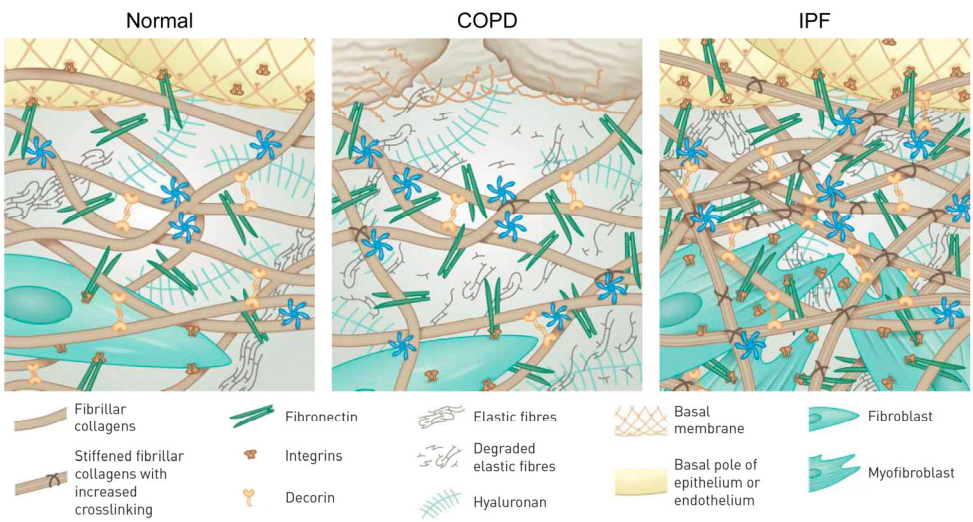

Figure 3. Extracellular matrix in normal lungs, COPD lungs and IPF lungs. Reproduced with permission of the © ERS 2018, European Respiratory Journal Jul 2017, 50 (1) 1601805; DOI: 10.1183/13993003.01805-2016.

been observed in lungs from patients with severe emphysema[124], which could have implications for collagen fibrillogenesis[125]. Versican content is increased in alveolar walls of COPD lungs[126] and fibroblasts isolated from distal airways of COPD patients show increased deposition of versican[127]. Of note, versican in COPD lungs is also negatively correlated with both FEV_1 and elastic fiber content[126], which could be a reflection of versican-mediated disruption of elastic fiber assembly. Elastin-binding protein plays an important role as a molecular chaperone during secretion of tropoelastin, and polysaccharides like CS and DS are known to suppress formation of elastic fibers[128,129], likely by disrupting the interaction between elastin-binding protein and tropoelastin. Since versican is a CS/DS proteoglycan, it has therefore been suggested that increased deposition of versican might contribute to aberrant elastic fiber formation in COPD lungs.

Degradation of elastic fibers is one of the hallmarks of COPD pathology and several studies have reported that COPD lungs have reduced levels of elastin or elastic fibers[16,130]. Chronic infiltration of leukocytes such as neutrophils and macrophages in COPD lungs leads to increased secretion of neutrophil elastase, MMP12 and other elastolytic enzymes, which causes elastic fiber degradation[131,132].

Extracellular matrix remodeling in IPF lungs

IPF lungs are subjected to substantial interstitial remodeling (fig. 3). The exaggerated ECM deposition characteristic of IPF is a consequence of hyperproliferation of fibroblasts and their differentiation into highly contractile myofibroblasts that produce large amounts of ECM components such as fibrillar collagens, fibronectin, proteoglycans and tenascin[24,133]. Experiments using atomic force microscopy have shown that IPF lung tissue is stiffer than normal lung tissue, both before and after decellularization[134]. This could be explained by increased ECM crosslinking catalyzed by lysyl oxidase and transglutaminase 2, as they are both increased in IPF lungs[135,136]. Intriguingly, fibroblasts assume a more pro-fibrotic phenotype and show increased ECM production when grown on a stiffer matrix, suggesting that mechanical properties of the ECM contribute to IPF pathogenesis by modulating cell function[134,137,138]. Indeed, another study showed that matrix stiffness acts in synergy with TGF-β1 to enhance expression of collagen I in human fibroblasts in a manner that depends on focal adhesion kinase/Akt signaling, and this effect was stronger in fibroblasts from IPF patients compared to controls[139].

Periostin is a pro-fibrotic ECM protein that has been shown to be increased in IPF lungs, and its expression was localized to fibroblastic foci[140]. The same study also showed that plasma levels of periostin in IPF patients are predictive of disease progression. Moreover, the hexameric ECM glycoprotein tenascin-C, which is involved in tissue repair, show increased expression in IPF lungs with pronounced deposition in

fibroblastic foci together with versican[141]. Fibroblastic foci display a light color in hematoxylin/eosin stainings and contain deposits of newly synthesized, immature collagen. Histologically, fibroblastic foci look like small and fairly uniform lesions in the IPF lung interstitium, but they actually have a heterogeneous and complex morphology and show large variation in size and shape, as has been shown by micro-computed tomography[142].

The HSPGs syndecan-1 and syndecan-2 also show increased expression in IPF lungs[143,144], while syndecan-4 has been shown to have anti-fibrotic properties in an in vivo model of pulmonary fibrosis[145]. Finally, HA is implicated in tissue injury[146] and increased levels of HA have been reported in bronchoalveolar lavage fluid from IPF patients[147]. Targeted overexpression of the HA-synthesizing enzyme hyaluronan synthase 2 in myofibroblasts also leads to enhanced pulmonary fibrosis in mice[148], suggesting that HA may contribute to the pathophysiology of IPF.

Aims

The overall objective of this thesis was to investigate how airway epithelial cell phenotype is modulated by an aberrant bronchial ECM in COPD and to study pathological alterations in the pulmonary ECM in COPD and IPF.

The specific aims of the studies included in this thesis were:

- To develop an ex vivo model for repopulating decellularized human bronchial scaffolds with primary normal human bronchial epithelial cells and study the cell phenotype after repopulation and differentiation on COPD and normal bronchial scaffolds (paper I).
- To study how epithelial cell phenotype in COPD airways is modulated by the relative influence from airway epithelial cells and bronchial ECM, and to study extracellular matrix alterations in bronchial airways of COPD patients (paper II).
- To quantify and study tissue distribution and fine structure of glycosaminoglycans in IPF lungs (paper III).
- To quantify and study tissue distribution of extracellular matrix proteins in COPD and IPF lungs (paper IV).

Methodology

This chapter provides an overview of the most important methods used in this thesis. Detailed descriptions of all materials and methods can be found in paper I-IV.

Human lungs

Lungs from healthy individuals and from patients with severe COPD (GOLD stage IV) or IPF were acquired from Sahlgrenska University Hospital in Gothenburg and Skåne University Hospital in Lund. The studies were approved by the Swedish Research Ethical Committees in Gothenburg and Lund and informed consent was obtained from all subjects or their closest relatives.

Decellularization

Bronchial airways were dissected from the lungs and frozen in liquid nitrogen. The frozen airways were cut into 500 µm thick cryosections, which were immediately placed in phosphate-buffered saline (PBS) at room temperature (RT). Any remaining parenchyma was removed and decellularization was performed by treating the sections with the following solutions: 4% (w/v) sodium deoxycholate (Sigma-Aldrich) for 2.5 hours, Hank's Balanced Salt Solution for 3x5 min, 1000 Kunitz units/ml of deoxyribonuclease I (DNase I) (Sigma-Aldrich D4527) with 0.5 mM $CaCl_2$ for 60 min and PBS for 3x5 min. All decellularization steps were done at RT on an orbital shaker set to 170 rpm, except the DNase I incubation, which was done at 37°C without agitation. The decellularized scaffolds were stored in PBS at 4˚C for up to 2 days before being used for repopulation. All PBS used during sectioning and decellularization had been supplemented with 50 U/ml penicillin, 50 µg/ml streptomycin, 50 µg/ml gentamicin and 2 µg/ml amphotericin B.

Quantification of DNA, sulfated glycosaminoglycans and elastin

Non-decellularized and decellularized bronchial airway tissue was dried at 50°C for 2.5 hours, followed by weighing, before extraction of DNA, GAGs or elastin. DNA was extracted using the DNeasy Blood & Tissue Kit (Qiagen 69504) and quantified using the Quant-iT PicoGreen dsDNA Assay Kit (Thermo Fisher P11496). Sulfated GAGs and soluble α-elastin were extracted and quantified using the Blyscan Sulfated GAG (Biocolor B1000) and Fastin (Biocolor F2000) Assay Kits, respectively. DNA, sulfated GAG and α-elastin concentrations in the extracts were normalized against dry tissue weight.

Cell culture, repopulation and differentiation

Paper I

Primary HBEC from a healthy donor were purchased from Lonza and cultured in Bronchial Epithelial Cell Growth Medium (BEGM) (Lonza CC-3170) before being frozen in passage 2. The cells were thawed and cultured in BEGM for 6 days with a medium change every 2-3 days. On the day of repopulation, the cells had a confluence of ~90% and they were detached using StemPro Accutase Cell Dissociation Reagent (Thermo Fisher). Decellularized scaffolds from COPD patients and healthy donors (n=3) were carefully placed on top of sterile polycarbonate Whatman filters (Sigma-Aldrich WHA110614), which were transferred to 6-well plates filled with BEGM, allowing them to float on the medium surface. The HBEC were carefully dispensed on top of the scaffolds, which were then incubated with the cells at 37°C. On the next day, 75% of the medium in each well was replaced with fresh BEGM. Differentiation was induced four days after the addition of cells to the scaffolds by exchanging the BEGM for a differentiation medium. The day of differentiation induction was defined as day 0. The differentiation medium was composed of 50% (v/v) BEGM Stock Solution, 50% (v/v) Dulbecco's Modified Eagle's Medium (DMEM) (Thermo Fisher 41965) Stock Solution and 0.05 µM retinoic acid (Sigma-Aldrich R2625). The DMEM Stock Solution had previously been supplemented with 1 mM sodium pyruvate, 2 mM L-glutamine and Minimal Essential Medium Non-Essential Amino Acids Solution (Thermo Fisher) at working concentration. All the included BEGM supplements had been added to the BEGM Stock Solution at two times the working concentration except for retinoic acid, which had been omitted. The scaffolds were cultured with differentiation medium for up to 35 days with a medium change every 2-3 days. New

differentiation medium with freshly added retinoic acid was prepared from the BEGM and DMEM Stock Solutions before each medium change. Repopulated scaffolds were collected at different time points. For histology, TUNEL (TdT-mediated dUTP Nick-End Labeling) staining and immunohistochemistry (IHC), scaffolds (n=3) were fixed in 4% formaldehyde for 20-24 hours at RT. Scaffolds designated for RNA sequencing (RNA-Seq) (n=3) were snap frozen in liquid nitrogen and stored at -80˚C. The experimental design for RNA-Seq and IHC is visualized in fig. 4.

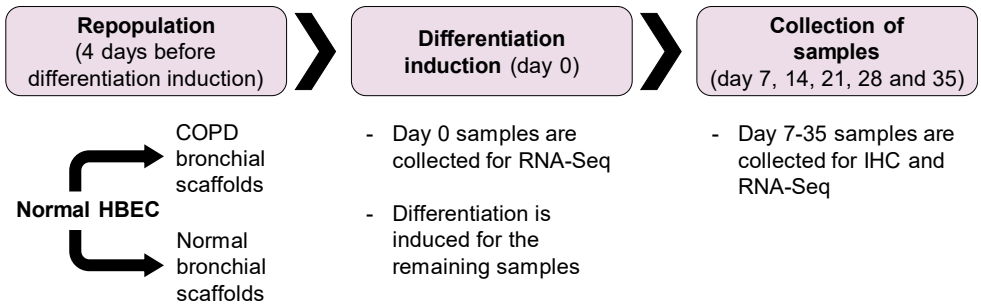

Figure 4. Experimental design for RNA sequencing (RNA-Seq) and immunohistochemistry (IHC) in paper I. Human bronchial epithelial cells (HBEC) from a healthy donor were seeded on decellularized bronchial scaffolds derived from COPD patients and healthy individuals (n=3). Differentiation was induced 4 days after seeding of cells (defined as day 0) and proceeded for 35 days.

Paper II

Isolation of human bronchial epithelial cells

Bronchial epithelial cells were isolated from bronchial airways dissected from COPD and healthy lungs. The airways were cut into shorter segments, which were incubated overnight at 4°C in S-MEM medium (Thermo Fisher) supplemented with 1 mg/ml protease (Sigma-Aldrich P5147), 50 U/ml penicillin, 50 µg/ml streptomycin, 50 µg/ml geneticin and 2 µg/ml amphotericin B. The airways were longitudinally cut to expose the mucosa, which was thoroughly scraped to detach epithelial cells. Cells were collected in DMEM medium (Thermo Fisher 31966) supplemented with 10% fetal bovine serum and the same antibiotics/antimycotics as the S-MEM medium. The suspension was filtered through a cell strainer, followed by incubation with deoxyribonuclease I (DNase I) (Sigma-Aldrich D4527) for 20 min at 37°C. Cells were centrifuged, resuspended in BEGM (Lonza CC-3170), and seeded in T75 cell culture flasks, followed by expansion and freezing.

Repopulation

Repopulation was performed as described for paper I, except the cells were in PneumaCult-Ex medium (Stemcell Technologies 05008) when seeded on the bronchial scaffolds and PneumaCult-ALI medium (Stemcell Technologies 05001) during the differentiation phase. COPD and normal HBEC (n=3) were repopulated on COPD and normal bronchial scaffolds (n=3). The cells were also seeded in transwell plates coated with bovine collagen I (Advanced Biomatrix), for culture at the air-liquid interface (ALI). The apical medium was removed on day 0 and the basolateral PneumaCult-Ex medium was exchanged for the PneumaCult-ALI medium. Repopulated scaffolds designated for RNA-Seq and protein extraction were collected and frozen in liquid nitrogen followed by storage at -80°C and repopulated scaffolds for histology were fixed in 4 % formaldehyde for 20-24 hours at RT. ALI cultures were lysed in RLT buffer (Qiagen), followed by freezing in liquid nitrogen and storage at -80°C. Day 0 was defined as the day of differentiation induction, i.e. when the PneumaCult-Ex medium was exchanged for the PneumaCult-ALI medium. The experimental design for the RNA-Seq study is visualized in fig. 5.

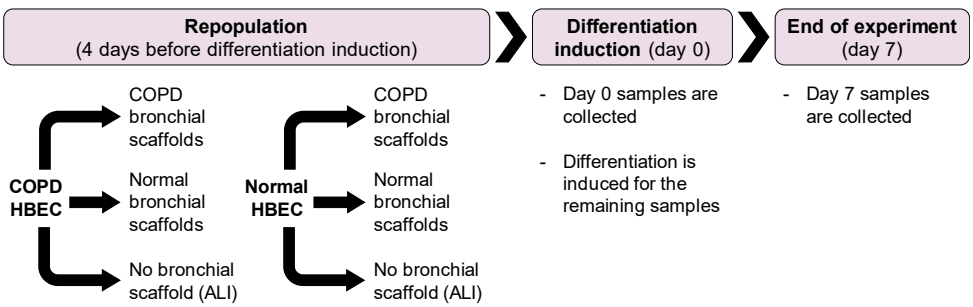

Figure 5. Experimental design for RNA sequencing in paper II. COPD and normal human bronchial epithelial cells (HBEC) (n=3) were seeded on decellularized bronchial scaffolds derived from COPD patients and healthy individuals (n=3) and in transwell plates for culture at the air-liquid interface (ALI). Samples were collected on the day of differentiation induction and after 7 days of differentiation.

Immunohistochemistry and histology

All antibodies used for IHC and their concentrations are described in detail in paper I, III and IV.

Paper I

Fixed bronchial scaffolds were embedded in histogel (Thermo Fisher) and dehydrated in ethanol and xylene, followed by paraffin embedding and sectioning. Before staining,

the tissue sections were deparaffinized in xylene and rehydrated in ethanol followed by deionized water. Different epitope retrieval methods were chosen based on the primary antibody. Heat-induced epitope retrieval was done in citrate (pH 6) buffer (collagen IV, FOXJ1, MUC5AC, Ki-67, ZO-1) or Tris/EDTA (pH 9) buffer (p63). Epitope retrieval with proteinase K was done for 15 min at 37°C (laminin) and with heparinase III overnight at RT (perlecan). Endogenous peroxidase activity was blocked with 1% hydrogen peroxide in methanol for 30 min, followed by blocking of endogenous biotin using a streptavidin/biotin blocking kit (Vector Laboratories). After blocking with 5% normal goat serum, 1% BSA and 0.05% Tween-20 for 30 min, the sections were incubated with the primary antibody overnight at 4°C. Mouse IgG isotype antibodies or rabbit Ig fraction were used as negative controls. The sections were then incubated with biotinylated secondary goat anti-mouse or anti-rabbit IgG (Vector Laboratories) for 1 h at RT. Following incubation with the avidin/biotin-based peroxidase complex Vectastain Elite ABC (Vector Laboratories), the sections were developed with the peroxidase substrate NovaRED (Vector Laboratories). Masson's trichrome staining was performed using a Masson's Trichrome Stain Kit (Sigma-Aldrich). Standard protocols were used for hematoxylin/eosin staining and alcian blue-periodic acid Schiff (AB-PAS) staining. Finally, the sections were counterstained with Mayer's hematoxylin, dehydrated in ethanol and xylene, and mounted with Pertex mounting medium. All antibodies were diluted in blocking buffer. Unless otherwise stated, all staining steps were done at RT.

Paper III

Cryosections of peripheral lung tissue from healthy donors (n=3) and IPF patients (n=4) were air-dried and rehydrated. For A04B08V stainings, endogenous peroxidase activity was blocked with 1% hydrogen peroxide in methanol for 30 min, followed by blocking of endogenous biotin using a streptavidin/biotin blocking kit (Vector Laboratories). After blocking with 1% BSA and 0.05% Tween-20 for 20 min, the tissue sections were incubated for 1 h at RT with a 1:10 dilution of the phage display-derived antibody fragment A04B08V. This step was followed by incubation with a 1:800 dilution of mouse anti-VSV-G antibody (clone P5D4) (Sigma-Aldrich) at RT for 1 h. The sections were then fixed in 4% formalin for 30 min and incubated with a biotinylated goat anti-mouse IgG antibody (Vector Laboratories) at RT for 1 h. Following incubation with the avidin/biotin-based peroxidase complex Vectastain Elite ABC (Vector Laboratories), the sections were developed with the peroxidase substrate NovaRED (Vector Laboratories). The sections were counterstained with Mayer's hematoxylin (Sigma-Aldrich), dehydrated and mounted with Pertex mounting medium. To verify the specificity of the stainings, the tissue sections were pre-treated overnight at 37◦C with a combination of heparinase I, II and III, each at 0.1 IU/ml.

For heparan sulfate and perlecan stainings, the sections were fixed in formalin immediately after air-drying and incubated with the primary antibody at 10 µg/ml (anti-heparan sulfate, 10E4 epitope, AMS Biotechnology) or 0.5 µg/ml (anti-perlecan, 7B5 clone, Thermo Fisher) for 2 h at RT, followed by incubation with a biotinylated goat anti-mouse IgG antibody and development according to procedures described above for A04B08V. The specificity of the anti-heparan sulfate antibody was verified by pre-treatment with heparinase I, II and III as described for A04B08V. For the anti-perlecan antibody, a mouse IgG1 isotype antibody was used as a negative control and the sections were pre-treated with heparinase for epitope retrieval. Sequential tissue sections were collected to be able to compare the staining patterns for A04B08V, 10E4 and perlecan in the same tissue regions.

Paper IV

Tissue sections were made from paraffin-embedded peripheral lung tissue from IPF patients, COPD patients and healthy donors (n=2). IHC staining was performed as described for paper I. Heat-induced epitope retrieval was done in citrate (pH 6) buffer (Agilent Technologies). An anti-asporin antibody (rabbit) (Sigma-Aldrich HPA024230) was used at 0.25 µg/ml and rabbit Ig fraction (Agilent Technologies) was used as a negative control.

Reversed-phase high-performance liquid chromatography

This analysis was performed by Annika Nybom and Oskar Hallgren.

Glycosaminoglycan isolation and digestion

Lyophilized and weighed tissue samples were incubated overnight with pronase and then with benzonase for 2 h to degrade polypeptides and DNA. Next, GAGs were purified on an anion spin column and desalted using spin columns with a cut-off size of 3 kDa by repeated addition of water. Sample amounts that corresponded to 0.3 mg of the initial dry tissue were used for each digestion. To generate disaccharides from chondroitin sulfate, dermatan sulfate and hyaluronic acid, GAGs were subjected to chondroitinase ABC degradation (10 mU) overnight. To degrade HS, the samples were incubated overnight with a mixture of heparinase I, II and III (10 mU of each).

Glycosaminoglycan disaccharide analysis

Disaccharide analysis was performed as previously described[149]. Briefly, fluorophore-labelling of the disaccharides was performed by adding 10 µl of 20 mM re-purified 2-aminoacridone (AMAC) to lyophilized samples, followed by a 20 min incubation at RT before the addition of 10 µl of 1 M $NaBH_3CN$ and incubation at 45◦C for 16 h. AMAC-labelled disaccharides were analyzed with reversed-phase high-performance liquid chromatography (RP-HPLC)-fluorescence on an X-Bridge BEH Shield RP18 (2.1 × 100 mm, 2.5 µm) column connected to a Thermo ScientificUltiMate 3000 Quaternary Analytical system with an FLD-3400RS fluorescence detector (excitation λ = 428 and emission λ = 525) set at 30◦C. 20 µl samples were diluted five-fold in running buffer (98% A: 60 mM NH_4OAc (pH 5.6) and 2% B: MeCN) and 2 µl were injected onto the column. Disaccharides were separated using a 39 min gradient run at 0.35 ml/min (0–1 min: 98% A, 1–3 min: 98–96% A, 3–26 min: 96–85% A, 26–28 min: 85–10% A, 28–32 min: 10% A, 32–34 min: 10–98% A, 34–39 min: 98% A). Quantification was done by comparison to known weights of standard disaccharides (Iduron), mock-treated in the same buffers and enzymes as the samples in each series of runs.

Image analysis

All IHC stained sections from repopulated scaffolds were scanned at 20 times magnification using a Zeiss Axio Scan.Z2 scanner. The virtual slides were imported into the Visiopharm Integrator System 6.0 software. Regions of interest in each tissue section were defined manually. All cells seen on the luminal side of each repopulated scaffold section were included in the image analysis. Counterstaining with hematoxylin allowed for counting of the total number of cells. The fraction of positive cells for each marker was calculated using Analysis Protocol Packages, which are protocols in the Visiopharm software that classify cells as positive or negative. At least 400 cells were counted per patient/donor and time point for each marker.

RNA sequencing

Repopulated bronchial scaffolds were disrupted and homogenized using a TissueLyser II bead mill (Qiagen) and RNA was extracted and isolated using the RNeasy 96 kit (Qiagen 74182), including on-column DNase I digestion. RNA integrity was evaluated on a 2100 Bioanalyzer system (Agilent Technologies) (paper I) or the Fragment Analyzer Automated CE platform (Advanced Analytical) (paper II) and quantification

was done using the Quant-iT RiboGreen RNA Assay Kit (Thermo Fisher R11490). RNA was diluted to 10 ng/µl (paper I) or 6 ng/µl (paper II) and used as input to create cDNA libraries using a TruSeq Stranded mRNA Library Preparation kit (Illumina RS-122-2103) with dual indexing following the manufacturer's instructions. Following validation on the Fragment Analyzer Automated CE platform (Advanced Analytical), the libraries were pooled in equimolar concentrations and diluted and denatured according to Illumina guidelines. RNA-Seq was performed using a High Output 1x76 bp kit on an Illumina NextSeq 500 platform. Experimental designs for the RNA-Seq studies in paper I and II are visualized in fig. 4 and 5, respectively.

Bioinformatic analysis

Paper I and II

RNA-Seq fastq files were processed using bcbio-nextgen (https://github.com/chapmanb/bcbio-nextgen), where reads were mapped to the human genome build hg38 (GRCh38.79) using hisat2 (version 2.0.5)[150], yielding between 5.3-20.6 M mapped reads (10.8 M on average) (paper I) and 7.3-15.8 M mapped reads (10.6 M on average) (paper II) with a ≥97% mapping frequency per sample. Gene level quantifications and counts were generated with featurecounts (version 1.4.4)[151] within bcbio-nextgen. ArrayStudio (OmicSoft) was used for further data analysis. Data for individual genes were plotted using log2-transformed DESeq2-normalized[152] counts. The scientific literature-based commercial software package Ingenuity Pathway Analysis (Qiagen) (https://www.qiagenbioinformatics.com/products/ingenuity-pathway-analysis) was used for upstream mediator analysis[153]. Drugs and non-endogenous chemicals were excluded from the analysis.

Paper II

Principal component analysis (PCA) was performed in ArrayStudio (OmicSoft). Gene ontology (GO) term enrichment search[154,155] was performed on the GO Consortium website (http://www.geneontology.org) against biological process annotations in the GO database (released 2018-04-04) and PANTHER (Protein Annotation Through Evolutionary Relationships) GO-slim database (version 13.1, released 2018-02-03)[156]. The reference list consisted of all GO-annotated genes detected in at least one RNA-Seq sample (17456 genes).

Enzyme-linked immunosorbent assay

Repopulated and non-repopulated bronchial scaffolds were disrupted and homogenized in RIPA lysis buffer (Thermo Fisher) with added protease inhibitors (Sigma-Aldrich) using a TissueLyser II bead mill (Qiagen). Following centrifugation, the protein concentrations in the supernatants were measured with the Pierce BCA protein assay kit (Thermo Fisher). Forkhead box J1 (FOXJ1) and beta-galactosidase (GLB1) were quantified using enzyme-linked immunosorbent assay (ELISA) kits for human FOXJ1 (Abbexa abx257844) and human GLB1 (Abbexa abx151616). FOXJ1 concentrations were normalized against GLB1 to account for varying numbers of cells on the scaffolds.

Mass spectrometry

For paper II, the mass spectrometry analysis was performed by the Proteomics Core Facility at Sahlgrenska Academy, Gothenburg University. For paper IV, the mass spectrometry analysis was performed by Emma Åhrman.

Paper II

Extraction, tryptic digestion and tandem mass tag labeling of proteins

Bronchial airways were dissected and decellularized as previously described[157], followed by freezing at -80°C. Samples were homogenized in lysis buffer (2% sodium dodecyl sulfate in 50 mM triethylammonium bicarbonate (TEAB)) and total protein concentration was determined, followed by processing using the filter-aided sample preparation method[158], as previously described[159]. Briefly, 30 µg of total protein from each sample were reduced with dithiothreitol, transferred to Nanosep 30k Omega filters (Pall Life Sciences), repeatedly washed using 8 M urea and alkylated with methyl methanethiosulfonate, followed by double digestion using trypsin at 37°C in digestion buffer (1% sodium deoxycholate and 50 mM TEAB). Samples were labeled using a 10-plex tandem isobaric mass tag (TMT) labeling kit (Thermo Fisher 90406), according to the manufacturer's instructions. Samples were combined and sodium deoxycholate was removed by acidification. The TMT-set was fractionated into 40 fractions using high pH reversed-phase chromatography (Waters XBridge BEH C18 3.0x150 mm, 3.5µm) with a gradient from 4% to 90% acetonitrile in 10 mM ammonium formate (pH 10.0) over 22 min, and concatenated into 20 fractions.

LC-MS/MS analysis and database search

Each fraction was analyzed on an Orbitrap Fusion Tribrid mass spectrometer (MS) as previously described[160], with some adjustments. Peptides were separated on a trap column (Thermo Fisher Acclaim Pepmap C18 100 µm x2 cm, 5 µm) together with an in-house packed C18 analytical column (75 µm x 32 cm, 3 µm) using an EASY-nanoLC 1200 system (Thermo Fisher) with a gradient from 4% to 80% acetonitrile in 0.2% formic acid over 80 min. MS scans were recorded at 120 000 resolution, the most intense precursor ions were selected (top speed of 3 seconds) for fragmentation (CID 35%) and MS and MS/MS spectra were recorded in ion trap with isolation window of 0.7 Da. Charge states 2 to 7 were selected for fragmentation and dynamic exclusion was set to 45 seconds with 10 ppm tolerance. The top 7 MS2 fragment ions were selected for MS3 fragmentation (HCD 60%) and detection in the Orbitrap at 50 000 resolution.

Data analysis was performed as previously described[160], using Proteome Discoverer version 2.2 (Thermo Fisher) and the Homo sapiens Swissprot database (20316 sequences). The precursor and fragment mass tolerance were set to 5 ppm and 0.6 Da. One missed cleavage was accepted, and variable modifications of methionine oxidation, fixed modifications of cysteine alkylation and TMT-labels at N-terminals and lysines were selected. Reporter ion intensities were quantified in MS3 spectra at 0.003 Da mass tolerance, using S/N threshold 19, and normalized against total protein abundance. Only values for unique peptides at a false discovery rate of 1% were used for quantification. One of the samples was used as denominator for calculation of relative abundances.

Paper IV

Protein extraction and MS sample preparation

Distal lung tissue was dissected from healthy donor lungs (n=5), COPD lungs (n=5) and dense and less dense regions of IPF lungs (n=6). The samples were homogenized with a FastPrep-96 instrument and proteins were consecutively extracted from the tissue into three separate fractions: soluble protein fraction, detergent-soluble protein fraction (labeled SDS fraction) and ECM-enriched fraction. The protein concentrations were determined with the Pierce BCA protein assay kit (Thermo Fisher). Samples representative of the soluble fraction and the SDS fraction from one healthy donor, one COPD patient and one IPF patient were separated on SDS-PAGE and digested in-gel as previously described[161], while samples representing the ECM-enriched fraction from the same subjects were prepared in solution; these samples were used for generation of the assay library. For samples to be analyzed in solution, standard protocols were used for reduction, alkylation, trypsin digestion and purification with

C18 reversed-phase spin columns prior to mass spectrometry analysis. Digested samples from the SDS fractions were cleaned up using SP3 beads[162].

LC-MS/MS analysis

LC-MS/MS analyses were performed on a Q-Exactive Plus mass spectrometer (Thermo Fisher). For the SDS-PAGE-separated protein samples, each lane was separated into 45 bands that were pooled into 10 MS injections. Peptides were separated on an EASY-nLC 1000 HPLC system (Thermo Fisher) connected to an EASY-Spray column (ID 75 μm×25 cm). The following gradient was used: 5% to 35% buffer B (0.1% formic acid, 100% acetonitrile) for 120 min, 35 to 95% buffer B for 5 min, and finally 95% buffer B for 10 min, at a flow rate of 300 nl/min. For data-dependent acquisition (DDA), full MS survey scans (resolution 70,000 at 200 m/z) at mass range 400–1600 m/z were followed by MS/MS scans (resolution 17,500 at 200 m/z) of the top 15 most intense ions. For data-independent acquisition (DIA), MS survey scans at mass range 400–1200 m/z were followed by 32 MS/MS full fragmentation scans with an isolation window of 26 m/z as previously described[161].

MS data analysis and assay library generation

MS searches were performed using the Trans-proteomic pipeline (TPP v4.7 POLAR VORTEX rev 0, build 201405161127) with peptideProphet, iProphet and MAYU[163-165]. The assay library used for DIA quantification was generated using spectraST, FDR calculations of 1% for peptide and protein were made with CLI and feature alignment was made with TRIC[166]. DIA data were analyzed using openSWATH[167], where the proteins were quantified by summing the intensities of their associated peptides. All data analyses were managed in openBIS[168]. Prior to statistical testing, protein abundances were normalized by dividing their intensities by the sum of all protein intensities per sample.

Results

Bronchial extracellular matrix from COPD patients induces altered gene expression in repopulated primary human bronchial epithelial cells (paper I)

In paper I, we aimed to investigate how global gene expression in normal HBEC is influenced by bronchial ECM derived from COPD patients. To this end, we developed an ex vivo model in which normal HBEC repopulate and differentiate on decellularized human bronchial scaffolds. We provided a comprehensive description of the model and presented results from global transcriptomic profiling in normal HBEC after repopulation on COPD or normal bronchial scaffolds followed by up to 35 days of differentiation.

Primary human bronchial epithelial cells differentiate into pseudostratified airway epithelium on decellularized bronchial scaffolds

The HBEC repopulated bronchial scaffolds from both healthy donors and COPD patients, and after 7 days of differentiation a continuous layer of cells was observed on the epithelial basement membrane (fig. 6, upper panel). Occasional cilia were present on the apical side of the repopulated epithelium on both normal and COPD scaffolds after 14 days of differentiation, but after 21 days the cilia had become more prominent (fig. 6, middle panel). At this point the cell layer had a more columnar morphology and an increased thickness compared to day 7. After 35 days of differentiation the cilia had increased in number and the epithelium had assumed a distinct pseudostratified morphology (fig. 6, lower panel).

Immunohistochemistry showed that the percentage of FOXJ1-positive and MUC5AC-positive cells increased over time on both COPD and normal bronchial scaffolds, demonstrating differentiation towards ciliated cells and goblet cells, respectively (fig. 7). This was accompanied by decreased expression of the basal cell marker p63 and the proliferation marker Ki-67, suggesting that basal cells differentiated into ciliated cells

and goblet cells on the bronchial scaffolds. There were no differences in expression of these markers in HBEC on COPD compared to normal bronchial scaffolds.

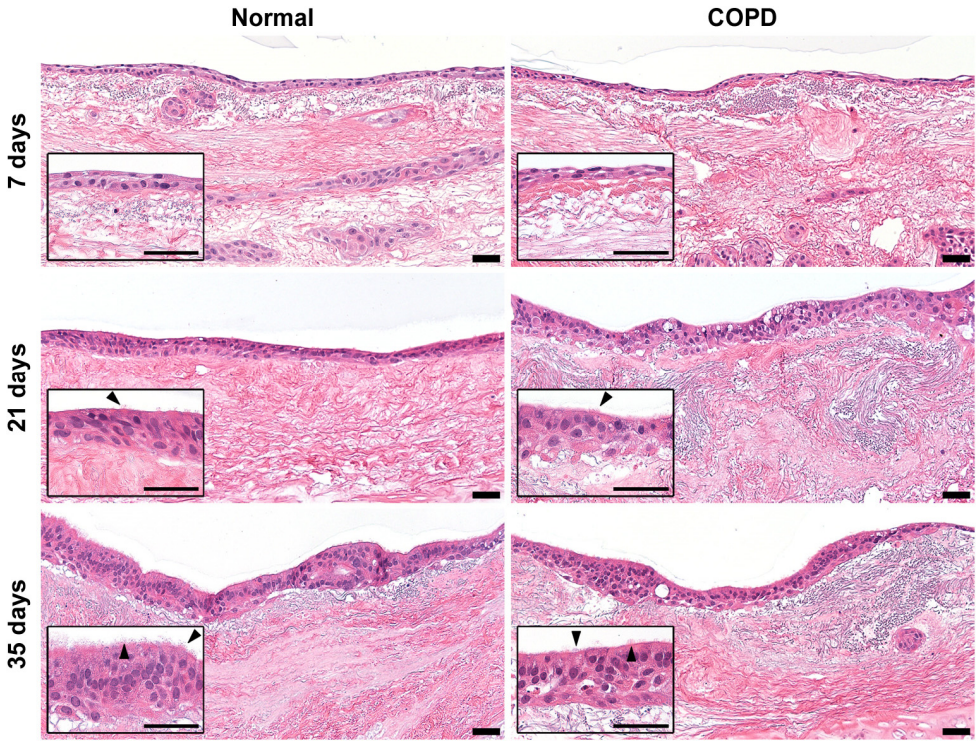

Figure 6. Normal HBEC develop cilia and assume a pseudostratified morphology on bronchial scaffolds from COPD patients and healthy individuals. Hematoxylin/eosin stainings of repopulated bronchial scaffolds after 7, 21 and 35 days of differentiation. Arrows: cilia. Scale bars: 50 µm.

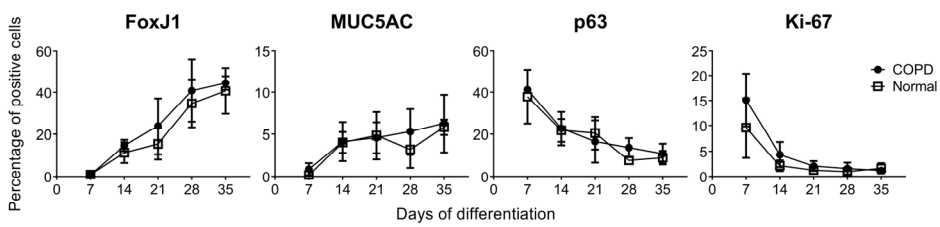

Figure 7. Normal HBEC differentiate into airway epithelium on bronchial scaffolds from COPD patients (circles) and healthy individuals (squares). Expression of FOXJ1 (ciliated cells), MUC5AC (goblet cells), p63 (basal cells) and Ki-67 (proliferation marker) based on image analysis of immunohistochemistry stainings of repopulated bronchial scaffolds. The number of positive cells for each marker was normalized against the total number of cells.

Bronchial ECM from COPD patients induces altered gene expression in repopulated human bronchial epithelial cells

RNA-Seq showed that a large number of genes were differentially expressed in HBEC on COPD compared to normal bronchial scaffolds with more pronounced differences early during differentiation. On day 0 (when the cells had been exposed to the scaffolds for 4 days), 2430 genes were differentially expressed, but after 7 and 14 days of differentiation that number had decreased to 701 and 256, respectively (fig. 8A-B). Later during differentiation (day 21-35), very few genes were differentially expressed.

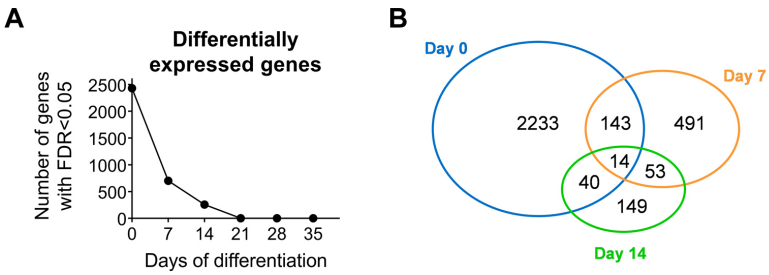

Figure 8. (**A**) Number and (**B**) overlap of differentially expressed genes in normal HBEC repopulated on COPD compared to normal bronchial scaffolds.

The bioinformatic tool Ingenuity Pathway Analysis was used to perform upstream mediator analysis based on the RNA-Seq data for genes differentially expressed on day 0, 7 and 14, respectively. The analysis generated positive and negative z scores that corresponded to a predicted increase or decrease in activity, respectively, in HBEC on COPD relative to normal bronchial scaffolds. Several mediators were predicted to have an altered activity in HBEC on COPD compared to normal scaffolds based on the expression patterns of genes downstream of those mediators (table 3).

Hepatocyte growth factor (HGF) was predicted to have decreased activity in HBEC on COPD scaffolds on both day 0 and 14, which was also reflected in the expression pattern for genes regulated by HGF (fig. 9A). On day 0, genes having a lower expression level in cells on COPD scaffolds included *MET* (HGF receptor), FOS-related antigen 1 (*FOSL1*), low density lipoprotein receptor (*LDLR*) and prostaglandin-endoperoxidase synthase 2 (*PTGS2*) (also known as cyclooxygenase 2). *FOSL1* and *LDLR* had a lower expression level on COPD scaffolds also on day 14, as well as the proto-oncogene FOS and nuclear receptor 4A1 (*NR4A1*).

Moreover, TGF-β1 activity was also predicted to be decreased in HBEC on COPD scaffolds on day 0. However, on day 7, TGF-β1 was predicted to have increased activity. Several genes known to be regulated downstream of TGF-β1 had a lower expression level in cells on COPD scaffolds on day 0, including TGF-β receptor 1 (*TGFBR1*), Snail family transcriptional repressor 2 (*SNAI2*) and *SMAD7* (fig. 9B). These genes were also differentially expressed on day 7, but at that time point *SNAI2* and *SMAD7* were more highly expressed in cells on COPD compared to normal scaffolds. Other TGF-β1-regulated genes also had a higher expression level in cells on COPD scaffolds on day 7, including connective tissue growth factor (*CTGF*), suppressor of cytokine signaling 3 (*SOCS3*) and Hes family basic helix-loop-helix transcription factor 1 (*HES1*). Some genes, like *FOS*, *NR4A1*, *SOCS3* and *HES1* had a similar overall expression pattern in cells on COPD and normal scaffolds, but with temporal differences, reaching their peak expression earlier on COPD scaffolds.

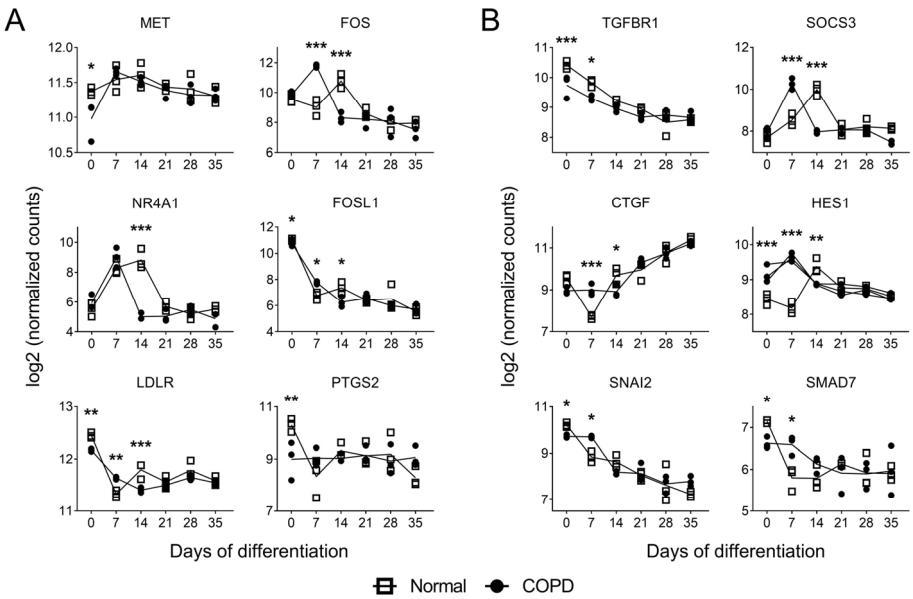

Figure 9. RNA sequencing data showing relative expression of genes regulated by (**A**) hepatocyte growth factor (HGF) and (**B**) transforming growth factor beta 1 (TGF-β1) in primary normal human bronchial epithelial cells during differentiation on normal (squares) or COPD (circles) bronchial scaffolds (n=3). *MET*=MET proto-oncogene, receptor tyrosine kinase (HGF receptor), *FOS*=Fos proto-oncogene (AP-1 transcription factor subunit), *FOSL1*=Fos-related antigen 1 (AP-1 transcription factor subunit), *LDLR*=low density lipoprotein receptor, *PTGS2*=prostaglandin-endoperoxide synthase 2 (cyclooxygenase 2), *NR4A1*=nuclear receptor 4A1, *TGFBR1*=TGF-β receptor 1, *SNAI2*= Snail family transcriptional repressor 2, *SMAD7*=SMAD family member 7, *CTGF*=connective tissue growth factor, *SOCS3*=suppressor of cytokine signaling 3, *HES1*=Hes family bHLH transcription factor 1. *FDR (False Discovery Rate)<0.05, **FDR<0.01, ***FDR<0.001.

Table 3. Upstream mediators predicted to have a changed activity in normal HBEC on COPD compared to normal bronchial scaffolds after 0, 7 and 14 days of differentiation, based on the expression pattern of the differentially expressed genes. Positive and negative activation z scores indicate increased and decreased activity, respectively, on COPD compared to normal scaffolds.

Normal HBEC on COPD compared to normal bronchial scaffolds on day 0, 7 and 14				
	Upstream mediator	Predicted activity	Activation z score	p value
Day 0	Estrogen receptor 1 (ESR1)	Decreased	-3.3	1.6E-08
	Hepatocyte growth factor (HGF)	Decreased	-3.2	1.8E-04
	Transforming growth factor beta 1 (TGFB1)	Decreased	-3.0	9.7E-09
	Interferon alpha 2 (IFNA2)	Increased	4.9	1.1E-04
	Interferon beta 1 (IFNB1)	Increased	4.2	8.5E-05
	Tumor protein p53 (TP53)	Increased	3.9	2.7E-10
	Interferon lambda 1 (IFNL1)	Increased	3.9	1.5E-04
	Tretinoin (all-trans retinoic acid)	Increased	3.3	2.6E-07
	Interferon alpha 1 (IFNA1)	Increased	3.1	6.6E-05
	Peroxisome proliferator activated receptor gamma (PPARG)	Increased	3.0	1.1E-04
Day 7	Interferon alpha 2 (IFNA2)	Decreased	-3.6	7.1E-06
	Interferon lambda 1 (IFNL1)	Decreased	-3.5	6.9E-07
	Interferon beta 1 (IFNB1)	Decreased	-3.4	8.4E-05
	Histone deacetylase (HDAC) (family)	Decreased	-3.2	1.9E-07
	Platelet-derived growth factor B (PDGFB)	Increased	4.7	7.4E-17
	Mitogen-activated protein kinase 1 (MAPK1)	Increased	3.9	1.2E-10
	Transforming growth factor beta 1 (TGFB1)	Increased	3.2	9.9E-11
	Tumor protein p53 (TP53)	Increased	3.2	9.4E-12
	CD40 ligand (CD40LG)	Increased	3.1	1.3E-07
	Endothelin 1 (EDN1)	Increased	3.1	2.3E-04
Day 14	Platelet-derived growth factor B (PDGFB)	Decreased	-4.8	6.7E-27
	Tumor necrosis factor alpha (TNF)	Decreased	-3.8	8.9E-16
	Nuclear factor kappa B (NF-kB) (family)	Decreased	-3.8	2.0E-08
	cAMP responsive element binding protein 1 (CREB1)	Decreased	-3.7	2.0E-13
	Calcium	Decreased	-3.7	8.2E-10
	Triggering receptor expressed on myeloid cells 1 (TREM1)	Decreased	-3.5	7.0E-10
	Coagulation factor II (thrombin) (F2)	Decreased	-3.3	6.4E-10
	Interferon gamma (IFNG)	Decreased	-3.2	2.5E-09
	Interleukin 1 beta (IL1B)	Decreased	-3.1	1.2E-20
	Hepatocyte growth factor (HGF)	Decreased	-3.1	3.1E-14

Bronchial epithelial cells from COPD patients show impaired ciliary development and altered cell cycle progression after repopulation on bronchial scaffolds (paper II)

In paper II, we aimed to study how airway epithelial remodeling in COPD patients depends on the relative influence from inherent defects in the HBEC themselves and the underlying ECM. We therefore performed global transcriptomic profiling (RNA-Seq) in COPD and normal HBEC after repopulation on bronchial scaffolds derived from COPD patients and healthy individuals. In addition, the cells were seeded in transwell plates for culture at the air-liquid interface (ALI). Finally, the matrisome composition of the bronchial scaffolds was analyzed by mass spectrometry.

Influence from bronchial epithelial cells and bronchial scaffolds on gene expression

PCA showed that the RNA-Seq samples were predominantly clustered based on differentiation time and whether the HBEC had grown on bronchial scaffolds or at the ALI. This was also reflected in the number of differentially expressed genes between day 0 and 7 samples and between samples representing HBEC on bronchial scaffolds and at the ALI (fig. 2 in paper II). When performed on day 0 and 7 samples separately, PCA revealed that COPD and normal HBEC grown on bronchial scaffolds formed two different clusters at both timepoints (fig. 10A). A separation was also seen between COPD and normal HBEC grown at the ALI, but it was less prominent, suggesting that bronchial scaffolds contribute to increased gene expression differences between COPD and normal HBEC. This was corroborated by a much larger number of differentially expressed genes between COPD and normal HBEC grown on bronchial scaffolds compared to those grown at the ALI (fig. 10B-C).

On day 0, PCA showed no separation between samples representing COPD and normal bronchial scaffolds (fig. 11A-B). However, in COPD HBEC on day 7, a separation could be seen between COPD and normal bronchial scaffold samples, while no such separation was seen for normal HBEC samples at the same timepoint (fig. 11C-D). In agreement with this observation, 1694 genes were found to be differentially expressed in COPD HBEC on COPD compared to normal scaffolds on day 7, while the corresponding number for normal HBEC was considerably lower (fig. 11E-F), demonstrating a fundamental difference between COPD and normal HBEC in terms of how gene expression is modulated by the bronchial scaffolds over time.

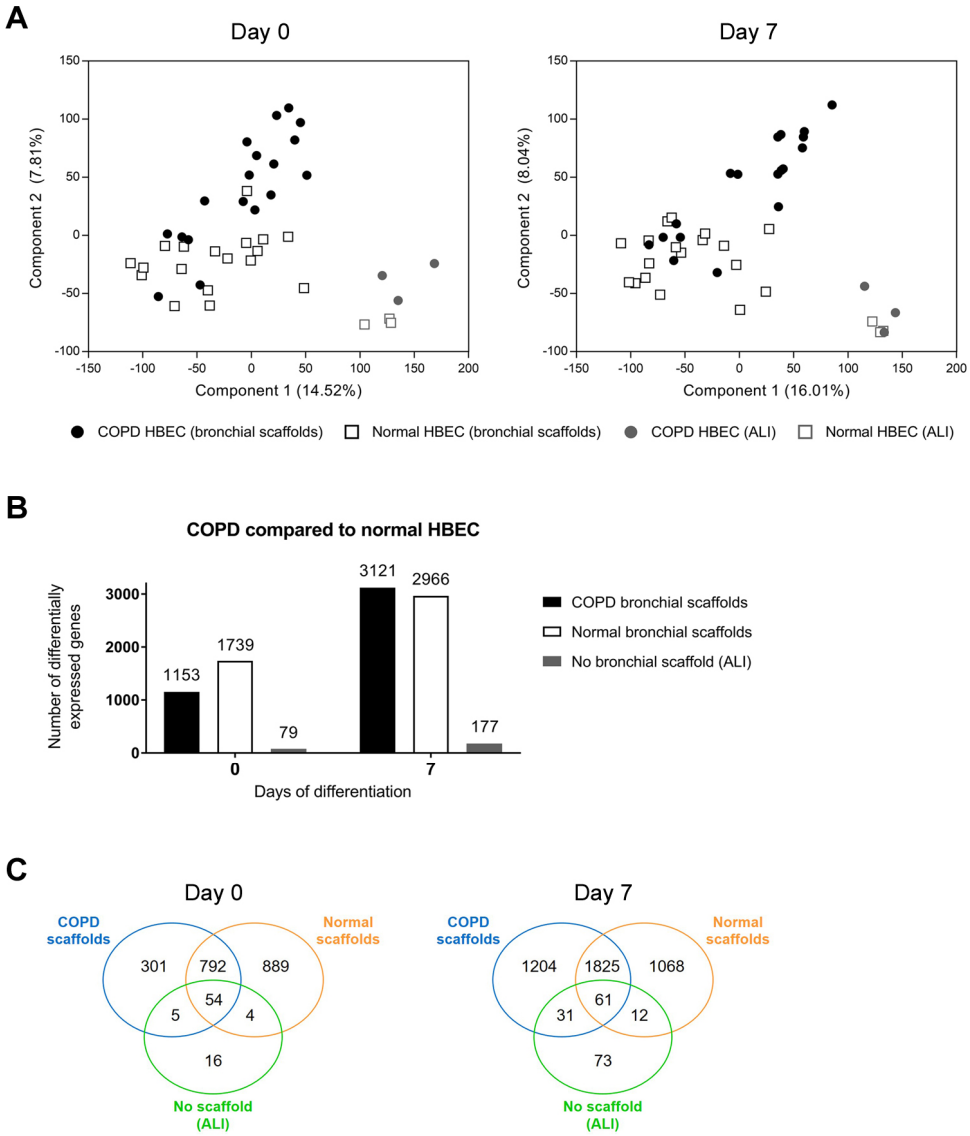

Figure 10. (**A**) Principal component analysis of RNA sequencing data for samples representing 0 days and 7 days of differentiation of primary HBEC on human bronchial scaffolds or at the air-liquid interface (ALI). Day 0 was defined as the day of differentiation induction, which was 4 days after seeding of cells. (**B**) Number and (**C**) overlap of differentially expressed genes in COPD compared to normal HBEC when grown on COPD scaffolds, normal scaffolds or at the ALI on day 0 and 7.

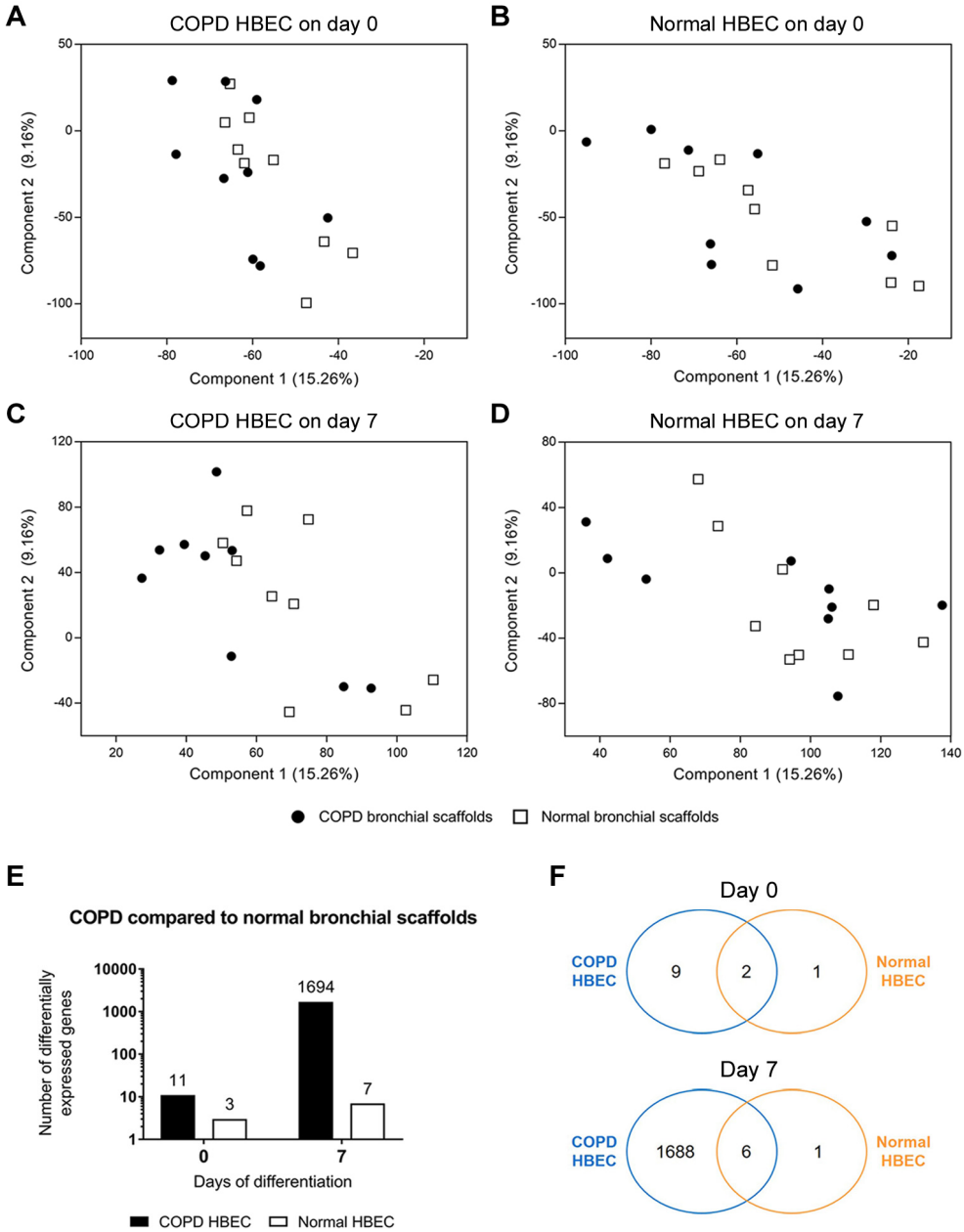

Figure 11. (**A-D**) Principal component analysis of RNA sequencing data for samples representing COPD and normal HBEC after 0 days (A-B) and 7 days (C-D) of differentiation on COPD or normal bronchial scaffolds. Day 0 was defined as the day of differentiation induction, which was 4 days after seeding of cells. (**E**) Number and (**F**) overlap of genes differentially expressed in COPD and normal HBEC on COPD compared to normal bronchial scaffolds.

Bronchial epithelial cells from COPD patients show impaired ciliated cell differentiation after repopulation on bronchial scaffolds

The temporal expression pattern of marker genes representing ciliated cells (*FOXJ1*), goblet cells (*MUC5AC*) and basal cells (*TP63*) indicated successful differentiation induction (fig. 12A) and was consistent with the results in paper I. Interestingly, however, the *FOXJ1* expression on day 7 was lower in COPD compared to normal HBEC on bronchial scaffolds, regardless of scaffold origin, a finding that was also confirmed at the protein level (fig. 12B). *TP63* expression was higher in COPD HBEC on bronchial scaffolds on day 7, but no differences were seen for *MUC5AC* (fig. 12A).

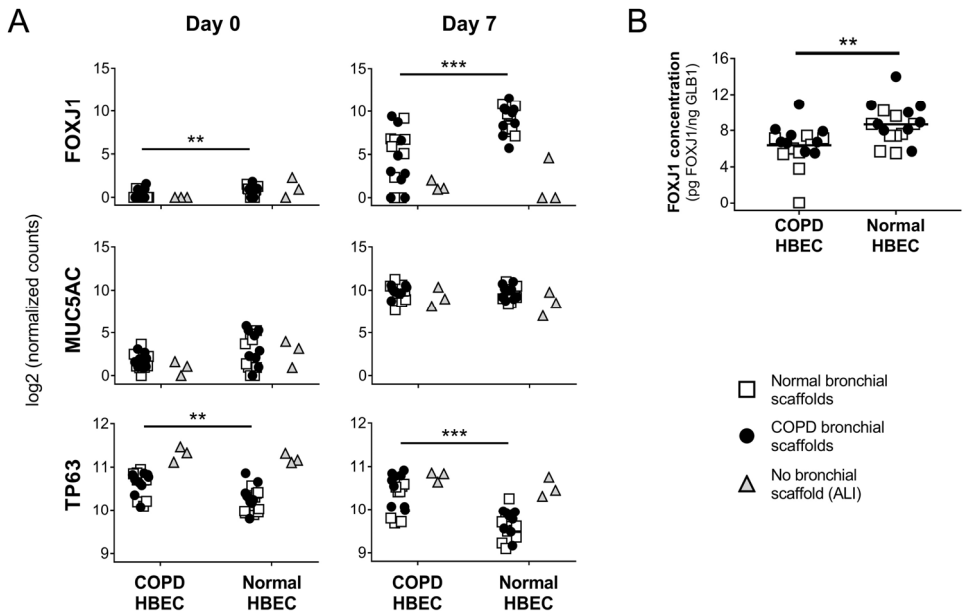

Figure 12. **(A)** Expression of forkhead box J1 (*FOXJ1*) (ciliated cells), mucin 5AC (*MUC5AC*) (goblet cells) and tumor protein p63 (*TP63*) (basal cells) from RNA sequencing in primary HBEC (n=3) repopulated on human bronchial scaffolds (n=3) or grown at the air-liquid interface (ALI). Day 0 was defined as the day of differentiation induction, which was 4 days after seeding of cells. FOXJ1 increased between day 0 and 7 in HBEC on scaffolds (FDR<0.001), but not at the ALI. *MUC5AC* increased between day 0 and 7 in all HBEC (FDR<0.001). *TP63* decreased between day 0 and 7 in all HBEC (FDR<0.001), except for COPD HBEC on COPD scaffolds. On day 0, *FOXJ1* was higher in COPD than normal HBEC on scaffolds. **(B)** Expression of FOXJ1 protein in primary HBEC (n=3) after 7 days of differentiation on human bronchial scaffolds (n=3). **FDR (False Discovery Rate)<0.01, ***FDR<0.001 in (A) and **p<0.01 in (B).

In concordance with the relative decrease of FOXJ1, GO term enrichment search showed an overrepresentation of genes annotated with biological process terms related to ciliogenesis among the genes differentially expressed in COPD compared to normal HBEC on scaffolds on day 7 (table 4). Numerous genes known to be involved in development and assembly of cilia showed a consistent pattern of lower expression in COPD HBEC on both diseased and normal bronchial scaffolds, including *ZMYND10*,

DRC1, *DNAI2*, *ARMC4*, *RSPH1*, *TMEM231*, *B9D1* and *CC2D2A* (fig. 13). Meanwhile, these differences were not seen in HBEC grown at the ALI and none of the genes were induced between day 0 and 7 in the absence of bronchial scaffolds (fig. S2 in paper II). In contrast, all genes were induced over time in HBEC that had grown on bronchial scaffolds (fig. 13). In summary, these results indicate that interactions with the bronchial scaffolds trigger an induction of ciliated cell differentiation in HBEC and that COPD HBEC have an impaired capacity to respond to this induction.

Table 4. Gene ontology (GO) term enrichment for genes differentially expressed in COPD compared to normal HBEC on normal bronchial scaffolds on day 7. Very similar results were obtained from GO term enrichment for genes differentially expressed in COPD compared to normal HBEC on COPD bronchial scaffolds on day 7 (shown in table 1 in paper II).

COPD compared to normal HBEC on normal bronchial scaffolds on day 7		
GO biological process	Fold enrichment	FDR
Cilium organization (GO:0044782)	2.6	5.7E-15
Cilium assembly (GO:0060271)	2.6	7.2E-14
Plasma membrane bounded cell projection assembly (GO:0120031)	2.3	2.1E-12
Cell projection assembly (GO:0030031)	2.3	3.0E-12
Cell projection organization (GO:0030030)	1.7	3.2E-11
Plasma membrane bounded cell projection organization (GO:0120036)	1.7	1.6E-10
Microtubule bundle formation (GO:0001578)	3.9	3.7E-09
Microtubule-based process (GO:0007017)	1.8	1.0E-08
Axoneme assembly (GO:0035082)	4.5	2.9E-08
Cilium movement (GO:0003341)	4.5	5.7E-08

Bronchial epithelial cells from COPD patients show increased cell cycle progression after repopulation on COPD bronchial scaffolds

GO term enrichment search was performed for the 1694 genes differentially expressed in COPD HBEC on COPD compared to normal bronchial scaffolds on day 7. An enrichment was seen for genes annotated with biological process terms such as chromosome segregation, cell proliferation, DNA replication and regulation of cell cycle (table 5). Also, the gene expression pattern indicated that several upstream mediators known to promote cell growth or cell cycle progression were predicted to have increased activity in COPD HBEC on COPD compared to normal scaffolds, while mediators that negatively regulate cell cycle progression were predicted to have decreased activity (table 3 in paper II). Several genes known to promote cell cycle

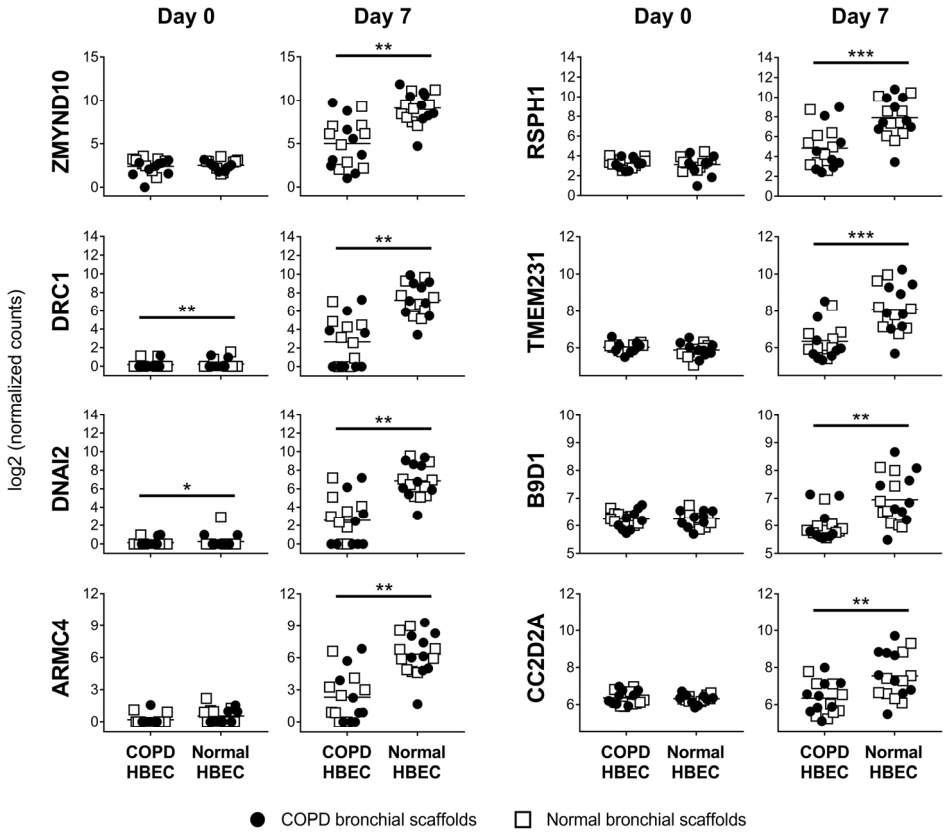

Figure 13. RNA sequencing data for genes implicated in ciliary development and assembly in primary HBEC (n=3) after 0 and 7 days of differentiation on human bronchial scaffolds (n=3). Day 0 was defined as the day of differentiation induction, which was 4 days after seeding of cells. All genes increased between day 0 and 7 in normal HBEC. In COPD HBEC, the following genes increased between day 0 and 7: *ZMYND10*, *ARMC4*, *RSPH1*, *DRC1* (normal scaffolds only), *DNAI2* (normal scaffolds only) and *TMEM231* (normal scaffolds only). On day 0, *DRC1* and *DNAI2* expression was higher in COPD HBEC. Means are indicated by horizontal lines. *ZMYND10*=zinc finger MYND-type-containing 10, *DRC1*=dynein regulatory complex subunit 1, *DNAI2*=dynein axonemal intermediate chain 2, *ARMC4*=armadillo repeat-containing 4, *RSPH1*=radial spoke head 1 homolog, *TMEM231*=transmembrane protein 231, *B9D1*=B9 domain-containing 1, *CC2D2A*=coiled-coil and C2 domain-containing 2A. *FDR (False Discovery Rate)<0.05, **FDR<0.01, ***FDR<0.001.

progression or cell division had a higher expression level on COPD scaffolds on day 7, including *E2F2*, *TTK*, *MCM10*, *ANLN*, *CCNB1*, *CCNA2* and *CDK1*, whereas *CDKN1A* and *CDKN2A* were both downregulated on COPD scaffolds (fig. 14). Furthermore, the proliferation marker *MKI67* was increased on COPD relative to normal scaffolds. Taken together, these data indicate increased cell cycle progression and proliferation of COPD HBEC when cultured on COPD compared to normal bronchial scaffolds.

Table 5. Gene ontology (GO) term enrichment for genes differentially expressed in COPD HBEC on COPD compared to normal bronchial scaffolds after 7 days of differentiation.

COPD HBEC on COPD compared to normal bronchial scaffolds on day 7		
GO-slim biological process	Fold enrichment	FDR
Chromosome segregation (GO:0007059)	3.4	4.2E-05
DNA metabolic process (GO:0006259)	2.1	8.9E-05
DNA replication (GO:0006260)	2.7	1.2E-04
Regulation of cell cycle (GO:0051726)	2.5	2.0E-04
Cellular process (GO:0009987)	1.1	5.9E-04
Cell cycle (GO:0007049)	1.6	6.5E-04
Metabolic process (GO:0008152)	1.2	4.4E-03
Translation (GO:0006412)	2.0	9.1E-03
Cell proliferation (GO:0008283)	2.8	1.6E-02
DNA recombination (GO:0006310)	3.1	1.6E-02
Biosynthetic process (GO:0009058)	1.3	1.9E-02
Phosphate-containing compound metabolic process (GO:0006796)	1.3	2.1E-02
DNA repair (GO:0006281)	2.0	2.9E-02
Mitosis (GO:0007067)	1.8	3.8E-02
Meiosis (GO:0007126)	2.6	3.9E-02

COPD bronchial scaffolds show an altered extracellular matrix composition

Mass spectrometry was performed to study ECM alterations in the bronchial scaffolds. In total, 3340 proteins were detected, 58 of which were differentially abundant in COPD compared to normal bronchial scaffolds. Among all detected proteins, 364 belonged to the matrisome as defined by Naba et al[65]. Many core matrisome components, such as ECM glycoproteins and collagens, were identified in the scaffolds, but also matrisome-associated proteins, like ECM regulators and secreted factors (fig. S5 in paper II). Thirteen matrisome proteins were differentially abundant in COPD compared to normal scaffolds (fig. S6 in paper II). Lysyl oxidase-like 1 (LOXL1), fibulin 5 (FBLN5), EGF-containing fibulin extracellular matrix protein 1 (EFEMP1), MMP12 and the complement C1q A (C1QA), B (C1QB) and C (C1QC) chains were all increased in COPD scaffolds. Proteins decreased in COPD scaffolds included insulin-like growth factor-binding protein 2 (IGFBP2), S100 calcium-binding protein A8 (S100A8) and A9 (S100A9) as well as the fibrinogen alpha (FGA), beta (FGB) and gamma (FGG) chains.

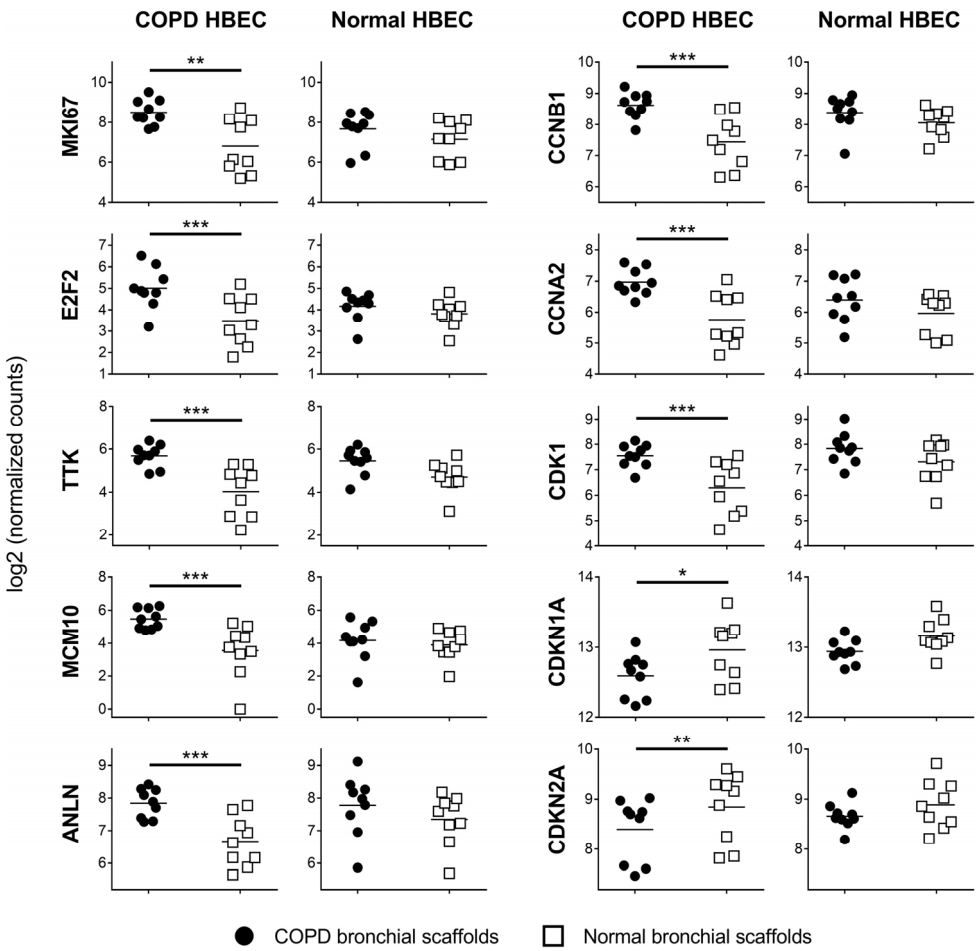

Figure 14. RNA sequencing data for genes implicated in cell cycle regulation and cell division in primary HBEC (n=3) after 7 days of differentiation on human bronchial scaffolds (n=3). Means are indicated by horizontal lines. *MKI67*= marker of proliferation Ki-67, *E2F2*=E2F transcription factor 2, *TTK*=TTK protein kinase, *MCM10*=minichromosome maintenance 10 replication initiation factor, *ANLN*=anillin actin-binding protein, *CCNB1*=cyclin B1, *CCNA2*=cyclin A2, *CDK1*=cyclin-dependent kinase 1, *CDKN1A*=cyclin-dependent kinase inhibitor 1A (p21), *CDKN2A*=cyclin-dependent kinase inhibitor 2A (p16-INK4A/p14-ARF). *FDR (False Discovery Rate)<0.05, **FDR<0.01, ***FDR<0.001.

Increased deposition of glycosaminoglycans and altered structure of heparan sulfate in IPF lungs (paper III)

Tissue remodeling in IPF is characterized by increased ECM deposition in the lung interstitium, and GAGs have an inherent ability to bind soluble mediators such as growth factors, which may contribute to remodeling in IPF lungs. In paper III, we aimed to quantify and analyze the fine structure of GAGs in dense and less dense regions of IPF lungs and in lungs from healthy individuals. In addition, we examined the tissue distribution of highly sulfated heparan sulfate in IPF and normal lungs by IHC.

Increased deposition of glycosaminoglycans in IPF lungs

Following enzymatic digestion of GAGs, CS/DS, HA and HS disaccharides were quantified with RP-HPLC. There was a general increase in the total pool of GAGs in both dense and less dense regions of IPF lungs compared to normal lungs (fig. 15), and the same pattern was seen for CS/DS, HA and HS individually. However, no differences were found between dense and less dense regions.

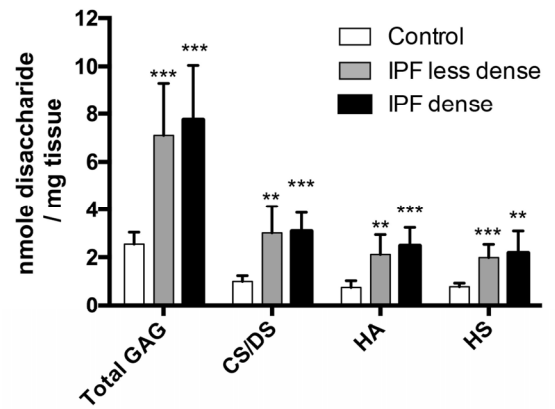

Figure 15. Glycosaminoglycan (GAG) abundance in healthy donor lungs (control) (n=7) and dense and less dense regions of IPF lungs (n=10). The quantification was done using reversed-phase high-performance liquid chromatography. CS/DS=chondroitin sulfate/dermatan sulfate, HA=hyaluronic acid, HS=heparan sulfate. *p<0.05, **p<0.01, ***p<0.001 (compared to control lungs).

Moreover, the total amount of sulfated CS/DS was increased in both dense and less dense regions of IPF lungs (fig. 16A). This was also seen for all subgroups of CS/DS disaccharides with specific sulfation patterns. To explore the relative composition of

different CS/DS disaccharides, the data for each disaccharide subgroup were normalized against the total levels of CS/DS (fig. 16B). In dense IPF lung tissue, there was a relative increase in the total amount of sulfated CS/DS and a relative decrease in non-sulfated CS/DS disaccharides. These results show that CS/DS GAGs have an increased abundance in IPF lungs, but that their overall fine structure is largely unchanged except for a slight increase in sulfation in more fibrotic regions.

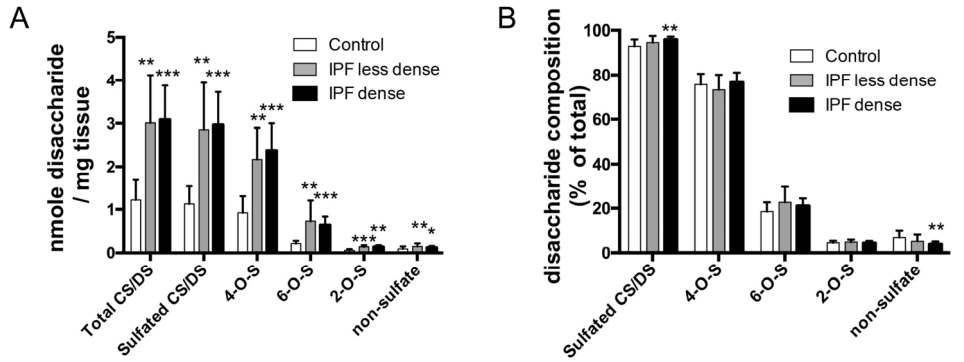

Figure 16. Absolute (**A**) and relative (**B**) levels of chondroitin sulfate/dermatan sulfate (CS/DS), including groups of disaccharides representing specific CS/DS sulfation patterns, in less dense and dense regions of IPF lungs (n=10) and in lungs from healthy individuals (control) (n=7). Total CD/DS: the sum of all CS/DS disaccharides, sulfated CS/DS: the sum of all sulfated CS/DS disaccharides, 4-O-S: the sum of 4-O sulfated CS/DS disaccharides, 6-O-S: the sum of 6-O sulfated CS/DS disaccharides, 2-O-S: the sum of 2-O sulfated CS/DS disaccharides, non-sulfate: non-sulfated CS/DS disaccharides. *p<0.05, **p<0.01, ***p<0.001 (compared to control lungs).

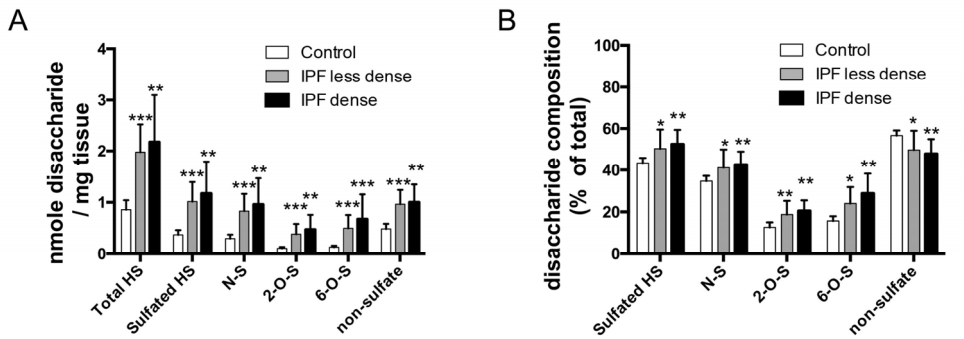

Figure 17. Absolute (**A**) and relative (**B**) levels of heparan sulfate (HS), including groups of disaccharides representing specific HS sulfation patterns, in less dense and dense regions of IPF lungs (n=10) and in lungs from healthy individuals (control) (n=7). Total HS: the sum of all HS disaccharides, sulfated HS: the sum of all sulfated HS disaccharides, N-S: the sum of N-sulfated HS disaccharides, 2-O-S: the sum of 2-O sulfated HS disaccharides, 6-O-S: the sum of 6-O sulfated HS disaccharides, non-sulfate: non-sulfated HS disaccharides. *p<0.05, **p<0.01, ***p<0.001 (compared to control lungs).

Heparan sulfate has an altered structure in IPF lungs

Similar to what was observed for CS/DS, the total levels of sulfated HS were also elevated in both dense and less dense regions of IPF lungs, and all analyzed subgroups of HS disaccharides showed the same pattern (fig. 17A). Furthermore, after normalization against total HS content, the total amount of sulfated HS and all subgroups of sulfated HS disaccharides also showed a relative increase in the IPF samples (fig. 17B). Meanwhile, a relative decrease was seen for non-sulfated HS disaccharides. These findings demonstrate that IPF lungs not only have increased HS deposition, but that HS in IPF lungs also has an altered fine structure as a result of increased sulfation.

Tissue distribution of highly sulfated heparan sulfate in IPF lungs

We used the phage display-derived antibody fragment A04B08V to detect a highly sulfated HS epitope in IPF and normal lung tissue. Pre-treatment with heparinase I, II and III was used to validate binding specificity. In normal lungs, A04B08V-specific staining was found in occasional airways and blood vessels, but the staining was generally weak and showed limited distribution (fig. 7 in paper III). In contrast, IPF lungs showed a stronger and more widespread A04B08V-specific staining, which was found in the border zone between areas of dense fibrosis and regions with more normal looking alveolar parenchyma (fig. 18, upper panel).

To investigate the general tissue distribution of HS, we used the anti-HS antibody 10E4, which has a much broader specificity for HS than A04B08V. The 10E4 staining pattern showed that HS is widely distributed in IPF lungs also in regions that were negative for A04B08V (fig. 18, middle panel). Furthermore, we analyzed expression of the perlecan core protein and found that it is highly abundant in basement membranes of airways, alveoli and blood vessels (fig. 18, lower panel). A04B08V-positive staining was predominantly found in basement membranes of blood vessels (fig. 19D, G and I) and airways (fig. 19A and C), but also in spindle-shaped cells in the alveolar interstitium (fig. 19F). Although the perlecan staining was much more widespread, there was an overlap between the A04B08V and perlecan staining patterns, especially in basement membranes, suggesting that perlecan might be one of the core proteins that harbor the highly sulfated HS chains. These results show that highly sulfated HS appears to be concentrated to areas of active remodeling in IPF lungs.

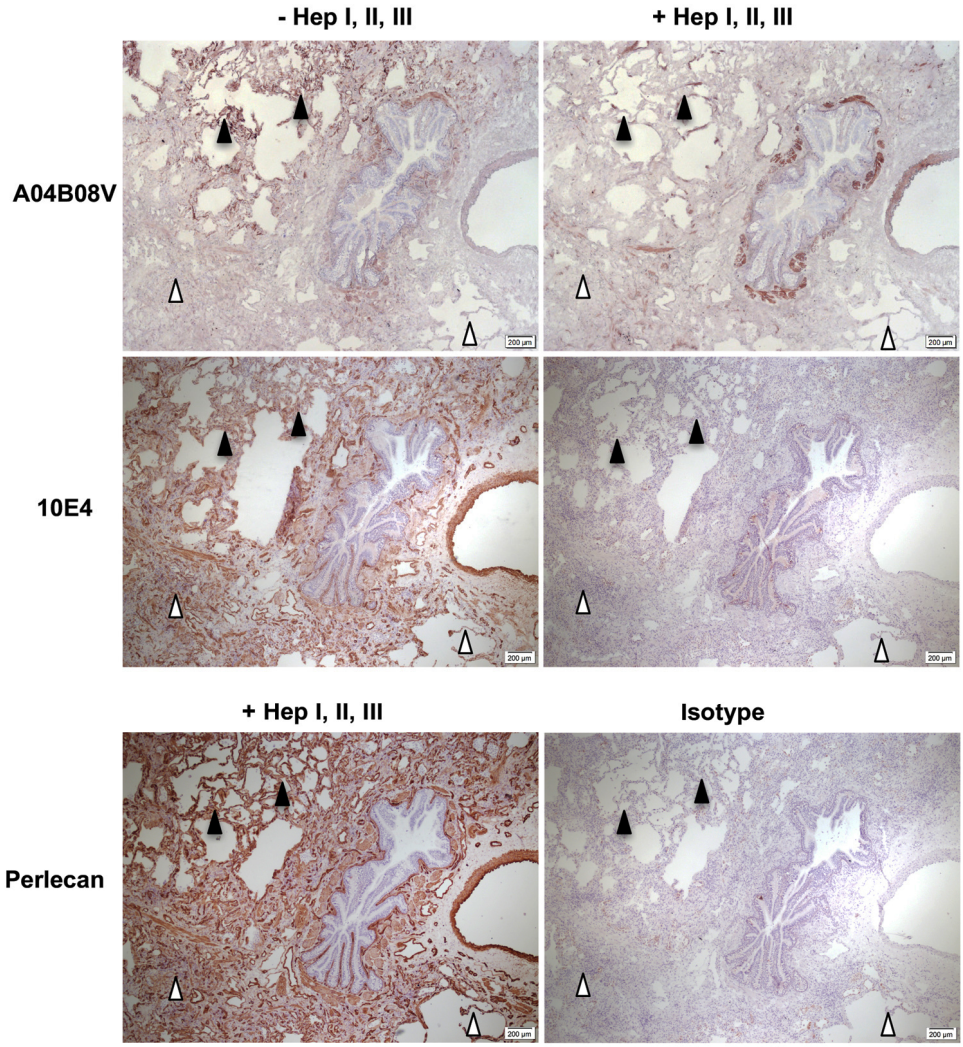

Figure 18. Location of highly sulfated heparan sulfate (HS) in the border zone between areas of dense fibrosis and more normal looking alveolar parenchyma in IPF lung. Staining for HS was performed on sequential cryosections with and without treatment with heparinase I, II and III. The A04B08V antibody fragment recognizes an N-sulfated HS octasaccharide with three consecutive 6-O-sulfate groups and an internal 2-O-sulfate group. The 10E4 antibody has a broader specificity and binds to less sulfated stretches of HS that contain N-sulfated glucosamine residues. Staining was also performed against the HS proteoglycan perlecan using heparinase treatment for epitope retrieval and a mouse IgG1 isotype antibody as negative control. Solid arrowheads indicate areas that are positive for A04B08V, 10E4 and perlecan. Open arrowheads indicate areas that are positive for 10E4 and perlecan but not A04B08V. Images are representative of n=4. Scale bars: 200 µm.

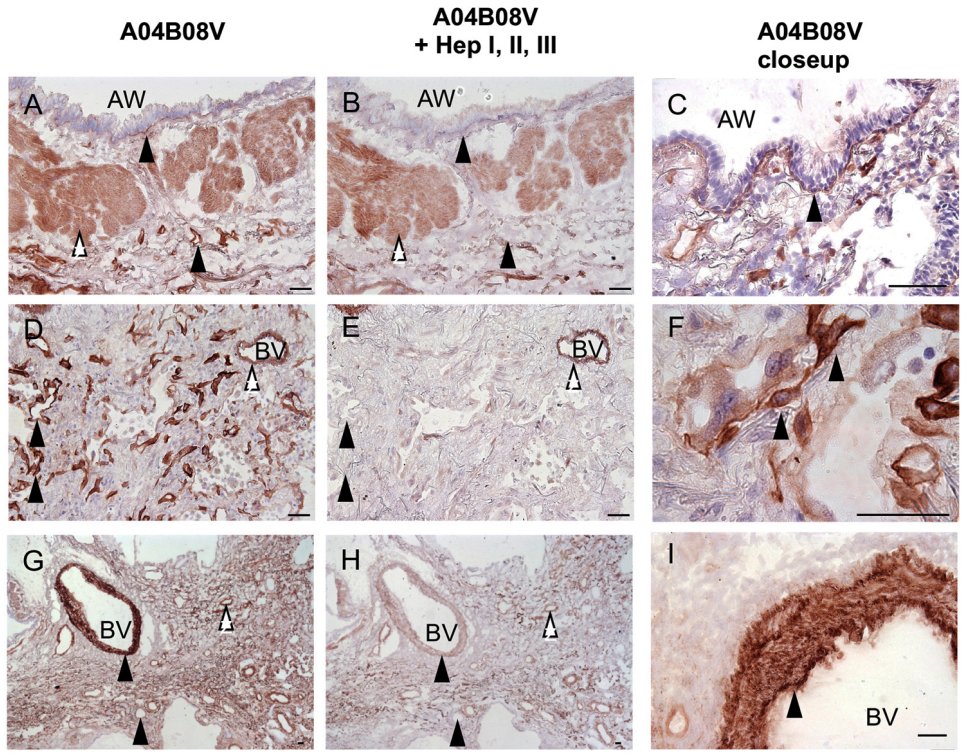

Figure 19. Location of highly sulfated heparan sulfate (HS) in sequential cryosections of IPF lung with (**B, E, H**) and without (**A, C, D, F, G, I**) treatment with heparinase I, II and III. The A04B08V antibody fragment recognizes an N-sulfated HS octasaccharide with three consecutive 6-O-sulfate groups and an internal 2-O-sulfate group. Solid and open arrowheads indicate heparinase-sensitive and heparinase-insensitive staining, respectively. **A** and **B** show a bronchiolar airway wall with A04B08V-positive staining in basement membranes of airway epithelium and small blood vessels. **D** and **E** show A04B08V-positive capillaries and small blood vessels in an area of dense fibrosis. **G** and **H** show a larger A04B08V-positive blood vessel surrounded by smaller blood vessels and airways. **C**, **F** and **I** show close-ups of A04B08V-positive staining in an airway wall (**C**), spindle-shaped cells in the alveolar interstitium (**F**) and a large blood vessel (**I**). AW=airway, BV=blood vessel. Images are representative of n=4. Scale bars: 50 µm.

Disease-specific extracellular matrix alterations in COPD and IPF lungs (paper IV)

In paper IV, we aimed to provide a comprehensive description of the human lung matrisome during tissue remodeling, which led to identification of several ECM proteins with altered abundance in COPD and IPF lungs.

Extractability of matrisome proteins

By using sequential tissue extraction, we isolated proteins in three consecutive fractions (labeled soluble, SDS and ECM-enriched), representing proteins with different extractability, from healthy donor lungs, COPD lungs and dense (IPF+) and less dense (IPF) regions of IPF lungs. Following quantification by mass spectrometry, the relative abundances of all detected proteins (fig. 20A) showed that the proportion of matrisome proteins was higher in the ECM-enriched fraction. The relative abundances of only the matrisome proteins were also visualized (fig. 20B), which revealed that core matrisome proteins such as collagens and ECM glycoproteins were significantly enriched in the ECM-enriched fraction, while secreted factors and ECM-affiliated proteins were mostly found in the soluble fraction. These results highlight that different classes of matrisome proteins have distinct solubility profiles and that the tissue extraction strategy is critical for proteomics studies that are focused on ECM proteins.

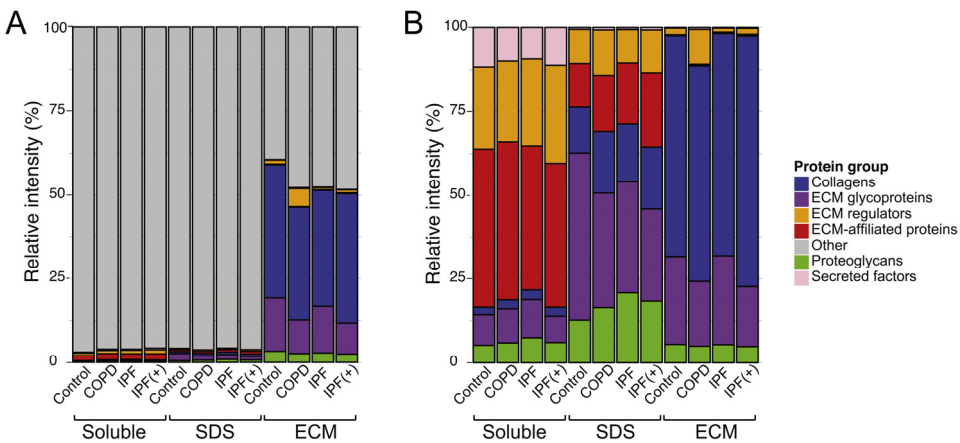

Figure 20. Relative abundances of (**A**) all detected proteins and (**B**) all detected matrisome proteins in each solubility fraction (soluble, SDS and ECM-enriched) in healthy donor lungs, COPD lungs and dense (IPF+) and less dense (IPF) regions of IPF lungs. Matrisome categories are shown to the right. Grey color represents non-matrisome proteins (other).

Disease-specific extracellular matrix alterations in COPD and IPF lungs

After summing the abundances in each of the three fractions, the total amount of each protein was compared between the diseased groups and the healthy control group, which led to identification of 25 proteins with significantly altered levels in COPD or IPF lungs (fig. 21). Several proteins known to promote cell adhesion were less abundant in dense regions of IPF lungs, including laminin β1 (LAMB1), laminin γ1 (LAMC1) and nidogen-1 (NID1), whereas the α1 and α2 chains of collagen VI (COL6A1, COL6A2) were both increased in the IPF+ samples (fig 22A). Also, the SLRP asporin (ASPN) was significantly increased in less dense regions of IPF lungs. Other proteins with altered abundance in IPF lungs included ADAM9, ITIH2, SERPINA6, SERPINB9, MUC16, CLC, COL16A1, PF4 and PF4V1 (fig. 21 and fig. S4 in paper IV).

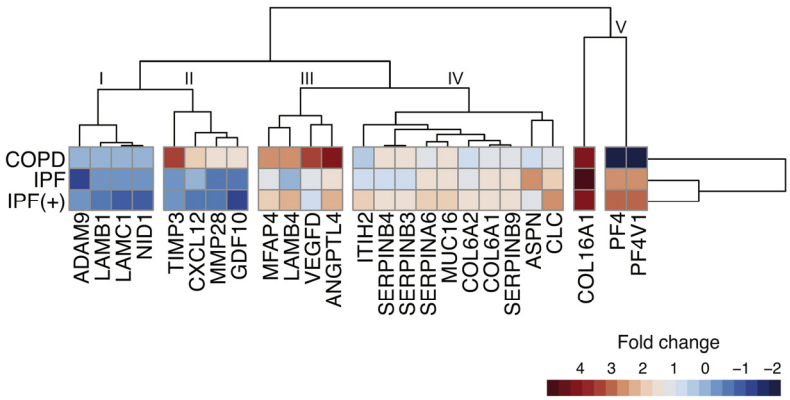

Figure 21. Matrisome proteins with altered expression in the COPD, IPF+ (dense) or IPF (less dense) groups compared to the healthy control group after unsupervised hierarchical clustering. The fold change represents the relative difference between the level of each protein in the diseased groups compared to the level in the healthy donor control group. ADAM9=disintegrin and metalloproteinase domain-containing protein 9, LAMB1=laminin subunit beta 1, LAMC1=laminin subunit gamma 1, NID1=nidogen-1, TIMP3=TIMP metalloproteinase inhibitor 3, CXCL12=C-X-C motif chemokine ligand 12, MMP28=matrix metalloproteinase 28, GDF10=growth differentiation factor 10, MFAP=microfibril-associated protein 4, LAMB4=laminin subunit beta 1, VEGFD=vascular endothelial growth factor D, ANGPTL4=angiopoietin-like 4, ITIH2=inter-alpha-trypsin inhibitor heavy chain 2, SERPINB4=serpin family B member 4, SERPINB3=serpin family B member 3, SERPINA6=serpin family A member 6, MUC16=mucin 16, COL6A2= collagen type VI alpha 2 chain, COL6A1=collagen type VI alpha 1 chain, SERPINB9=serpin family B member 9, ASPN=asporin, CLC=Charcot-Leyden crystal galectin, COL16A1=collagen type XVI alpha 1 chain, PF4=platelet factor 4, PF4V1= platelet factor 4 variant 1.

In COPD lungs, increased levels were seen for proteins that participate in regulation of the ECM, including MMP28, TIMP3, SERPINB3, SERPINB4, GDF10 and CXCL12 (fig. 22B). Also, MFAP4, LAMB4, VEGFD and ANGPTL4 were all more highly abundant in the COPD group, whereas no matrisome proteins were decreased in COPD compared to healthy control samples. (fig. 21 and fig. S4 in paper IV).

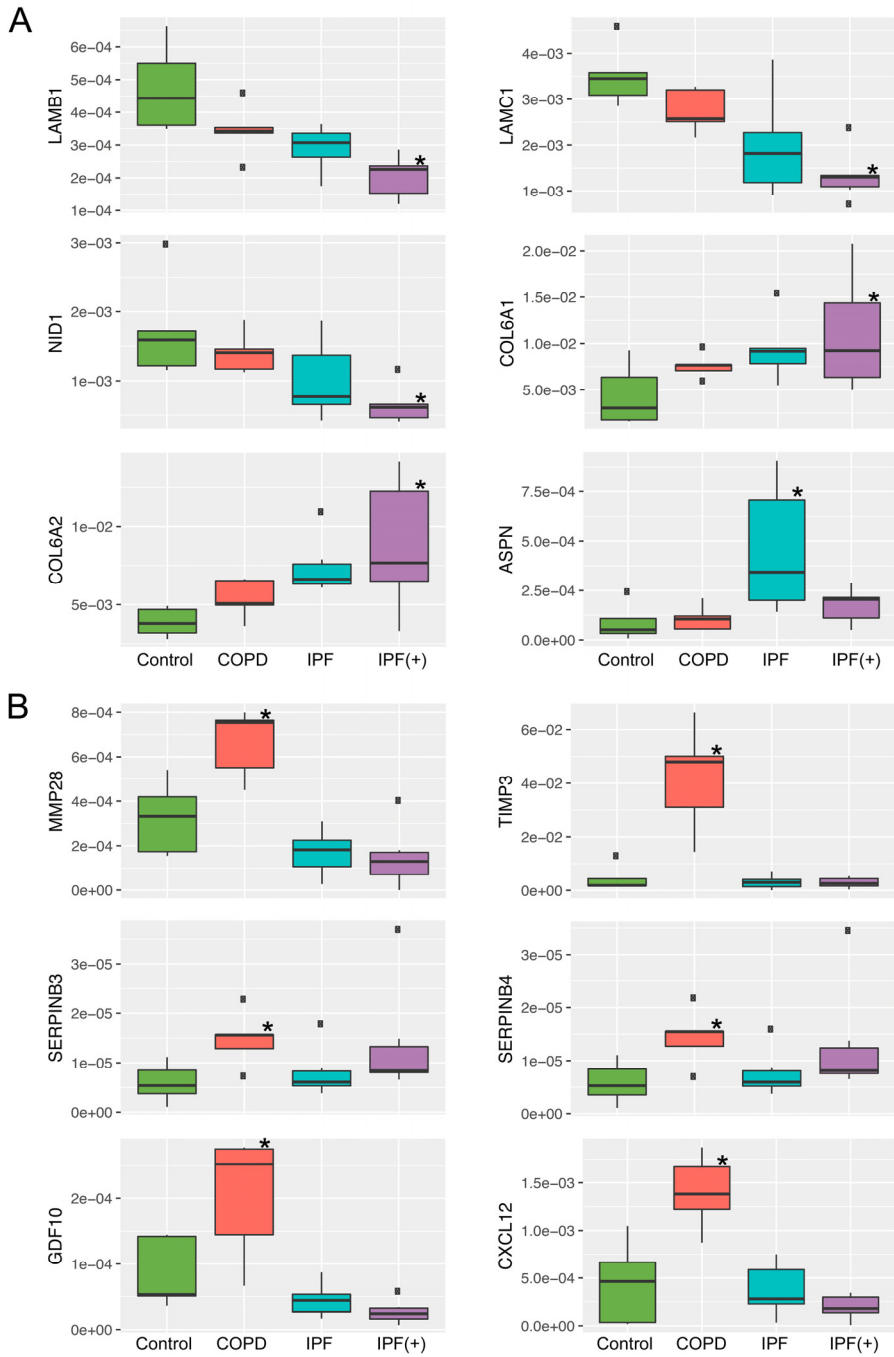

Figure 22. Matrisome proteins with differential abundance in (**A**) IPF and (**B**) COPD lungs Shown are relative intensities from mass spectrometry of proteins extracted from healthy donor lungs, COPD lungs and dense (IPF+) and less dense (IPF) regions of IPF lungs. See fig. 21 for description of acronyms. *p<0.05.

Asporin show increased deposition in IPF lungs and is found in honeycomb structures and fibroblastic foci

IHC was performed to study tissue distribution of asporin in lungs from healthy donors, IPF patients and COPD patients. In normal lungs, weak staining was found in the lamina propria of bronchioles (fig. 23A), but no staining was seen in blood vessels (fig. 23B) or in the alveolar parenchyma (fig. 23C). However, the staining pattern in IPF lungs revealed a more widespread distribution of asporin. Staining was found in bronchioles (fig. 23D), alveolar septa (fig. 23E), alveolar openings (not shown) and in more dense, fibrotic regions (fig. 23F), but no staining was present in blood vessels (fig. 23G). Moreover, strong staining was found in areas with low cell density in honeycomb structures (fig. 23H) and fibroblastic foci (fig. 23I). These findings confirm the increased asporin levels seen in IPF lungs in the mass spectrometry analysis, and the expression pattern suggests a potential role for asporin in pulmonary remodeling in IPF.

Tissue distribution of asporin in COPD lungs

In contrast, COPD lungs showed a very different staining pattern compared to IPF lungs. Strong staining was found in blood vessels (fig. 23J), while no staining could be seen in airways (fig. 23K), alveolar septa (fig. 23L) or alveolar openings (not shown). Although the mass spectrometry showed no difference in the total amount of asporin between COPD and control samples (fig. 22A), the IHC results suggest that asporin distribution is affected in COPD lungs. In addition, asporin was increased in the SDS fraction from COPD tissue compared to the same fraction from normal lungs (fig. 4C in paper IV), which could be a reflection of altered asporin solubility in COPD compared to healthy lungs.

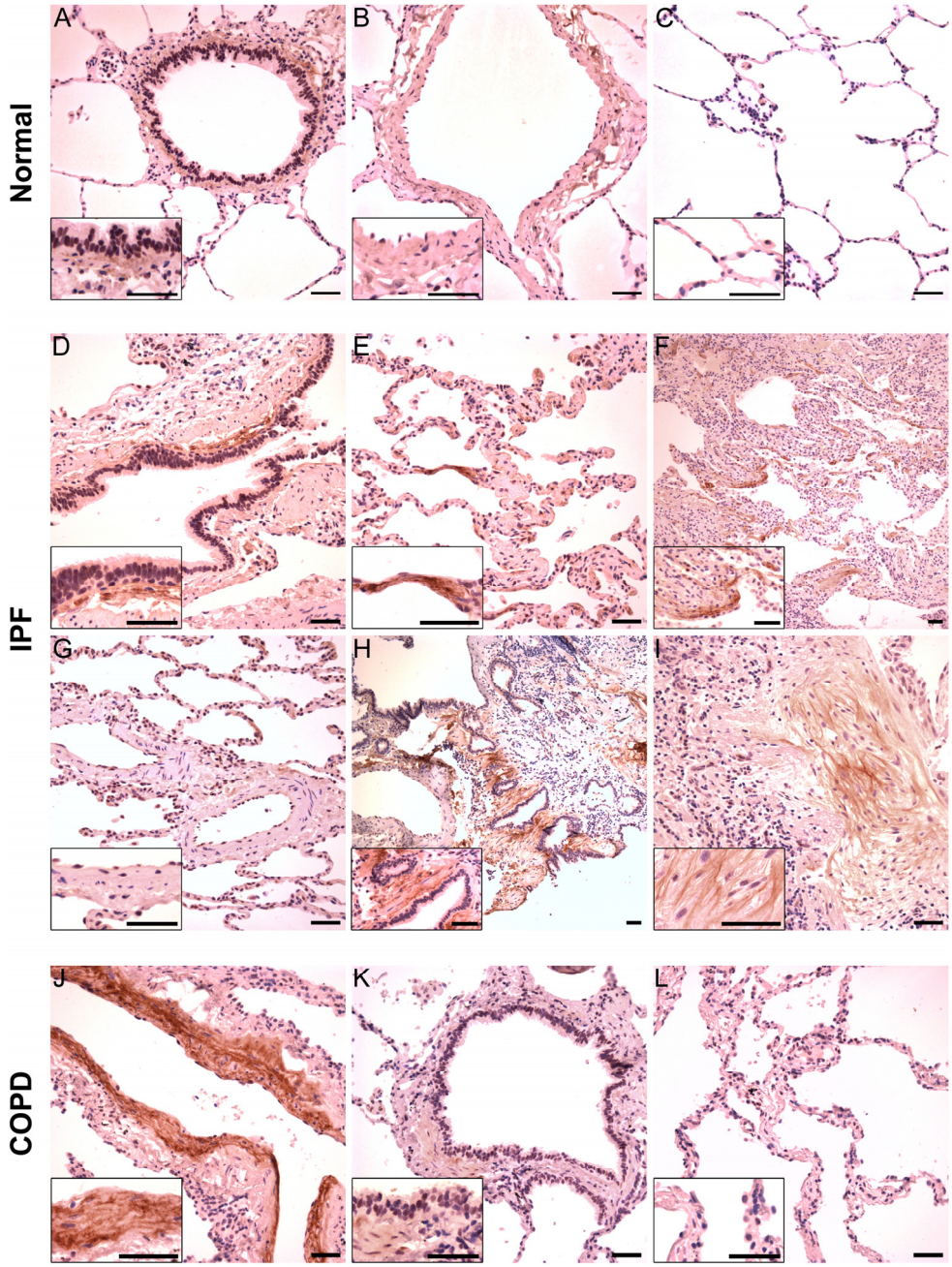

Figure 23. Tissue distribution of asporin in normal lung (**A-C**) and lungs from IPF (**D-I**) and COPD (**J-L**) patients. Insets show the same images at higher magnification. Images are representative of n=2. Scale bars: 50 μm.

Discussion

The ECM is known to influence cell function, either indirectly by harboring mediators such as growth factors or by directly participating in activation of cell surface receptors. The pulmonary ECM is remodeled in COPD and IPF, but much is yet to be learned about the nature of these alterations and especially how they affect cell function. In this thesis, we aimed to examine in detail how the pulmonary ECM is altered in COPD and IPF, with a particular focus on how pathological alterations in the bronchial ECM modulate epithelial cell phenotype in COPD airways. We provide data that demonstrate how the phenotype of airway epithelial cells in COPD depends both on inherent defects in the epithelial cells themselves and on alterations in the ECM microenvironment. Furthermore, we identify changes in quantity and distribution of several components of the pulmonary ECM in COPD and IPF lungs.

Several studies have shed light on how the ECM has an intrinsic potential for directing specification and differentiation of lung epithelial cells. Gilpin et al. repopulated decellularized human lung tissue slices with lung progenitor cells derived from human induced pluripotent stem cells, and the repopulated cells expressed epithelial markers such as E-cadherin and FOXJ1 after 5 days of culture[169]. Furthermore, the repopulated cells also showed increased expression of the lung progenitor cell marker Nkx2-1 compared to cells not cultured on lung scaffolds, thus confirming enhanced lung epithelial specification for cells grown on a native ECM. Shojaie et al. showed that repopulated decellularized rat lung scaffolds could direct differentiation of definitive endodermal cells, derived from murine embryonic stem cells, into ciliated cells, club cells and basal cells[170]. Of note, the temporal expression pattern of FOXJ1, p63 and Ki-67 was very similar to our findings in repopulated HBEC on bronchial scaffolds, even though both the scaffolds and the cells have very different origins in the two studies. Also, by pre-treating the lung scaffolds with heparinase, Shojaie et al. showed that HS and its associated factors are essential for supporting the observed differentiation, which underlines the powerful impact GAGs can have on cell function.

Parker et al. repopulated decellularized lung tissue from IPF patients and healthy donors with normal and IPF-derived fibroblasts[171]. Interestingly, they found fibroblast gene expression to be more influenced by the disease state of the ECM than that of the fibroblasts. In contrast, we concluded that epithelial cell gene expression in COPD airways is more dependent on the disease state of the HBEC than that of the ECM. This could mean that different cell types in the lung are differently affected by disease-

related changes in the ECM, but it may also reflect the fact that different lung diseases were investigated. In addition, the scaffolds used by Parker et al. included peripheral lung, whereas our study was focused specifically on bronchial airways. Wagner et al. repopulated normal and emphysematous lung scaffolds with HBEC and found that normal scaffolds could support repopulated HBEC for up to 21 days following inoculation of cells, whereas no HBEC were present in the emphysematous scaffolds after day 7[172]. They also performed immunohistochemistry to assess proliferation and apoptosis following repopulation, and the results were consistent with our observations in normal HBEC repopulated on bronchial scaffolds, which showed a rapid decline in proliferation after repopulation and minimal apoptosis. Moreover, in contrast to the study by Wagner et al, we observed viable HBEC also on diseased scaffolds at timepoints as late as day 35. This is not surprising though, considering that we did not use parenchymal but bronchial scaffolds, which are obviously less affected by emphysema.

In COPD, dysfunctional mucociliary clearance increases the risk of chronic cough and exacerbations induced by respiratory infections, which are typical clinical features of the disease. The mucociliary escalator is critically dependent on adequate ciliary function, and decreased ciliary beating and shortened cilia in COPD airways[11,12] contribute to the inability to clear mucus and pathogens from the airways. Our results indicate that the ECM plays a role in initiating ciliated cell differentiation, thus emphasizing the need for a native ECM to adequately recapitulate microenvironmental cues during differentiation of airway epithelium. The data we present imply that the transcriptional program governing motile cilia development in HBEC is influenced by signaling downstream of receptors that interact with the ECM. Moreover, we found that COPD HBEC failed to properly induce ciliated cell differentiation when grown on bronchial scaffolds, which suggests that intrinsic defects in the COPD HBEC prevent this process. Such defects may have an epigenetic origin since the COPD HBEC in our study all came from smokers or ex-smokers, and cigarette smoke is known to induce both ciliary dysfunction[48,50,51] and epigenetic alterations[173] in airway epithelial cells. Apart from motile cilia, which are present in the airways and a few other organs, most cell types are equipped with non-motile cilia, also known as primary cilia[174]. Motile and primary cilia have a similar ultrastructure, but primary cilia are mainly involved in chemosensing and mechanosensing. Little is known about influence from the ECM on ciliary development, but collagen I has been shown to promote growth of primary cilia in embryonic fibroblast-like cells in vitro[175]. Furthermore, it has recently been reported that the number of primary cilia is substantially increased in COPD airway epithelium and they were primarily found on basal cells[176]. Primary cilia are known to regulate differentiation of cells with motile cilia in the airways[174], suggesting that they might have played a role also in our study.

COPD patients have a markedly increased risk of developing lung cancer, although the mechanistic links between the two diseases are not clear[20]. The gene expression pattern we found in repopulated COPD HBEC indicates that bronchial ECM in COPD airways promotes hyperproliferation of epithelial cells, which suggests that ECM alterations in the bronchial airways may contribute to increased lung cancer risk in COPD patients. Our findings may also have implications for basal cell hyperplasia, an early pathological change in COPD airway epithelium[2].

Our data demonstrate increased deposition and sulfation of HS in IPF lungs. In agreement with this, Lu et al. also found a relative increase in HS 6-O-sulfation in IPF lungs, but they did not investigate other HS sulfation patterns[177]. In the same study, IPF lungs were reported to have increased expression of HS 6-O-sulfotransferase 1 (HS6ST1) and 2 (HS6ST2) mRNA, yet our results show decreased levels of HS6ST2 and no change in HS6ST1 mRNA in IPF tissue. These different outcomes could be due to the large heterogeneity that exists within IPF lungs as well as between patients. HS is implicated in formation of elastic fibers and has been shown to interfere with the binding between tropoelastin and the glycoprotein fibrillin-1, the main component of microfibrils[178]. Formation of elastic fibers depends on microfibrils, since tropoelastin monomers are deposited onto microfibrils in the ECM during elastic fiber assembly[92]. Additionally, increased elastic fiber degradation has been reported in IPF patients, as they have increased levels of peptide fragments and amino acids that are specific for elastin in their circulation[179,180]. In light of this, the increased levels of HS we observed in IPF lungs may be related to dysregulated elastic fiber homeostasis in IPF.

We found asporin to be more highly expressed in IPF lungs and it was enriched in areas that show signs of active remodeling. Asporin is known to bind TGF-β1 and blocks TGF-β1-induced expression of ECM genes in chondrocytes[181]. Furthermore, TGF-β1 induces expression of asporin[182], which suggests the existence of a regulatory feedback loop. Since TGF-β1 is a potent pro-fibrotic mediator and plays an important role in development of pulmonary fibrosis[183], the increased asporin deposition in IPF lungs may be a consequence of augmented secretion of TGF-β1. Also, profound alterations in GAG content and structure have been reported in the skin of asporin-deficient mice, including an increased amount of CS/DS, lower levels of HS and decreased HS sulfation[184]. This is intriguing considering that we found an increase in both asporin and HS, along with increased HS sulfation, in IPF lungs. To date, asporin has mainly been linked to diseases of bones and joints, especially osteoarthritis[185], but almost no studies have implicated this SLRP in chronic lung diseases. However, Booth et al. analyzed decellularized lungs from IPF patients and healthy donors with mass spectrometry and also found asporin to be elevated in IPF lungs[134]. The increased deposition of asporin we found in honeycomb structures and fibroblastic foci in IPF lungs suggests that it is implicated in the remodeling process, and a relevant question is whether asporin participates in driving disease progression or if the increased deposition is a downstream consequence of another pathological mechanism.

Godin et al. investigated how aging affects the murine lung proteome and how gene expression is modulated in HBEC and human lung fibroblasts after repopulation on decellularized lungs from mice at different ages[186]. They found that several laminins are downregulated with age and that both HBEC and fibroblasts produced less laminin following repopulation on lung scaffolds from old compared to young mice. We found both laminin β1 and γ1 to be downregulated in IPF lungs, and Booth et al. also identified laminins as being less abundant in decellularized IPF lungs compared to controls. Taken together, these findings make sense considering that IPF is a disease characterized by accelerated aging[32] and many cellular and molecular changes in IPF lungs are consistent with premature aging, especially in epithelial cells, which show telomere attrition[31], cellular senescence[30] and mitochondrial dysfunction[187]. Also, taking into account that epithelial cells in IPF lungs are known to undergo apoptosis and EMT[24], it is not surprising that we see a decrease in basement membrane proteins like laminin β1, laminin γ1 and nidogen-1 in IPF lungs. Meanwhile, the elevated levels of collagen VI we found in IPF lungs may be associated with an increased presence of fibroblasts and myofibroblasts, as collagen VI is known to anchor connective tissue cells to the ECM[90] and regulate fibroblast motility[188]. In addition, Booth et al. also reported higher levels of the α1 and α2 chains of collagen VI in IPF lungs[134]. The observed downregulation of ADAM9 in IPF lungs is intriguing considering that Adam9$^{-/-}$ mice are protected from developing a COPD-like lung phenotype in response to cigarette smoke, and bronchial epithelial cells in COPD patients show increased expression of ADAM9[189]. This could mean that ADAM9 plays opposing roles in COPD and IPF.

Lung tissue destruction in COPD is intimately associated with an imbalance between protease and antiprotease activity[190]. We found MMP12 to be increased in COPD bronchial scaffolds as well as in the SDS protein fraction derived from peripheral COPD lung tissue. MMP12 is an elastolytic enzyme with a strong connection to emphysema[190]. It is mainly produced by macrophages, which suggests that the observed increase in MMP12 may be a result of augmented macrophage infiltration. MMP12 activity is also associated with activation of TGF-β, as shown by an in vivo study where integrin $\alpha_V\beta_6$-deficient mice developed MMP12-dependent emphysema because of their inability to activate latent TGF-β in an integrin $\alpha_V\beta_6$-dependent manner[191]. This raises the possibility that the increased MMP12 content in COPD lungs is a consequence of impaired activation of TGF-β. In addition to MMP12, COPD bronchial scaffolds also displayed increased levels of FBLN5, EFEMP1 (fibulin 3) and LOXL1. All of these proteins are known to bind tropoelastin or be directly involved in homeostasis of elastic fibers[192-194] and their altered abundance may reflect a compensatory mechanism for elastic fiber loss in COPD lungs, which show decreased elastin content not only in alveolar parenchyma but also in airway walls[16]. In addition, microfibril-associated protein 4 plays a role in organizing elastic fibers and it was increased in the SDS fraction from peripheral COPD lung tissue[195]. Moreover, several protease inhibitors were more highly expressed in COPD lungs, including SERPINB3,

SERPINB4 and TIMP3. In COPD patients, increased levels of SERPINB3 have been reported in the epithelial lining fluid in response to acute smoking[196] and both SERPINB3 and SERPINB4 are known to have cytoprotective functions[197]. TIMP3 is the only TIMP found in the ECM and Timp3$^{-/-}$ mice start to develop airspace enlargement perinatally[198]. A polymorphism in the TIMP3 gene has also been associated with smoking status and the risk of developing COPD[199]. Taking all of this into account, it is not unlikely that the increased presence of SERPINB3, SERPINB4 and TIMP3 in COPD lungs is the result of a protective response to lung tissue damage. Finally, the increased expression of MMP28 is also consistent with COPD pathology as it regulates recruitment and polarization of macrophages and promotes lung inflammation and remodeling[200]. Taken together, these results point to dysregulation of proteolytic activity and aberrant elastic fiber homeostasis, which are both characteristic features of COPD.

Conclusions

The following conclusions can be drawn based on the results in this thesis:

- Normal HBEC can differentiate into pseudostratified airway epithelium on COPD and normal bronchial scaffolds. COPD bronchial scaffolds induce altered gene expression in normal HBEC.

- COPD HBEC have an impaired ability to initiate ciliated cell differentiation when grown on bronchial scaffolds. COPD HBEC show increased cell cycle progression when grown on COPD compared to normal bronchial scaffolds.

- IPF lungs display increased deposition of glycosaminoglycans and altered structure of heparan sulfate. Highly sulfated heparan sulfate is located in spindle-shaped cells in the alveolar interstitium and in the border zone between areas of dense fibrosis and more normal looking alveolar parenchyma in basement membranes of airways and blood vessels.

- Asporin expression in IPF lungs is enriched in areas that show signs of active remodeling, and IPF and COPD lungs display marked differences in asporin tissue distribution. IPF lungs show altered expression of proteins that regulate cell adhesion, and COPD lungs show altered expression of proteins that regulate proteolytic activity and elastic fiber homeostasis.

Future perspective

This thesis has provided novel insight into ECM alterations in COPD and IPF and how the ECM modulates epithelial cell phenotype in COPD airways, but new questions have also emerged that should be addressed in future studies.

It would be of great interest to identify the mechanistic links between specific bronchial ECM alterations and increased epithelial cell proliferation in COPD airways. This could potentially lead to identification of proteins that could be targeted pharmacologically to prevent epithelial remodeling that leads to basal cell hyperplasia and increased lung cancer risk in COPD patients. Moreover, our findings raise the question of why the gene expression pattern show induction of ciliary genes in HBEC on bronchial scaffolds but not at the ALI. Is ciliated cell differentiation triggered by the scaffolds because of their biochemical composition or because of the structural cues they offer? One of the challenges of studying how tissue-derived ECM scaffolds influence cell behavior is the complexity of the system, which can make it difficult to delineate which factors in the ECM are the main contributors to observed effects on cell phenotype. In this case, a good place to start would be to investigate the proteins we identified as differentially abundant in COPD bronchial scaffolds compared to controls. To isolate the effects of specific proteins on cell function, a simplified system would be preferred. Growing epithelial cells at the air-liquid interface in transwell plates coated with the protein of interest would offer the possibility of analyzing effects on differentiation. Another option could be to seed cells in collagen gels that contain the protein as this would offer a more three-dimensional environment, but epithelial cell differentiation would likely not be feasible. In addition, it would be preferable to choose an experimental setup where you could selectively degrade specific ECM components enzymatically and see how that affects the phenotype of epithelial cells in the presence of the protein being investigated.

Furthermore, our findings from the repopulation model are mostly based on transcriptomic data, although we did confirm differential expression of FOXJ1 also on the protein level. Logical next steps would be to conduct further validation on the protein level and, importantly, to validate the findings using functional studies. We did attempt to isolate HBEC from repopulated scaffolds with the aim of using flow cytometry to run cell cycle analysis and thereby validate the gene expression pattern of increased proliferation observed in repopulated COPD HBEC. Unfortunately, the cell yield we obtained following cell isolation was too low to generate reliable results.

Since IPF lungs showed increased deposition and altered structure of HS, a relevant question is whether these alterations contribute to creating a more pro-fibrotic ECM landscape. Also, it would be of interest to investigate whether asporin regulates production and structure of GAGs in the lungs during pulmonary fibrosis, as we found both asporin and HS to be increased in IPF lungs, and altered deposition and structure of GAGs have been reported in the skin of asporin-deficient mice[184]. The bleomycin model is a frequently used in vivo model of pulmonary fibrosis that could be useful for testing this hypothesis, provided that such a study included both asporin-deficient and wildtype mice. Finally, because of limited tissue supply we only had access to lung tissue samples from patients with end-stage COPD and IPF, but exploring the dynamics of pulmonary ECM remodeling during progression from mild to severe disease could provide valuable information on key drivers behind the remodeling process.

Populärvetenskaplig sammanfattning (Summary in Swedish)

Över 300 miljoner människor i världen lider av kroniskt obstruktiv lungsjukdom (KOL). Sjukdomsbilden är mångfacetterad och varierar mycket mellan patienter, men typiska symptom är andnöd och kronisk hosta. Rökning är den vanligaste orsaken till att man drabbas. För många KOL-patienter går sjukdomen i skov och man löper en ökad risk att få infektioner i lungorna. Symptomen blir värre över tid och man får allt svårare att andas ut ordentligt, vilket beror både på förträngningar i luftvägarna och nedbrytning av lungvävnaden. Denna nedbrytning gör att man successivt förlorar fler och fler av de miljontals mikroskopiska lungblåsor som bygger upp lungorna. Lungblåsorna kallas även alveoler och är nödvändiga för blodets syresättning och avlägsnandet av koldioxid från kroppen. Cellerna som täcker insidan av luftvägarna kallas epitelceller och de förändras i KOL-patienters lungor. De epitelceller som bär på flimmerhår minskar i antal och epitelceller som producerar slem blir allt fler. Flimmerhåren är viktiga eftersom de har som uppgift att transportera slemmet upp mot svalget och därmed rensa lungorna från bakterier och andra skadliga partiklar som man har andats in. Ett minskat antal flimmerhår och en ökad mängd slem gör att KOL-patienter behöver hosta ofta för att rensa luftvägarna.

Idiopatisk pulmonell fibros (IPF) är en annan kronisk lungsjukdom som innebär att den normala vävnaden i patientens lungor successivt förändras till att bli ärrvävnad. Lungorna blir stela och kan inte expandera ordentligt under andning och överföringen av syre till blodet fungerar allt sämre ju mer ärrvävnad som bildas. Sjukdomen har ingen känd orsak, men rökning ökar risken att drabbas och det finns även genetiska riskfaktorer.

Alla kroppens organ är uppbyggda av ett stort antal celler, men utrymmet mellan cellerna är långt ifrån tomt. Här finns ett omfattande nätverk av molekyler som bildar en stödstruktur för cellerna. Detta nätverk kallas för det extracellulära matrix (ECM) och består av ett stort antal proteiner och kolhydrater som utsöndras från cellerna och bildar något som fungerar ungefär som en byggnadsställning cellerna kan fästa vid. Detta ECM-nätverk bidrar dock inte enbart med strukturellt stöd, utan kan dessutom påverka hur celler fungerar genom att binda till molekyler som sitter på cellernas utsida. Det finns forskning som pekar på att ECM-nätverket ser annorlunda ut i lungorna hos

patienter med KOL och IPF. Syftet med det här forskningsprojektet har varit att i detalj studera hur ECM-nätverket är förändrat i lungor från KOL- och IPF-patienter och att undersöka om sådana förändringar är en del av förklaringen till varför epitelcellerna i luftvägarna förändras i den sjuka lungan. För att testa detta utvecklades en ny metod där luftvägar dissekerades från både sjuka och friska lungor och sedan behandlades i olika lösningar så att alla celler tvättades bort men ECM-nätverket blev kvar. Därefter tillfördes epitelceller, som tidigare isolerats från andra lungor, till de tvättade luftvägarna så att de kunde fästa vid luftvägarnas ECM-nätverk. Ett flertal analysmetoder användes sedan för att undersöka hur epitelcellerna hade påverkats och för att ta reda på vilka proteiner och kolhydrater som bygger upp ECM-nätverket.

Resultaten visade att epitelcellerna i KOL-patienters luftvägar förändras både på grund av cellernas inneboende defekter och på grund av förändringar i ECM-nätverket de växer inom. ECM-nätverket visade sig stimulera utveckling av flimmerhår. De processer i epitelcellerna som styr den tidiga utvecklingen av flimmerhår var störda i epitelceller som kom från KOL-patienter jämfört med epitelceller från friska personer. Dessutom visade epitelceller från KOL-patienter tecken på att vilja växa fortare om de kom i kontakt med ECM-nätverk från KOL-patienter jämfört med ECM-nätverk från friska personer. Detta visar att sjukdomsrelaterade förändringar både inne i cellerna och i ECM-nätverket har betydelse för hur cellerna fungerar i KOL-patienters luftvägar. Analysen av hur ECM-nätverket är förändrat i sjuka lungor visade att en specifik typ av kolhydrater, så kallade glykosaminoglykaner, är mer vanligt förekommande i IPF-patienters lungor än i friska lungor. Ett flertal olika proteiner i ECM-nätverket uppvisade också högre eller lägre nivåer i lungor från patienter med KOL och IPF jämfört med lungor från friska personer.

Det behövs ökad kunskap om hur ECM-nätverket är förändrat i KOL- och IPF-patienters lungor och hur detta påverkar lungans celler, eftersom det kan leda till nya idéer och strategier kring hur man kan bromsa eller till och med stoppa sjukdomsförloppet. Förhoppningen är att resultaten från det här forskningsprojektet bidrar till att förbättra möjligheterna för utveckling av nya behandlingsformer som kan hjälpa patienter som lider av dessa svåra lungsjukdomar.

Acknowledgements

I want to express my sincere gratitude to everyone who have supported me inside and outside the lab during all these years.

First and foremost, I want to thank my supervisors **Xiaohong Zhou**, **Oskar Hallgren** and **Gunilla Westergren-Thorsson**. Your guidance, support and knowledge have helped me develop a lot as a scientist.

Thanks to all my fantastic friends, colleagues and lab mates, past and present, at AstraZeneca Gothenburg:

Lisa Öberg, for your invaluable bioinformatic work, and **Outi Vaarala**, for your important contributions to paper I and II.

My lab mates at HA3: **Martijn Manson**, **Sara Bursomanno**, **Lina Odqvist**, **Paulina Kucharzewska**, **Carla Winkler**, **Tina Jellesmark Jensen**, **Anatoly Dzgoev**, **Yue Cui**, **Zala Rojnik** and **Thomas Hochdörfer**.

Johan Mattsson, for nice lunches, pub visits and for teaching me about beer, trees and flow cytometry.

The Hemsedal ski gang: **Maria Ahlefelt** (thanks for keeping me company by the microtome), **Sonya Jackson**, **Corinne Hamblet** (thanks for guiding me through DC), **Kristofer Thörn**, **Micke Bengtsson**, **Kumar Krishnaswamy**, **Arpita Singh**, **Jeremie Boucher**, **Rebecca Riise**, **Gabriel Skogberg**, **Bryan Egner** and **Rob Sheppard**.

All my office mates: **Fanyi Jiang**, **Gustav Johansson**, **Engin Baturcam**, **Elisabeth Ax** and **Stefan Vollmer**.

Thanks also to **Karolina Öst**, **Amy DeMicco**, **Graham Belfield** and everyone in IMED RIA who have contributed in different ways.

Thanks to all my colleagues at BMC in Lund: **Linda Elowsson Rendin**, **Oskar Rosmark**, **Emma Åhrman**, **Sara Rolandsson Enes**, **Emil Tykesson**, **Maria Weitoft**, **Anders Malmström**, **Catharina Müller**, **Anna Löfdahl**, **Mariam Bagher**, **Annika Nybom**, **Anna-Karin Larsson Callerfelt**, **Annika Andersson-Sjöland**, **Marie Wildt**, **Lena Thiman**, **Lisa Karlsson**, **Kristina Rydell-Törmänen**, **Jenny Wigén**, **Mattias Magnusson**, **Anders Aspberg** and **Leif Eriksson**.

One of the best decisions I made during my PhD education was to take up lindy hop in 2016. I want to say thanks to all my dance buddies at West Coast Jitterbugs for reminding me that there is a world outside the lab: **Catharina**, **Jakob**, **Erika**, **Stellan**, **Vard**, **Amanda**, **Anti**, **Jens**, **Johan**, **Emelie**, **Lars**, **Yara**, **Marika**, **Naemi**, **Sandra** and **Pinar**.

Finally, I want to thank my family for all your love and support. Tack **mamma**, **pappa**, **Ulle**, **Stefan**, **Martin**, **Iba**, **Malte**, **Noemi**, **Iris**, **Elmer** och **Sixten**!

References

1 Rabe, K. F. & Watz, H. Chronic obstructive pulmonary disease. *Lancet (London, England)* **389**, 1931-1940, doi:10.1016/s0140-6736(17)31222-9 (2017).

2 Crystal, R. G. Airway basal cells. The "smoking gun" of chronic obstructive pulmonary disease. *American journal of respiratory and critical care medicine* **190**, 1355-1362, doi:10.1164/rccm.201408-1492PP (2014).

3 Plantier, L. *et al.* Physiology of the lung in idiopathic pulmonary fibrosis. *European respiratory review : an official journal of the European Respiratory Society* **27**, doi:10.1183/16000617.0062-2017 (2018).

4 Mouw, J. K., Ou, G. & Weaver, V. M. Extracellular matrix assembly: a multiscale deconstruction. *Nature reviews. Molecular cell biology* **15**, 771-785, doi:10.1038/nrm3902 (2014).

5 Barnes, P. J. Cellular and molecular mechanisms of chronic obstructive pulmonary disease. *Clinics in chest medicine* **35**, 71-86, doi:10.1016/j.ccm.2013.10.004 (2014).

6 Ramsey, S. D. & Hobbs, F. D. Chronic obstructive pulmonary disease, risk factors, and outcome trials: comparisons with cardiovascular disease. *Proceedings of the American Thoracic Society* **3**, 635-640, doi:10.1513/pats.200603-094SS (2006).

7 Vogelmeier, C. F. *et al.* Global Strategy for the Diagnosis, Management, and Prevention of Chronic Obstructive Lung Disease 2017 Report. GOLD Executive Summary. *American journal of respiratory and critical care medicine* **195**, 557-582, doi:10.1164/rccm.201701-0218PP (2017).

8 McDonough, J. E. *et al.* Small-airway obstruction and emphysema in chronic obstructive pulmonary disease. *The New England journal of medicine* **365**, 1567-1575, doi:10.1056/NEJMoa1106955 (2011).

9 Hogg, J. C., Macklem, P. T. & Thurlbeck, W. M. Site and nature of airway obstruction in chronic obstructive lung disease. *The New England journal of medicine* **278**, 1355-1360, doi:10.1056/nejm196806202782501 (1968).

10 Innes, A. L. *et al.* Epithelial mucin stores are increased in the large airways of smokers with airflow obstruction. *Chest* **130**, 1102-1108, doi:10.1378/chest.130.4.1102 (2006).

11 Yaghi, A., Zaman, A., Cox, G. & Dolovich, M. B. Ciliary beating is depressed in nasal cilia from chronic obstructive pulmonary disease subjects. *Respir Med* **106**, 1139-1147, doi:10.1016/j.rmed.2012.04.001 (2012).

12 Hessel, J. *et al.* Intraflagellar transport gene expression associated with short cilia in smoking and COPD. *PloS one* **9**, e85453, doi:10.1371/journal.pone.0085453 (2014).

13 Hogg, J. C. *et al.* The nature of small-airway obstruction in chronic obstructive pulmonary disease. *The New England journal of medicine* **350**, 2645-2653, doi:10.1056/NEJMoa032158 (2004).

14 Rigden, H. M. *et al.* Squamous Metaplasia Is Increased in the Bronchial Epithelium of Smokers with Chronic Obstructive Pulmonary Disease. *PloS one* **11**, e0156009, doi:10.1371/journal.pone.0156009 (2016).

15 Shaykhiev, R. *et al.* Cigarette smoking reprograms apical junctional complex molecular architecture in the human airway epithelium in vivo. *Cellular and molecular life sciences : CMLS* **68**, 877-892, doi:10.1007/s00018-010-0500-x (2011).

16 Eurlings, I. M. *et al.* Similar matrix alterations in alveolar and small airway walls of COPD patients. *BMC pulmonary medicine* **14**, 90, doi:10.1186/1471-2466-14-90 (2014).

17 Kulkarni, T., O'Reilly, P., Antony, V. B., Gaggar, A. & Thannickal, V. J. Matrix Remodeling in Pulmonary Fibrosis and Emphysema. *American journal of respiratory cell and molecular biology* **54**, 751-760, doi:10.1165/rcmb.2015-0166PS (2016).

18 Kent, B. D., Mitchell, P. D. & McNicholas, W. T. Hypoxemia in patients with COPD: cause, effects, and disease progression. *International journal of chronic obstructive pulmonary disease* **6**, 199-208, doi:10.2147/copd.s10611 (2011).

19 Chaouat, A., Naeije, R. & Weitzenblum, E. Pulmonary hypertension in COPD. *The European respiratory journal* **32**, 1371-1385, doi:10.1183/09031936.00015608 (2008).

20 Houghton, A. M. Mechanistic links between COPD and lung cancer. *Nature reviews. Cancer* **13**, 233-245, doi:10.1038/nrc3477 (2013).

21 Beghe, B., Rabe, K. F. & Fabbri, L. M. Phosphodiesterase-4 inhibitor therapy for lung diseases. *American journal of respiratory and critical care medicine* **188**, 271-278, doi:10.1164/rccm.201301-0021PP (2013).

22 Barnes, P. J. Theophylline. *Pharmaceuticals (Basel, Switzerland)* **3**, 725-747, doi:10.3390/ph3030725 (2010).

23 Kew, K. M., Dias, S. & Cates, C. J. Long-acting inhaled therapy (beta-agonists, anticholinergics and steroids) for COPD: a network meta-analysis. *The Cochrane database of systematic reviews*, Cd010844, doi:10.1002/14651858.CD010844.pub2 (2014).

24 Martinez, F. J. *et al.* Idiopathic pulmonary fibrosis. *Nature reviews. Disease primers* **3**, 17074, doi:10.1038/nrdp.2017.74 (2017).

25 Mathai, S. K., Newton, C. A., Schwartz, D. A. & Garcia, C. K. Pulmonary fibrosis in the era of stratified medicine. *Thorax* **71**, 1154-1160, doi:10.1136/thoraxjnl-2016-209172 (2016).

26 Raghu, G. *et al.* An official ATS/ERS/JRS/ALAT statement: idiopathic pulmonary fibrosis: evidence-based guidelines for diagnosis and management. *American journal of respiratory and critical care medicine* **183**, 788-824, doi:10.1164/rccm.2009-040GL (2011).

27 Cavazza, A. *et al.* The role of histology in idiopathic pulmonary fibrosis: an update. *Respir Med* **104 Suppl 1**, S11-22, doi:10.1016/j.rmed.2010.03.013 (2010).

28 Selman, M. & Pardo, A. Revealing the pathogenic and aging-related mechanisms of the enigmatic idiopathic pulmonary fibrosis. an integral model. *American journal of respiratory and critical care medicine* **189**, 1161-1172, doi:10.1164/rccm.201312-2221PP (2014).

29 King, T. E., Jr., Pardo, A. & Selman, M. Idiopathic pulmonary fibrosis. *Lancet (London, England)* **378**, 1949-1961, doi:10.1016/s0140-6736(11)60052-4 (2011).

30 Minagawa, S. *et al.* Accelerated epithelial cell senescence in IPF and the inhibitory role of SIRT6 in TGF-beta-induced senescence of human bronchial epithelial cells. *American journal of physiology. Lung cellular and molecular physiology* **300**, L391-401, doi:10.1152/ajplung.00097.2010 (2011).

31 Alder, J. K. *et al.* Short telomeres are a risk factor for idiopathic pulmonary fibrosis. *Proceedings of the National Academy of Sciences of the United States of America* **105**, 13051-13056, doi:10.1073/pnas.0804280105 (2008).

32 Selman, M., Lopez-Otin, C. & Pardo, A. Age-driven developmental drift in the pathogenesis of idiopathic pulmonary fibrosis. *The European respiratory journal* **48**, 538-552, doi:10.1183/13993003.00398-2016 (2016).

33 Noble, P. W. *et al.* Pirfenidone in patients with idiopathic pulmonary fibrosis (CAPACITY): two randomised trials. *Lancet (London, England)* **377**, 1760-1769, doi:10.1016/s0140-6736(11)60405-4 (2011).

34 King, T. E., Jr. *et al.* A phase 3 trial of pirfenidone in patients with idiopathic pulmonary fibrosis. *The New England journal of medicine* **370**, 2083-2092, doi:10.1056/NEJMoa1402582 (2014).

35 Richeldi, L. *et al.* Efficacy and safety of nintedanib in idiopathic pulmonary fibrosis. *The New England journal of medicine* **370**, 2071-2082, doi:10.1056/NEJMoa1402584 (2014).

36 Reichmann, W. M., Yu, Y. F., Macaulay, D., Wu, E. Q. & Nathan, S. D. Change in forced vital capacity and associated subsequent outcomes in patients with newly diagnosed idiopathic pulmonary fibrosis. *BMC pulmonary medicine* **15**, 167, doi:10.1186/s12890-015-0161-5 (2015).

37 Montoro, D. T. *et al.* A revised airway epithelial hierarchy includes CFTR-expressing ionocytes. *Nature*, doi:10.1038/s41586-018-0393-7 (2018).

38 Crystal, R. G., Randell, S. H., Engelhardt, J. F., Voynow, J. & Sunday, M. E. Airway epithelial cells: current concepts and challenges. *Proceedings of the American Thoracic Society* **5**, 772-777, doi:10.1513/pats.200805-041HR (2008).

39 Georas, S. N. & Rezaee, F. Epithelial barrier function: at the front line of asthma immunology and allergic airway inflammation. *The Journal of allergy and clinical immunology* **134**, 509-520, doi:10.1016/j.jaci.2014.05.049 (2014).

40 Amatngalim, G. D. *et al.* Antibacterial Defense of Human Airway Epithelial Cells from Chronic Obstructive Pulmonary Disease Patients Induced by Acute Exposure to Nontypeable Haemophilus influenzae: Modulation by Cigarette Smoke. *Journal of innate immunity* **9**, 359-374, doi:10.1159/000455193 (2017).

41 Mori, K. *et al.* Synergistic Proinflammatory Responses by IL-17A and Toll-Like Receptor 3 in Human Airway Epithelial Cells. *PloS one* **10**, e0139491, doi:10.1371/journal.pone.0139491 (2015).

42 Choksi, S. P., Lauter, G., Swoboda, P. & Roy, S. Switching on cilia: transcriptional networks regulating ciliogenesis. *Development (Cambridge, England)* **141**, 1427-1441, doi:10.1242/dev.074666 (2014).

43 Rajavelu, P. *et al.* Airway epithelial SPDEF integrates goblet cell differentiation and pulmonary Th2 inflammation. *J Clin Invest* **125**, 2021-2031, doi:10.1172/jci79422 (2015).

44 Chen, G. *et al.* Foxa3 induces goblet cell metaplasia and inhibits innate antiviral immunity. *American journal of respiratory and critical care medicine* **189**, 301-313, doi:10.1164/rccm.201306-1181OC (2014).

45 Saetta, M. *et al.* Goblet cell hyperplasia and epithelial inflammation in peripheral airways of smokers with both symptoms of chronic bronchitis and chronic airflow limitation. *American journal of respiratory and critical care medicine* **161**, 1016-1021, doi:10.1164/ajrccm.161.3.9907080 (2000).

46 Sethi, S. & Murphy, T. F. Infection in the pathogenesis and course of chronic obstructive pulmonary disease. *The New England journal of medicine* **359**, 2355-2365, doi:10.1056/NEJMra0800353 (2008).

47 Leopold, P. L. *et al.* Smoking is associated with shortened airway cilia. *PloS one* **4**, e8157, doi:10.1371/journal.pone.0008157 (2009).

48 Simet, S. M. *et al.* Long-term cigarette smoke exposure in a mouse model of ciliated epithelial cell function. *American journal of respiratory cell and molecular biology* **43**, 635-640, doi:10.1165/rcmb.2009-0297OC (2010).

49 Sisson, J. H. *et al.* Smoke and viral infection cause cilia loss detectable by bronchoalveolar lavage cytology and dynein ELISA. *American journal of respiratory and critical care medicine* **149**, 205-213, doi:10.1164/ajrccm.149.1.8111584 (1994).

50 Schamberger, A. C., Staab-Weijnitz, C. A., Mise-Racek, N. & Eickelberg, O. Cigarette smoke alters primary human bronchial epithelial cell differentiation at the air-liquid interface. *Scientific reports* **5**, 8163, doi:10.1038/srep08163 (2015).

51 Brekman, A., Walters, M. S., Tilley, A. E. & Crystal, R. G. FOXJ1 prevents cilia growth inhibition by cigarette smoke in human airway epithelium in vitro. *American journal of*

respiratory cell and molecular biology **51**, 688-700, doi:10.1165/rcmb.2013-0363OC (2014).

52 Heijink, I. H., Noordhoek, J. A., Timens, W., van Oosterhout, A. J. & Postma, D. S. Abnormalities in airway epithelial junction formation in chronic obstructive pulmonary disease. *American journal of respiratory and critical care medicine* **189**, 1439-1442, doi:10.1164/rccm.201311-1982LE (2014).

53 Heijink, I. H., Brandenburg, S. M., Postma, D. S. & van Oosterhout, A. J. Cigarette smoke impairs airway epithelial barrier function and cell-cell contact recovery. *The European respiratory journal* **39**, 419-428, doi:10.1183/09031936.00193810 (2012).

54 de Boer, W. I. *et al.* Expression of epidermal growth factors and their receptors in the bronchial epithelium of subjects with chronic obstructive pulmonary disease. *American journal of clinical pathology* **125**, 184-192, doi:10.1309/w1ax-kgt7-ua37-x257 (2006).

55 Ramos, F. L., Krahnke, J. S. & Kim, V. Clinical issues of mucus accumulation in COPD. *International journal of chronic obstructive pulmonary disease* **9**, 139-150, doi:10.2147/copd.s38938 (2014).

56 Kim, V. *et al.* Chronic bronchitis and current smoking are associated with more goblet cells in moderate to severe COPD and smokers without airflow obstruction. *PloS one* **10**, e0116108, doi:10.1371/journal.pone.0116108 (2015).

57 Takeyama, K. *et al.* Activation of epidermal growth factor receptors is responsible for mucin synthesis induced by cigarette smoke. *American journal of physiology. Lung cellular and molecular physiology* **280**, L165-172, doi:10.1152/ajplung.2001.280.1.L165 (2001).

58 Shi, J. *et al.* Cigarette Smoke-Induced Acquired Dysfunction of Cystic Fibrosis Transmembrane Conductance Regulator in the Pathogenesis of Chronic Obstructive Pulmonary Disease. **2018**, 6567578, doi:10.1155/2018/6567578 (2018).

59 Kalluri, R. & Weinberg, R. A. The basics of epithelial-mesenchymal transition. *The Journal of Clinical Investigation* **119**, 1420-1428, doi:10.1172/JCI39104 (2009).

60 Zeisberg, M. & Neilson, E. G. Biomarkers for epithelial-mesenchymal transitions. *The Journal of Clinical Investigation* **119**, 1429-1437, doi:10.1172/JCI36183 (2009).

61 Milara, J., Peiro, T., Serrano, A. & Cortijo, J. Epithelial to mesenchymal transition is increased in patients with COPD and induced by cigarette smoke. *Thorax* **68**, 410-420, doi:10.1136/thoraxjnl-2012-201761 (2013).

62 Gohy, S. T. *et al.* Imprinting of the COPD airway epithelium for dedifferentiation and mesenchymal transition. *The European respiratory journal* **45**, 1258-1272, doi:10.1183/09031936.00135814 (2015).

63 Araya, J. *et al.* Squamous metaplasia amplifies pathologic epithelial-mesenchymal interactions in COPD patients. *J Clin Invest* **117**, 3551-3562, doi:10.1172/jci32526 (2007).

64 Mecham, R. P. Overview of extracellular matrix. *Current protocols in cell biology* **Chapter 10**, Unit 10.11, doi:10.1002/0471143030.cb1001s57 (2012).

65 Naba, A. *et al.* The matrisome: in silico definition and in vivo characterization by proteomics of normal and tumor extracellular matrices. *Molecular & cellular proteomics : MCP* **11**, M111.014647, doi:10.1074/mcp.M111.014647 (2012).

66 Iozzo, R. V. & Schaefer, L. Proteoglycan form and function: A comprehensive nomenclature of proteoglycans. *Matrix biology : journal of the International Society for Matrix Biology* **42**, 11-55, doi:10.1016/j.matbio.2015.02.003 (2015).

67 Elfenbein, A. & Simons, M. Syndecan-4 signaling at a glance. *Journal of cell science* **126**, 3799-3804, doi:10.1242/jcs.124636 (2013).

68 Mohammadi, M., Olsen, S. K. & Ibrahimi, O. A. Structural basis for fibroblast growth factor receptor activation. *Cytokine & growth factor reviews* **16**, 107-137, doi:10.1016/j.cytogfr.2005.01.008 (2005).

69 Huang, R. *et al.* Inhibition of versican synthesis by antisense alters smooth muscle cell phenotype and induces elastic fiber formation in vitro and in neointima after vessel injury. *Circulation research* **98**, 370-377, doi:10.1161/01.RES.0000202051.28319.c8 (2006).

70 Sanches, J. C. *et al.* Collagen fibril organization in the pregnant endometrium of decorin-deficient mice. *Journal of anatomy* **216**, 144-155, doi:10.1111/j.1469-7580.2009.01170.x (2010).

71 Hildebrand, A. *et al.* Interaction of the small interstitial proteoglycans biglycan, decorin and fibromodulin with transforming growth factor beta. *The Biochemical journal* **302 (Pt 2)**, 527-534 (1994).

72 Baker, S. M. *et al.* TGF-beta/extracellular matrix interactions in dentin matrix: a role in regulating sequestration and protection of bioactivity. *Calcified tissue international* **85**, 66-74, doi:10.1007/s00223-009-9248-4 (2009).

73 Handel, T. M., Johnson, Z., Crown, S. E., Lau, E. K. & Proudfoot, A. E. Regulation of protein function by glycosaminoglycans--as exemplified by chemokines. *Annual review of biochemistry* **74**, 385-410, doi:10.1146/annurev.biochem.72.121801.161747 (2005).

74 Prydz, K. Determinants of Glycosaminoglycan (GAG) Structure. *Biomolecules* **5**, 2003-2022, doi:10.3390/biom5032003 (2015).

75 Xu, D. & Esko, J. D. Demystifying heparan sulfate-protein interactions. *Annual review of biochemistry* **83**, 129-157, doi:10.1146/annurev-biochem-060713-035314 (2014).

76 Abramsson, A. *et al.* Defective N-sulfation of heparan sulfate proteoglycans limits PDGF-BB binding and pericyte recruitment in vascular development. *Genes & development* **21**, 316-331, doi:10.1101/gad.398207 (2007).

77 Desai, U. R., Petitou, M., Bjork, I. & Olson, S. T. Mechanism of heparin activation of antithrombin. Role of individual residues of the pentasaccharide activating sequence in the recognition of native and activated states of antithrombin. *The Journal of biological chemistry* **273**, 7478-7487 (1998).

78 Rauch, U., Feng, K. & Zhou, X. H. Neurocan: a brain chondroitin sulfate proteoglycan. *Cellular and molecular life sciences : CMLS* **58**, 1842-1856, doi:10.1007/pl00000822 (2001).

79 Yamaguchi, Y. Brevican: a major proteoglycan in adult brain. *Perspectives on developmental neurobiology* **3**, 307-317 (1996).

80 Roughley, P. J. & Mort, J. S. The role of aggrecan in normal and osteoarthritic cartilage. *Journal of experimental orthopaedics* **1**, 8, doi:10.1186/s40634-014-0008-7 (2014).

81 Andersson-Sjoland, A. *et al.* Versican in inflammation and tissue remodeling: the impact on lung disorders. *Glycobiology* **25**, 243-251, doi:10.1093/glycob/cwu120 (2015).

82 Giri, S. N. *et al.* Antifibrotic effect of decorin in a bleomycin hamster model of lung fibrosis. *Biochemical pharmacology* **54**, 1205-1216 (1997).

83 Kolb, M., Margetts, P. J., Sime, P. J. & Gauldie, J. Proteoglycans decorin and biglycan differentially modulate TGF-beta-mediated fibrotic responses in the lung. *American journal of physiology. Lung cellular and molecular physiology* **280**, L1327-1334, doi:10.1152/ajplung.2001.280.6.L1327 (2001).

84 Nastase, M. V., Iozzo, R. V. & Schaefer, L. Key roles for the small leucine-rich proteoglycans in renal and pulmonary pathophysiology. *Biochimica et biophysica acta* **1840**, 2460-2470, doi:10.1016/j.bbagen.2014.01.035 (2014).

85 Sarrazin, S., Lamanna, W. C. & Esko, J. D. Heparan sulfate proteoglycans. *Cold Spring Harb Perspect Biol* **3**, doi:10.1101/cshperspect.a004952 (2011).

86 Morgan, M. R., Humphries, M. J. & Bass, M. D. Synergistic control of cell adhesion by integrins and syndecans. *Nature reviews. Molecular cell biology* **8**, 957-969, doi:10.1038/nrm2289 (2007).

87 Okina, E., Manon-Jensen, T., Whiteford, J. R. & Couchman, J. R. Syndecan proteoglycan contributions to cytoskeletal organization and contractility. *Scandinavian journal of medicine & science in sports* **19**, 479-489, doi:10.1111/j.1600-0838.2009.00941.x (2009).

88 Bezakova, G. & Ruegg, M. A. New insights into the roles of agrin. *Nature reviews. Molecular cell biology* **4**, 295-308, doi:10.1038/nrm1074 (2003).

89 Khoshnoodi, J., Pedchenko, V. & Hudson, B. G. Mammalian collagen IV. *Microscopy research and technique* **71**, 357-370, doi:10.1002/jemt.20564 (2008).

90 Cescon, M., Gattazzo, F., Chen, P. & Bonaldo, P. Collagen VI at a glance. *Journal of cell science* **128**, 3525-3531, doi:10.1242/jcs.169748 (2015).

91 Mecham, R. P. Elastin in lung development and disease pathogenesis. *Matrix biology : journal of the International Society for Matrix Biology*, doi:10.1016/j.matbio.2018.01.005 (2018).

92 Baldwin, A. K., Simpson, A., Steer, R., Cain, S. A. & Kielty, C. M. Elastic fibres in health and disease. *Expert reviews in molecular medicine* **15**, e8, doi:10.1017/erm.2013.9 (2013).

93 Singh, P., Carraher, C. & Schwarzbauer, J. E. Assembly of fibronectin extracellular matrix. *Annual review of cell and developmental biology* **26**, 397-419, doi:10.1146/annurev-cellbio-100109-104020 (2010).

94 Mao, Y. & Schwarzbauer, J. E. Fibronectin fibrillogenesis, a cell-mediated matrix assembly process. *Matrix biology : journal of the International Society for Matrix Biology* **24**, 389-399, doi:10.1016/j.matbio.2005.06.008 (2005).

95 Nguyen, N. M. & Senior, R. M. Laminin isoforms and lung development: all isoforms are not equal. *Developmental biology* **294**, 271-279, doi:10.1016/j.ydbio.2006.03.032 (2006).

96 Pozzi, A., Yurchenco, P. D. & Iozzo, R. V. The nature and biology of basement membranes. *Matrix biology : journal of the International Society for Matrix Biology* **57-58**, 1-11, doi:10.1016/j.matbio.2016.12.009 (2017).

97 Ho, M. S., Bose, K., Mokkapati, S., Nischt, R. & Smyth, N. Nidogens-Extracellular matrix linker molecules. *Microscopy research and technique* **71**, 387-395, doi:10.1002/jemt.20567 (2008).

98 Uechi, G., Sun, Z., Schreiber, E. M., Halfter, W. & Balasubramani, M. Proteomic View of Basement Membranes from Human Retinal Blood Vessels, Inner Limiting Membranes, and Lens Capsules. *Journal of proteome research*, doi:10.1021/pr5002065 (2014).

99 Durbeej, M. Laminins. *Cell and tissue research* **339**, 259-268, doi:10.1007/s00441-009-0838-2 (2010).

100 Aumailley, M. *et al.* A simplified laminin nomenclature. *Matrix biology : journal of the International Society for Matrix Biology* **24**, 326-332, doi:10.1016/j.matbio.2005.05.006 (2005).

101 Poschl, E. *et al.* Collagen IV is essential for basement membrane stability but dispensable for initiation of its assembly during early development. *Development (Cambridge, England)* **131**, 1619-1628, doi:10.1242/dev.01037 (2004).

102 Brown, J. C., Sasaki, T., Gohring, W., Yamada, Y. & Timpl, R. The C-terminal domain V of perlecan promotes beta1 integrin-mediated cell adhesion, binds heparin, nidogen and fibulin-2 and can be modified by glycosaminoglycans. *European journal of biochemistry* **250**, 39-46 (1997).

103 Talts, J. F., Andac, Z., Gohring, W., Brancaccio, A. & Timpl, R. Binding of the G domains of laminin alpha1 and alpha2 chains and perlecan to heparin, sulfatides, alpha-dystroglycan and several extracellular matrix proteins. *The EMBO journal* **18**, 863-870, doi:10.1093/emboj/18.4.863 (1999).

104 Behrens, D. T. *et al.* The epidermal basement membrane is a composite of separate laminin- or collagen IV-containing networks connected by aggregated perlecan, but not by nidogens. *The Journal of biological chemistry* **287**, 18700-18709, doi:10.1074/jbc.M111.336073 (2012).

105 Gubbiotti, M. A., Neill, T. & Iozzo, R. V. A current view of perlecan in physiology and pathology: A mosaic of functions. *Matrix biology : journal of the International Society for Matrix Biology* **57-58**, 285-298, doi:10.1016/j.matbio.2016.09.003 (2017).

106 Coraux, C., Roux, J., Jolly, T. & Birembaut, P. Epithelial cell-extracellular matrix interactions and stem cells in airway epithelial regeneration. *Proceedings of the American Thoracic Society* **5**, 689-694, doi:10.1513/pats.200801-010AW (2008).

107 Rosmark, O. *et al.* Quantifying extracellular matrix turnover in human lung scaffold cultures. **8**, 5409, doi:10.1038/s41598-018-23702-x (2018).

108 Srichai, M. B. & Zent, R. Integrin Structure and Function. *In Cell-Extracellular Matrix Interactions in Cancer (chapter 2)*, doi:10.1007/978-1-4419-0814-8_2 (2010).

109 Moser, M., Legate, K. R., Zent, R. & Fassler, R. The tail of integrins, talin, and kindlins. *Science (New York, N.Y.)* **324**, 895-899, doi:10.1126/science.1163865 (2009).

110 White, S. R., Wojcik, K. R., Gruenert, D., Sun, S. & Dorscheid, D. R. Airway epithelial cell wound repair mediated by alpha-dystroglycan. *American journal of respiratory cell and molecular biology* **24**, 179-186, doi:10.1165/ajrcmb.24.2.3993 (2001).

111 Winder, S. J. The complexities of dystroglycan. *Trends in biochemical sciences* **26**, 118-124 (2001).

112 Kikkawa, Y. & Miner, J. H. Review: Lutheran/B-CAM: a laminin receptor on red blood cells and in various tissues. *Connective tissue research* **46**, 193-199, doi:10.1080/03008200500344074 (2005).

113 DiGiacomo, V. & Meruelo, D. Looking into laminin receptor: critical discussion regarding the non-integrin 37/67-kDa laminin receptor/RPSA protein. *Biological reviews of the Cambridge Philosophical Society* **91**, 288-310, doi:10.1111/brv.12170 (2016).

114 Li, S. *et al.* Laminin-sulfatide binding initiates basement membrane assembly and enables receptor signaling in Schwann cells and fibroblasts. *The Journal of cell biology* **169**, 179-189, doi:10.1083/jcb.200501098 (2005).

115 Senbanjo, L. T. & Chellaiah, M. A. CD44: A Multifunctional Cell Surface Adhesion Receptor Is a Regulator of Progression and Metastasis of Cancer Cells. *Frontiers in cell and developmental biology* **5**, 18, doi:10.3389/fcell.2017.00018 (2017).

116 Bourguignon, L. Y., Shiina, M. & Li, J. J. Hyaluronan-CD44 interaction promotes oncogenic signaling, microRNA functions, chemoresistance, and radiation resistance in cancer stem cells leading to tumor progression. *Advances in cancer research* **123**, 255-275, doi:10.1016/b978-0-12-800092-2.00010-1 (2014).

117 Leitinger, B. Discoidin domain receptor functions in physiological and pathological conditions. *International review of cell and molecular biology* **310**, 39-87, doi:10.1016/b978-0-12-800180-6.00002-5 (2014).

118 Borza, C. M. *et al.* Discoidin domain receptor 1 kinase activity is required for regulating collagen IV synthesis. *Matrix biology : journal of the International Society for Matrix Biology* **57-58**, 258-271, doi:10.1016/j.matbio.2016.11.009 (2017).

119 Eswaramoorthy, R. *et al.* DDR1 regulates the stabilization of cell surface E-cadherin and E-cadherin-mediated cell aggregation. *Journal of cellular physiology* **224**, 387-397, doi:10.1002/jcp.22134 (2010).

120 Roberts, M. E., Magowan, L., Hall, I. P. & Johnson, S. R. Discoidin domain receptor 1 regulates bronchial epithelial repair and matrix metalloproteinase production. *The European respiratory journal* **37**, 1482-1493, doi:10.1183/09031936.00039710 (2011).

121 Annoni, R. *et al.* Extracellular matrix composition in COPD. *The European respiratory journal* **40**, 1362-1373, doi:10.1183/09031936.00192611 (2012).

122 Kranenburg, A. R. *et al.* Enhanced bronchial expression of extracellular matrix proteins in chronic obstructive pulmonary disease. *American journal of clinical pathology* **126**, 725-735 (2006).

123 Hogg, J. C., McDonough, J. E., Gosselink, J. V. & Hayashi, S. What drives the peripheral lung-remodeling process in chronic obstructive pulmonary disease? *Proceedings of the American Thoracic Society* **6**, 668-672, doi:10.1513/pats.200907-079DP (2009).

124 van Straaten, J. F. *et al.* Proteoglycan changes in the extracellular matrix of lung tissue from patients with pulmonary emphysema. *Modern pathology : an official journal of the United States and Canadian Academy of Pathology, Inc* **12**, 697-705 (1999).

125 Douglas, T., Heinemann, S., Bierbaum, S., Scharnweber, D. & Worch, H. Fibrillogenesis of collagen types I, II, and III with small leucine-rich proteoglycans decorin and biglycan. *Biomacromolecules* **7**, 2388-2393, doi:10.1021/bm0603746 (2006).

126 Merrilees, M. J. *et al.* Changes in elastin, elastin binding protein and versican in alveoli in chronic obstructive pulmonary disease. *Respiratory research* **9**, 41, doi:10.1186/1465-9921-9-41 (2008).

127 Hallgren, O. *et al.* Altered fibroblast proteoglycan production in COPD. *Respiratory research* **11**, 55, doi:10.1186/1465-9921-11-55 (2010).

128 Hinek, A. & Wilson, S. E. Impaired elastogenesis in Hurler disease: dermatan sulfate accumulation linked to deficiency in elastin-binding protein and elastic fiber assembly. *The American journal of pathology* **156**, 925-938, doi:10.1016/s0002-9440(10)64961-9 (2000).

129 Hinek, A. *et al.* Decreased elastin deposition and high proliferation of fibroblasts from Costello syndrome are related to functional deficiency in the 67-kD elastin-binding protein. *American journal of human genetics* **66**, 859-872, doi:10.1086/302829 (2000).

130 Black, P. N. *et al.* Changes in elastic fibres in the small airways and alveoli in COPD. *The European respiratory journal* **31**, 998-1004, doi:10.1183/09031936.00017207 (2008).

131 Elkington, P. T. & Friedland, J. S. Matrix metalloproteinases in destructive pulmonary pathology. *Thorax* **61**, 259-266, doi:10.1136/thx.2005.051979 (2006).

132 Baraldo, S. *et al.* Matrix metalloproteinase-2 protein in lung periphery is related to COPD progression. *Chest* **132**, 1733-1740, doi:10.1378/chest.06-2819 (2007).

133 Klingberg, F., Hinz, B. & White, E. S. The myofibroblast matrix: implications for tissue repair and fibrosis. *The Journal of pathology* **229**, 298-309, doi:10.1002/path.4104 (2013).

134 Booth, A. J. *et al.* Acellular normal and fibrotic human lung matrices as a culture system for in vitro investigation. *American journal of respiratory and critical care medicine* **186**, 866-876, doi:10.1164/rccm.201204-0754OC (2012).

135 Calderwood, C. *et al.* P113 Secreted Lysyl Oxidase is Elevated in the Bronchoalveolar Lavage Fluid of Patients with Idiopathic Pulmonary Fibrosis. *Thorax* **67**, A111-A111, doi:10.1136/thoraxjnl-2012-202678.396 (2012).

136 Olsen, K. C. *et al.* Transglutaminase 2 and its role in pulmonary fibrosis. *American journal of respiratory and critical care medicine* **184**, 699-707, doi:10.1164/rccm.201101-0013OC (2011).

137 Liu, F. *et al.* Feedback amplification of fibrosis through matrix stiffening and COX-2 suppression. *The Journal of cell biology* **190**, 693-706, doi:10.1083/jcb.201004082 (2010).

138 Marinkovic, A., Liu, F. & Tschumperlin, D. J. Matrices of physiologic stiffness potently inactivate idiopathic pulmonary fibrosis fibroblasts. *American journal of respiratory cell and molecular biology* **48**, 422-430, doi:10.1165/rcmb.2012-0335OC (2013).

139 Gimenez, A. *et al.* Dysregulated Collagen Homeostasis by Matrix Stiffening and TGF-beta1 in Fibroblasts from Idiopathic Pulmonary Fibrosis Patients: Role of FAK/Akt. *International journal of molecular sciences* **18**, doi:10.3390/ijms18112431 (2017).

140 Naik, P. K. *et al.* Periostin promotes fibrosis and predicts progression in patients with idiopathic pulmonary fibrosis. *American journal of physiology. Lung cellular and molecular physiology* **303**, L1046-1056, doi:10.1152/ajplung.00139.2012 (2012).

141 Estany, S. *et al.* Lung fibrotic tenascin-C upregulation is associated with other extracellular matrix proteins and induced by TGFbeta1. *BMC pulmonary medicine* **14**, 120, doi:10.1186/1471-2466-14-120 (2014).

142 Jones, M. G. *et al.* Three-dimensional characterization of fibroblast foci in idiopathic pulmonary fibrosis. *JCI insight* **1**, doi:10.1172/jci.insight.86375 (2016).

143 Kliment, C. R. *et al.* Oxidative stress alters syndecan-1 distribution in lungs with pulmonary fibrosis. *The Journal of biological chemistry* **284**, 3537-3545, doi:10.1074/jbc.M807001200 (2009).

144 Ruiz, X. D. *et al.* Syndecan-2 is a novel target of insulin-like growth factor binding protein-3 and is over-expressed in fibrosis. *PloS one* **7**, e43049, doi:10.1371/journal.pone.0043049 (2012).

145 Jiang, D. *et al.* Inhibition of pulmonary fibrosis in mice by CXCL10 requires glycosaminoglycan binding and syndecan-4. *J Clin Invest* **120**, 2049-2057, doi:10.1172/jci38644 (2010).

146 Teder, P. *et al.* Resolution of lung inflammation by CD44. *Science (New York, N.Y.)* **296**, 155-158, doi:10.1126/science.1069659 (2002).

147 Bjermer, L., Lundgren, R. & Hallgren, R. Hyaluronan and type III procollagen peptide concentrations in bronchoalveolar lavage fluid in idiopathic pulmonary fibrosis. *Thorax* **44**, 126-131 (1989).

148 Li, Y. *et al.* Severe lung fibrosis requires an invasive fibroblast phenotype regulated by hyaluronan and CD44. *The Journal of experimental medicine* **208**, 1459-1471, doi:10.1084/jem.20102510 (2011).

149 Stachtea, X. N. *et al.* Dermatan Sulfate-Free Mice Display Embryological Defects and Are Neonatal Lethal Despite Normal Lymphoid and Non-Lymphoid Organogenesis. *PloS one* **10**, e0140279, doi:10.1371/journal.pone.0140279 (2015).

150 Kim, D., Langmead, B. & Salzberg, S. L. HISAT: a fast spliced aligner with low memory requirements. **12**, 357-360, doi:10.1038/nmeth.3317 (2015).

151 Liao, Y., Smyth, G. K. & Shi, W. featureCounts: an efficient general purpose program for assigning sequence reads to genomic features. *Bioinformatics (Oxford, England)* **30**, 923-930, doi:10.1093/bioinformatics/btt656 (2014).

152 Love, M. I., Huber, W. & Anders, S. Moderated estimation of fold change and dispersion for RNA-seq data with DESeq2. *Genome biology* **15**, 550, doi:10.1186/s13059-014-0550-8 (2014).

153 Kramer, A., Green, J., Pollard, J., Jr. & Tugendreich, S. Causal analysis approaches in Ingenuity Pathway Analysis. *Bioinformatics (Oxford, England)* **30**, 523-530, doi:10.1093/bioinformatics/btt703 (2014).

154 Ashburner, M. *et al.* Gene ontology: tool for the unification of biology. The Gene Ontology Consortium. *Nature genetics* **25**, 25-29, doi:10.1038/75556 (2000).

155 Expansion of the Gene Ontology knowledgebase and resources. *Nucleic acids research* **45**, D331-d338, doi:10.1093/nar/gkw1108 (2017).

156 Mi, H. *et al.* PANTHER version 11: expanded annotation data from Gene Ontology and Reactome pathways, and data analysis tool enhancements. *Nucleic acids research* **45**, D183-d189, doi:10.1093/nar/gkw1138 (2017).

157 Hedstrom, U. *et al.* Bronchial extracellular matrix from COPD patients induces altered gene expression in repopulated primary human bronchial epithelial cells. *Scientific reports* **8**, 3502, doi:10.1038/s41598-018-21727-w (2018).

158 Wisniewski, J. R., Zougman, A., Nagaraj, N. & Mann, M. Universal sample preparation method for proteome analysis. *Nature methods* **6**, 359-362, doi:10.1038/nmeth.1322 (2009).

159 Chursa, U. *et al.* Overexpression of protein kinase STK25 in mice exacerbates ectopic lipid accumulation, mitochondrial dysfunction and insulin resistance in skeletal muscle. *Diabetologia* **60**, 553-567, doi:10.1007/s00125-016-4171-5 (2017).

160 Oras, J. *et al.* Anaesthetic-induced cardioprotection in an experimental model of the Takotsubo syndrome - isoflurane vs. propofol. *Acta anaesthesiologica Scandinavica* **61**, 309-321, doi:10.1111/aas.12857 (2017).

161 Malmstrom, E. *et al.* Large-scale inference of protein tissue origin in gram-positive sepsis plasma using quantitative targeted proteomics. **7**, 10261, doi:10.1038/ncomms10261 (2016).

162 Hughes, C. S. *et al.* Ultrasensitive proteome analysis using paramagnetic bead technology. *Molecular systems biology* **10**, 757, doi:10.15252/msb.20145625 (2014).

163 Deutsch, E. W. *et al.* A guided tour of the Trans-Proteomic Pipeline. *Proteomics* **10**, 1150-1159, doi:10.1002/pmic.200900375 (2010).

164 Deutsch, E. W. *et al.* Trans-Proteomic Pipeline, a standardized data processing pipeline for large-scale reproducible proteomics informatics. *Proteomics. Clinical applications* **9**, 745-754, doi:10.1002/prca.201400164 (2015).

165 Reiter, L. *et al.* Protein identification false discovery rates for very large proteomics data sets generated by tandem mass spectrometry. *Molecular & cellular proteomics : MCP* **8**, 2405-2417, doi:10.1074/mcp.M900317-MCP200 (2009).

166 Rost, H. L. *et al.* TRIC: an automated alignment strategy for reproducible protein quantification in targeted proteomics. **13**, 777-783, doi:10.1038/nmeth.3954 (2016).

167 Rost, H. L. *et al.* OpenSWATH enables automated, targeted analysis of data-independent acquisition MS data. **32**, 219-223, doi:10.1038/nbt.2841 (2014).

168 Bauch, A. *et al.* openBIS: a flexible framework for managing and analyzing complex data in biology research. *BMC bioinformatics* **12**, 468, doi:10.1186/1471-2105-12-468 (2011).

169 Gilpin, S. E. *et al.* Enhanced lung epithelial specification of human induced pluripotent stem cells on decellularized lung matrix. *The Annals of thoracic surgery* **98**, 1721-1729; discussion 1729, doi:10.1016/j.athoracsur.2014.05.080 (2014).

170 Shojaie, S. *et al.* Acellular Lung Scaffolds Direct Differentiation of Endoderm to Functional Airway Epithelial Cells: Requirement of Matrix-Bound HS Proteoglycans. *Stem Cell Reports* **4**, 419-430, doi:10.1016/j.stemcr.2015.01.004 (2015).

171 Parker, M. W. *et al.* Fibrotic extracellular matrix activates a profibrotic positive feedback loop. *J Clin Invest* **124**, 1622-1635, doi:10.1172/jci71386 (2014).

172 Wagner, D. E. *et al.* Comparative decellularization and recellularization of normal versus emphysematous human lungs. *Biomaterials* **35**, 3281-3297, doi:10.1016/j.biomaterials.2013.12.103 (2014).

173 Liu, F. *et al.* Epigenomic alterations and gene expression profiles in respiratory epithelia exposed to cigarette smoke condensate. *Oncogene* **29**, 3650-3664, doi:10.1038/onc.2010.129 (2010).

174 Jain, R. *et al.* Temporal relationship between primary and motile ciliogenesis in airway epithelial cells. *American journal of respiratory cell and molecular biology* **43**, 731-739, doi:10.1165/rcmb.2009-0328OC (2010).

175 Xu, Q. *et al.* Type I collagen promotes primary cilia growth through down-regulating HDAC6-mediated autophagy in confluent mouse embryo fibroblast 3T3-L1 cells. *Journal of bioscience and bioengineering* **125**, 8-14, doi:10.1016/j.jbiosc.2017.07.012 (2018).

176 Perotin, J. M. *et al.* Alteration of primary cilia in chronic obstructive pulmonary disease. *The European respiratory journal*, doi:10.1183/13993003.00122-2018 (2018).

177 Lu, J., Auduong, L., White, E. S. & Yue, X. Up-regulation of heparan sulfate 6-O-sulfation in idiopathic pulmonary fibrosis. *American journal of respiratory cell and molecular biology* **50**, 106-114, doi:10.1165/rcmb.2013-0204OC (2014).

178 Cain, S. A. *et al.* Heparan sulfate regulates fibrillin-1 N- and C-terminal interactions. *The Journal of biological chemistry* **283**, 27017-27027, doi:10.1074/jbc.M803373200 (2008).

179 de Brouwer, B. *et al.* Increased circulating desmosine and age-dependent elastinolysis in idiopathic pulmonary fibrosis. *Respiratory research* **19**, 45, doi:10.1186/s12931-018-0747-6 (2018).

180 Kristensen, J. H. *et al.* Levels of circulating MMP-7 degraded elastin are elevated in pulmonary disorders. *Clinical biochemistry* **48**, 1083-1088, doi:10.1016/j.clinbiochem.2015.07.009 (2015).

181 Nakajima, M. *et al.* Mechanisms for asporin function and regulation in articular cartilage. *The Journal of biological chemistry* **282**, 32185-32192, doi:10.1074/jbc.M700522200 (2007).

182 Kou, I., Nakajima, M. & Ikegawa, S. Expression and regulation of the osteoarthritis-associated protein asporin. *The Journal of biological chemistry* **282**, 32193-32199, doi:10.1074/jbc.M706262200 (2007).

183 Fernandez, I. E. & Eickelberg, O. The impact of TGF-beta on lung fibrosis: from targeting to biomarkers. *Proceedings of the American Thoracic Society* **9**, 111-116, doi:10.1513/pats.201203-023AW (2012).

184 Maccarana, M. *et al.* Asporin-deficient mice have tougher skin and altered skin glycosaminoglycan content and structure. **12**, e0184028, doi:10.1371/journal.pone.0184028 (2017).

185 Xu, L., Li, Z., Liu, S. Y., Xu, S. Y. & Ni, G. X. Asporin and osteoarthritis. *Osteoarthritis and cartilage* **23**, 933-939, doi:10.1016/j.joca.2015.02.011 (2015).

186 Godin, L. M. *et al.* Decreased Laminin Expression by Human Lung Epithelial Cells and Fibroblasts Cultured in Acellular Lung Scaffolds from Aged Mice. *PloS one* **11**, e0150966, doi:10.1371/journal.pone.0150966 (2016).

187 Bueno, M. *et al.* PINK1 deficiency impairs mitochondrial homeostasis and promotes lung fibrosis. *J Clin Invest* **125**, 521-538, doi:10.1172/jci74942 (2015).

188 Theocharidis, G. *et al.* Type VI Collagen Regulates Dermal Matrix Assembly and Fibroblast Motility. *The Journal of investigative dermatology* **136**, 74-83, doi:10.1038/jid.2015.352 (2016).

189 Wang, X. *et al.* A Disintegrin and A Metalloproteinase-9 (ADAM9): A Novel Proteinase Culprit with Multifarious Contributions to COPD. doi:10.1164/rccm.201711-2300OC (2018).

190 Houghton, A. M. Matrix metalloproteinases in destructive lung disease. *Matrix biology : journal of the International Society for Matrix Biology* **44-46**, 167-174, doi:10.1016/j.matbio.2015.02.002 (2015).

191 Morris, D. G. *et al.* Loss of integrin alpha(v)beta6-mediated TGF-beta activation causes Mmp12-dependent emphysema. *Nature* **422**, 169-173, doi:10.1038/nature01413 (2003).

192 Liu, X. *et al.* Elastic fiber homeostasis requires lysyl oxidase-like 1 protein. *Nature genetics* **36**, 178-182, doi:10.1038/ng1297 (2004).

193 Yanagisawa, H. *et al.* Fibulin-5 is an elastin-binding protein essential for elastic fibre development in vivo. *Nature* **415**, 168-171, doi:10.1038/415168a (2002).

194 Kobayashi, N. *et al.* A comparative analysis of the fibulin protein family. Biochemical characterization, binding interactions, and tissue localization. *The Journal of biological chemistry* **282**, 11805-11816, doi:10.1074/jbc.M611029200 (2007).

195 Pilecki, B. *et al.* Characterization of Microfibrillar-associated Protein 4 (MFAP4) as a Tropoelastin- and Fibrillin-binding Protein Involved in Elastic Fiber Formation. *The Journal of biological chemistry* **291**, 1103-1114, doi:10.1074/jbc.M115.681775 (2016).

196 Franciosi, L. *et al.* Susceptibility to COPD: differential proteomic profiling after acute smoking. *PloS one* **9**, e102037, doi:10.1371/journal.pone.0102037 (2014).

197 Askew, D. J. & Silverman, G. A. Intracellular and extracellular serpins modulate lung disease. *Journal of perinatology : official journal of the California Perinatal Association* **28 Suppl 3**, S127-135, doi:10.1038/jp.2008.150 (2008).

198 Leco, K. J. *et al.* Spontaneous air space enlargement in the lungs of mice lacking tissue inhibitor of metalloproteinases-3 (TIMP-3). *J Clin Invest* **108**, 817-829, doi:10.1172/jci12067 (2001).

199 Korytina, G. F. *et al.* [Association of the MMP3, MMP9, ADAM33 and TIMP3 genes polymorphic markers with development and progression of chronic obstructive pulmonary disease]. *Molekuliarnaia biologiia* **46**, 487-499 (2012).

200 Manicone, A. M. *et al.* Matrix Metalloproteinase-28 Is a Key Contributor to Emphysema Pathogenesis. *The American journal of pathology* **187**, 1288-1300, doi:10.1016/j.ajpath.2017.02.008 (2017).

Printed by Media-Tryck, Lund 2018 NORDIC SWAN ECOLABEL 3041 0903

FACULTY OF MEDICINE

Department of Experimental Medical Science

Lund University, Faculty of Medicine
Doctoral Dissertation Series 2018:153
ISBN 978-91-7619-722-6
ISSN 1652-8220